



HAL
open science

Analysis of Absence Epileptic Seizures Using Depth Cortical Measurements

Saeed Akhavanbahabadi

► **To cite this version:**

Saeed Akhavanbahabadi. Analysis of Absence Epileptic Seizures Using Depth Cortical Measurements. Signal and Image processing. Université Grenoble Alpes; University of Teheran, 2019. English. NNT : 2019GREAT063 . tel-02527359

HAL Id: tel-02527359

<https://theses.hal.science/tel-02527359>

Submitted on 1 Apr 2020

HAL is a multi-disciplinary open access archive for the deposit and dissemination of scientific research documents, whether they are published or not. The documents may come from teaching and research institutions in France or abroad, or from public or private research centers.

L'archive ouverte pluridisciplinaire **HAL**, est destinée au dépôt et à la diffusion de documents scientifiques de niveau recherche, publiés ou non, émanant des établissements d'enseignement et de recherche français ou étrangers, des laboratoires publics ou privés.

THÈSE

Pour obtenir le grade de

DOCTEUR DE LA COMMUNAUTÉ UNIVERSITÉ GRENOBLE ALPES

Préparé dans le cadre d'une co-tutelle entre **la Communauté Université Grenoble Alpes et Université de Tehran**

Spécialité : **Signal, Image, Parole, Télécommunication (SIPT)**

Arrêté ministériel : le 6 janvier 2005 - 7 août, 2006

Présentée par

Saeed AKHAVAN

Thèse dirigée par **Christian Jutten et Hamid Soltanian-Zadeh**
et co-encadrée par **Ronald Phlypo et Mahmoud Kamarei**

préparée au sein des **Laboratoires Grenoble Images Parole Signal Automatique (GIPSA) et Biomedical Engineering (BME)**

dans **les École Doctorale d'Electronique, Electrotechnique, Automatique, Traitement du Signal (EEATS) et le Département d'Ingénierie Électrique**

Analyse des Crises d'Epilepsie à l'Aide de Mesures de Profondeur

Thèse soutenue publiquement le **27 November, 2019,**

devant le jury composé de :

M. Mohammad Bagher Shamsollahi

Professeur, Université de Sharif, Président

M. Kamal Setarehdan

Professeur, Université de Tehran, Rapporteur

M. François Cabestaing

Professeur, Université de Lille, Rapporteur

M. Massoud Babaie-Zadeh

Professeur, Université de Sharif, Examineur

M. Gholamali Hossein-Zadeh

Professeur, Université de Tehran, Examineur

M. Carole Lartizien

Professeur, Université de Lyon, Examineur



ACKNOWLEDGMENTS

I would like to express my sincere gratitude to my advisors, Prof. Christian Jutten, Prof. Hamid Soltanian-Zadeh, Prof. Mahmoud Kamarei, and Dr. Ronald Phlypo for their endless patience, motivation, enthusiasm, and knowledge. Beside my advisers, I would like to thank Prof. Depaulis and Dr. Studer for providing the data that I explored. They helped me a lot to understand the data. Definitely, I could not finish my PhD without their help.

I am grateful to the jury members: Prof. Shamsollahi, Prof. Setarehdan, Prof. Cabestaing, Prof. Babaie-Zadeh, Prof. Lartizien and Prof. Hossein-Zadeh. In particular, I am so grateful to the reviewers Prof. Setarehdan and Prof. Cabestaing who helped me to revise my thesis accurately.

I acknowledge that my PhD was funded by the European project 2012-ERC-Adv-320684 CHESS. I appreciate the European Union for funding my PhD.

At the end, my sincere gratitude goes to my family and Dr. Amini for all their spiritual support throughout my life and my study.

Abstract

Absence epilepsy syndrome is accompanied with sudden appearance of seizures in different regions of the brain. The sudden generalization of absence seizures to every region of the brain shows the existence of a mechanism which can quickly synchronizes the activities of the majority of neurons in the brain. The presence of such a mechanism challenges our information about the integrative properties of neurons and the functional connectivity of brain networks. For this reason, many researchers have tried to recognize the main origin of absence seizures. Recent studies have suggested a theory regarding the origin of absence seizures which states that somatosensory cortex drives the thalamus during the first cycles of absence seizures, while thereafter, cortex and thalamus mutually drive each other and continue absence seizures.

This theory motivated the neuroscientists in Grenoble Institute of Neurosciences (GIN) to record data from different layers of somatosensory cortex of Genetic Absence Epilepsy Rats from Strasbourg (GAERS), which is a well-validated animal model for absence epilepsy, to explore the main starting region of absence seizures locally. An electrode with $E = 16$ sensors was vertically implanted in somatosensory cortex of GAERS, and potentials were recorded. In this study, we aim to localize the onset layers of somatosensory cortex during absence seizures and investigate the temporal evolution and dynamics of absence seizures using the recorded data. It is worth mentioning that all previous studies have investigated absence seizures using the data recorded from different regions of the brain, while this is the first study that performs the local exploration of absence seizures using the data recorded from different layers of somatosensory cortex, i.e., the main starting region of absence seizures.

Using factor analysis, source separation, and blind deconvolution methods in different scenarios, we show that 1) the top and bottom layers of somatosensory cortex activate more than the other layers during absence seizures, 2) there is a background epileptic activity during absence seizures,

3) there are few activities or states which randomly activate with the background epileptic activity to generate the absence seizures, and 4) one of these states is dominant, and the others are unstable.

Keywords— Absence Seizure, Spatio-Temporal Analysis, Spike and Wave Discharges, State, Markovian Model, Epileptic Activity, Factor Analysis, Static and Dynamic Sources, Source Separation, Blind Deconvolution

CONTENTS

List of Figures	xi
List of Tables	xvii
List of Abbreviations	xix
1 Problem Sketch: Absence Epilepsy and Challenges	1
2 Spatio-Temporal Modeling of Absence Seizures	9
2.1 Main Idea	10
2.2 Model Definition	11
2.2.1 CSD as a representation of LFP	11
2.2.2 Definition of Epileptic Activity	13
2.2.3 Model for Generation of Spikes	14
2.2.4 Model for Absence Seizure	15
2.3 Data Processing Pipeline	17
2.3.1 Reference Removal	17
2.3.2 LFP Extraction	18
2.3.3 CSD Extraction	18
2.3.4 Seizure Detection	20
2.3.5 Spike Detection	20
2.3.6 Aligning and Stacking Spikes	20
2.3.7 Parameters Estimation	21
2.3.8 Validation of Model	26
2.4 Results	28

2.4.1	Training Phase: Estimation of Parameters	28
2.4.2	Testing Phase: Validation of Model	39
2.5	Discussion	42
2.6	Conclusion	45
3	Static and Dynamic Modeling of Absence Seizures	47
3.1	Main Idea	47
3.2	Model Definition	49
3.3	Problem Formulation	51
3.4	Proposed Method	54
3.4.1	Extraction of The Static Structure and The Number of Dynamic Sources	54
3.4.2	Extraction of Dynamic Sources	57
3.4.3	Extraction of Static Sources and Dynamic Structure	58
3.5	Simulation and Experimental Results	59
3.5.1	Simulations	59
3.5.2	Depth Recordings	62
3.6	Conclusion	74
4	Characterizing Absence Seizures Using Blind Deconvolution	75
4.1	Main Idea	75
4.2	Model and Problem Definition	77
4.3	Proposed Method	79
4.4	Experimental Results	80
4.4.1	Simulation	80
4.4.2	Neural Recording	84
4.5	Conclusion	89
5	Conclusion and Perspectives	91
6	Publications	95

A	Effect of First-Order Markovian Dependency on Parameters Estimation	97
B	Performing The Expectation Step in Spatio-Temporal Modeling of Absence seizures	99
	B.1 Forward Procedure	99
	B.2 Backward Procedure	100
C	Extracting The Model Parameters in Static and Dynamic Modeling of Absence Seizures	103
	C.1 Extraction of The static structure in static and dynamic modeling of seizures	103
	C.2 Extracting auto-correlation matrix of static sources in static and dynamic modeling of seizures	104
	C.3 Extraction of $\mathbf{R}_B^{(k)}$ in static and dynamic modeling of seizures	105
	Bibliography	107

LIST OF FIGURES

1.1	The axial view of implementation scheme in the data acquisition.	5
1.2	The recording electrode and a recorded absence seizure. The beginning and the end of the absence seizure are indicated by t_{onset} and t_{offset} , respectively.	5
2.1	The recording electrode, an absence seizure and a spike (in the green frame) isolated from the raw data. The beginning and the end of the absence seizure are indicated by t_{onset} and t_{offset} , respectively.	10
2.2	Interaction of current sources and sinks generating LFPs at one instant. The points and the curves in the middle plot respectively show the current source and sink, and the corresponding equipotential lines. We can assign a CSD vector to a LFP vector at every time point as explained in 2.3.3. CSD is shown by color coding to clearly show the organization of sources and sinks in different layers of somatosensory cortex.	12
2.3	CSD representation of an epileptic activity. An epileptic activity is described by two characteristics, spatial topography and temporal representation. The CSD map over time ($0 \leq t \leq T$) is shown by color coding to clearly show the organization of sources and sinks in different layers of somatosensory cortex.	13

2.4	Proposed model for the generation of a spike. The considered spike is constructed by a linear superposition of $J = 2$ epileptic activities (or factors). Each epileptic activity is described by two characteristics; 1) the spatial topography (with colorcoded positive and negative values) and 2) the temporal representation.	15
2.5	There are S states under first-order Markovian model during an absence seizure. Each spike, which is specified by a color rectangle, is generated when the corresponding state is activated. The activated state for the k^{th} spike is shown by $q_k \in \{1, 2, \dots, S\}$	16
2.6	Proposed model for the generation of spikes during an absence seizure considering $S = 2$ states and $J = 2$ factors in each state.	16
2.7	Block diagram of the proposed pipeline for 1) pre-processing the data, 2) estimating the unknown parameters of the model, and 3) validation of the results.	17
2.8	Considered cylinders for sources and sinks in iCSD method. z_i ($i = 1, 2, \dots, 16$) shows the positions of the sensors on the electrode.	19
2.9	Estimated parameters of the considered model for the training absence seizure. The probability of transition between the states is shown in the left plot. The obtained factors associated with the first and second states are respectively shown in the first and second rows of the right plot.	29
2.10	The CSD maps of the factors for the training absence seizure. The probability of transition between the states is shown in the left plot. The CSD maps of the obtained factors associated with the first and second states are respectively shown in the first and second rows of the right plot.	29
2.11	Sequence of states for the training absence seizure consisting of $K = 390$ spikes.	30

2.12 Spikes and their states during the windows specified in Fig. 2.11.	31
2.13 (a) Contributions of factors and (b) their joint distribution in each state for the training absence seizure. The average of $\mathbf{c}_j^{(s)}$ is shown by red dashed line in (a) and the average of each joint distribution is shown by a red square in (b).	32
2.14 The average of the CSD representations of the spikes in each state.	33
2.15 The sequence of states for four absence seizures of the first rat which consist of $K_1 = 87$, $K_2 = 94$, $K_3 = 95$ and $K_4 = 88$ spikes, respectively.	34
2.16 (a) The contributions of factors and (b) their joint distribution in each state for the fourth absence seizure of the first rat. The average of $\mathbf{c}_j^{(s)}$ is shown by red dashed line in (a), and the average of each joint distribution is shown by a red square in (b).	35
2.17 Estimated parameters of the proposed model for an absence seizure of the second rat. The probability of transition between the states is shown in the left plot. The obtained factors associated with the first and second states are respectively shown in the first and second rows of the right plot.	37
2.18 The CSD maps of the factors for an absence seizure of the second rat. The probability of transition between the states is shown in the left plot. The CSD maps of the obtained factors associated with the first and second states are respectively shown in the first and second rows of the right plot.	37
2.19 The sequence of states for an absence seizure of the second rat.	38

2.20	(a) The contributions of factors and (b) their joint distribution in each state for an absence seizure of the second rat. The average of $\mathbf{c}_j^{(s)}$ is shown by red dashed line in (a) and the average of each joint distribution is shown by a red square in (b).	38
2.21	The average of the CSD representations of the spikes in each state for an absence seizure of the second rat.	39
2.22	Final spatio-temporal model for the generation of spikes during absence seizures of the first and second rats.	43
3.1	From left to right, the recording electrode, an absence seizure and a time window (length of 87.5 ms) which consists of $n = 16$ spikes from different channels. The absence seizure onset and the end of the absence seizure are indicated by t_{onset} and t_{offset} , respectively.	48
3.2	Static and dynamic sources for three consecutive time windows. The static sources ($\mathbf{s}_1, \mathbf{s}_2, \mathbf{s}_3$) and the dynamic sources ($\mathbf{u}_1, \mathbf{u}_2, \mathbf{u}_3$) are shown in the left and right sides of the sensors, respectively.	50
3.3	The actual and estimated number of dynamic sources in different time windows ($\text{SNR} = 20\text{ dB}$).	61
3.4	The actual and estimated static sources in the marked region of Fig. 3.3. The vertical dashed line shows the boundary of the time windows.	61
3.5	The actual and estimated signals for the first static source in a specific time window in different SNR. The top left figure shows the actual static source.	63
3.6	The estimated static structure (left) and the estimated static source in different time windows (right) for the training absence seizure. To better show the static sources, they are normalized. The average of the static sources is shown in red.	64

3.7	The estimated dynamic structure (left) and the estimated dynamic source in different time windows (right) for the training absence seizure. To better show the dynamic structures, they are normalized.	64
3.8	There are three clusters in the dynamic sources. The average of each cluster is shown in red.	65
3.9	One kind of the dynamic spikes (sources) is added to the background spike (static source) to generate the spike time windows during the training absence seizure. MUX stands for multiplexer which only allows one dynamic spike to pass in each time window.	66
3.10	Sequence of clusters for the training absence seizure.	67
3.11	Sequence of clusters for one of the absence seizures from the first rat which consists of $K = 88$ spike time windows.	67
3.12	The static structure (left) and sources (right) obtained from one of the absence seizures of the second rat with $K = 560$ time windows.	68
3.13	The dynamic structures (left) and sources (right) obtained from one of the absence seizures of the second rat with $K = 560$ time windows.	69
3.14	The obtained average of clusters for the dynamic and static sources in the second rat. One kind of the dynamic spikes (sources) is added to the background spike (static source) to generate the spike time windows during the absence seizures.	69
3.15	Sequence of clusters for one of the absence seizures of the second rat which consists of $K = 560$ time windows.	70
4.1	(a) the noisy data where the spike detection is difficult, and (b) the clean data where the spike detection can be easily performed.	76
4.2	An absence seizure is modeled by a linear combination of R epileptic activities which have spatio-temporal representations.	77

4.3	Characteristics of the activities generating the simulated data. The top and the bottom figures show the characteristics of the first and the second activity, respectively.	81
4.4	The simulated data in the noise-free model. The data is generated by a linear superposition of two activities.	82
4.5	The estimated spikes of the first activity in different SNR. The top left figure shows the original spike.	83
4.6	The estimated spikes of the second activity in different SNR. The top left figure shows the original spike.	83
4.7	(a) The CSDs and the spikes of the epileptic activities generating the absence seizure. (b) Two seconds of the time series of the epileptic activities, and (c) the corresponding absence seizure.	85
4.8	The CSDs and the spikes of the epileptic activities in the second rat.	87
A.1	Scatter plot of two consecutive signals generated under first-order Markovian model. Assigning \mathbf{X}_k to one of the states is not independent form the activated state for \mathbf{X}_{k-1} . Assume that $\mathbf{a}_1^{(s)}$ shows the factor associated with the s^{th} state. . . .	97

LIST OF TABLES

2.1	Relative reconstruction error for five absence seizures of the first rat, which consist of $K_1 = 87$, $K_2 = 94$, $K_3 = 95$, $K_4 = 88$, and $K_5 = 390$ spikes. The diagonal and non-diagonal entries of the table respectively show Er_{train} and Er_{test} .	40
2.2	Relative reconstruction error for four absence seizures of the second rat which consist of $K_1 = 181$, $K_2 = 300$, $K_3 = 350$, $K_4 = 260$ and $K_5 = 146$ spikes. The diagonal and non-diagonal entries of the table respectively show Er_{train} and Er_{test} .	40
2.3	Relative reconstruction error by considering the absence seizures of the first and second rat as the training and testing data, respectively. The bad results are due to the high inter-rats variability, and consequently, it is not possible to use the parameters learned from one rat for the other rats.	41
2.4	The cross correlation coefficient between the spatial topographies of the atoms obtained from the first and second rat.	41
2.5	The average and variance of the contribution of each factor in the generation of spikes for five absence seizures of the first rat. k_s , \bar{c}_s and $\sigma_{c_s}^2$ for $s = \{1, 2\}$ respectively show the number of spikes, the average and variance of the contribution of each factor corresponding to the s^{th} state. Also, k_c , \bar{c}_c and $\sigma_{c_c}^2$ are corresponded to the common factor.	45
3.1	Performance of the proposed method in different SNR.	62

3.2	Reconstruction error for 5 different absence seizures of the first rat. The absence seizures respectively consist of $K_1 = 87$, $K_2 = 94$, $K_3 = 95$, $K_4 = 88$ and $K_5 = 390$ time windows. The diagonal and non-diagonal entries of the table respectively show Er_{train} and Er_{test}	72
3.3	The cross correlation coefficient between the obtained structures from the first and second rat.	73
3.4	The cross correlation coefficient between the obtained sources from the first and second rat.	73
4.1	Performance of the proposed method in different SNR.	83
4.2	The average and variance of the non-zero entries of the time series in four absence seizures of the first rat. l_i shows the number of non-zero entries of the i^{th} time series, and m_i and σ_i^2 represent the corresponding average and variance.	86
4.3	The cross correlation coefficient between the obtained CSDs from two absence seizures of the first rat whose lengths are 19.3 sec and 18.5 sec, respectively.	87
4.4	The cross correlation coefficient between the obtained spikes from two absence seizures of the first rat whose lengths are 19.3 sec and 18.5 sec, respectively.	88
4.5	The cross correlation coefficient between the obtained CSDs from two absence seizures recorded from the first and second rats whose lengths are 19.3 sec and 21.4 sec, respectively.	88
4.6	The cross correlation coefficient between the obtained spikes from two absence seizures recorded from the first and second rats whose lengths are 19.3 sec and 21.4 sec, respectively.	89

LIST OF ABBREVIATIONS

AWGN	Additive White Gaussian Noise
BSS	Blind Source Separation
CSD	Current Source Density
EEG	Electroencephalogram
EM	Expectation Maximization
fMRI	Functional Magnetic Resonance Imaging
GAERS	Genetic Absence Epilepsy Rats from Strasbourg
GIN	Grenoble Institute of Neurosciences
GP	Gaussian Process
ICA	Independent Component Analysis
iid	Independent and Identically Distributed
LFP	Local Field Potential
LTI	Linear Time-Invariant
LVA	Latent Variable Analysis
MLE	Maximum Likelihood Estimator
MSE	Mean Squared Error
pdf	Probability Density Function
WAG/Rij	Wistar Absence Glaxo from Rijswik

1 PROBLEM SKETCH: ABSENCE EPILEPSY AND CHALLENGES

Absence epilepsy is a form of epilepsy with genetic origins which is higher prevalent in children and young adults [Pardoe et al. (2008); Bernhardt et al. (2009); Williams et al. (2016)]. It is accompanied by sudden seizures that affect the patients' consciousness [Caraballo et al. (2008); Chipaux et al. (2013); Killory et al. (2011)]. In fact, the emergence of seizures associated with appearance of spike and wave discharges in electroencephalogram (EEG) recordings is an indication of absence epilepsy [Panayiotopoulos (2008); Das et al. (2006)]. Absence seizures are usually treated using anti-epileptic drugs like ethosuximide (Zarontin), but some of the patients are drug-resistant [Panayiotopoulos (2010)]. Patients who are drug-resistant must be operated for breaking to neuronal structure responsible of the absence seizure. Thus it is mandatory to have a better understanding and accurate localization on spatial and time origins of absence seizures. In this purpose, researchers have used animal models to understand the process by which the absence seizures are generated. Since absence seizures simultaneously occur in many regions of the brain and the duration of absence seizures is not fixed [Panayiotopoulos (2008)], localizing their origins (spatial analysis) [Meeren et al. (2002); Marten et al. (2009); Polack et al. (2007)] and investigating their dynamics (temporal analysis) [Amor et al. (2009); Moeller et al. (2010); Amini et al. (2014)] have been challenging problems over the past decades. In fact, we can prevent the origins from communicating with other regions of the brain to stop propagating the absence seizures if we

have a comprehensive spatio-temporal analysis from absence seizures. The importance of modelling absence seizures as spatio-temporal patterns has been discussed in [Baier et al. (2012)].

In the spatial domain, researchers have studied the epileptic events leading to absence seizures [Williams et al. (2016); Polack (2016)]. The sudden generalization of absence seizures to every region of the brain shows the existence of a mechanism which can quickly synchronizes the activities of the majority of neurons in the brain [Polack (2016)]. The presence of such a mechanism challenges our information about the integrative properties of neurons and the functional connectivity of brain networks. Hence, researchers have tried to accurately define the networks involved in absence seizures and their starting points (origins) [Panayiotopoulos (2010); Vlachos et al. (2017)]. Several theories have been suggested about the main origin of seizures. Some researches point to a faulty thalamus as the origin, while others consider an hyper-excitable region in the cortex area as the origin of absence seizures [Meeren et al. (2002); Avoli (2012)]. The most recent theory filling the gap between cortical and thalamic origin is that both cortex and thalamus participate in the generation of absence seizures [Meeren et al. (2002); Steriade (2003)]. By studying non-linear similarities between signals recorded from multiple zones of cortex and thalamus in the Wistar Absence Glaxo from Rijswik (WAG/Rij) rat model, which is an animal model for absence epilepsy, it has been shown that during the first cycles of absence seizures, somatosensory cortex drives thalamus, while thereafter, somatosensory cortex and thalamus drive each other until the end of absence seizures. Existence of a cortical starter has also been recognized in Genetic Absence Epilepsy Rat from Strasbourg (GAERS), which is one of the well-validated animal models for absence epilepsy [Depaulis et al. (2016); Depaulis and Van Luijtelaar (2005)]. For GAERS, it has been reported that spike-and-wave discharges (SWDs) [Archer et al. (2003); Hamandi et al. (2008)], which are the most important indication of absence seizures, start from somatosensory cortex more than 90% of the time [Polack et al. (2007)].

In the temporal domain, the challenge is about the dynamics of brain activities within the absence seizures. As a major work in this domain, authors of [Amini et al. (2014)] studied the temporal evolution of absence seizures using intracranial EEG (iEEG) recordings from different regions of GAERS brain. At first, source separation methods are applied on temporal sliding windows of the data and the relevant temporal sources are estimated for each window. Then, the temporal sources are compared quantitatively, giving a map of dynamic behavior. By analyzing this map, it has been shown that the relevant sources become more stationary after a latency from the onset of absence seizures. Dynamic analysis of absence seizures has also been done in humans [Moeller et al. (2009); Wu et al. (2017); Moeller et al. (2010)]. For instance in [Moeller et al. (2009)], the EEG-fMRI data were acquired from 13 patients suffering from absence epilepsy. Then, by applying gamma function regressors on sliding time windows of the data, and calculating the F-value, it was shown that the cortical activations and deactivations tend to occur earlier than the thalamic responses during absence seizures. As another example in [Wu et al. (2017)], neuromagnetic sources were volumetrically scanned with accumulated source imaging from 14 patients. Then, effective connectivity networks of the entire brain, including the cortico–thalamo network, were evaluated at the source level through Granger causality analysis [Seth et al. (2015)]. The obtained results show that the cortico–thalamic effective connectivity increases during absence seizures. Moreover, the direction of the connectivity is predominantly from the cortex to the thalamus in the beginning of absence seizures.

All previous works spatially or temporally analyze absence seizures using the data recorded from different areas of the brain, while in this study, the focus is on the analysis of different cortical layers of somatosensory cortex as the main onset region of absence seizures. In order to attain a comprehensive spatio-temporal analysis of absence seizures, a data set was acquired in Grenoble Institute of Neurosciences (GIN) from different layers of somatosensory cortex of GAERS. Using the recorded data, we aim to: 1) localize the

onset layers of somatosensory cortex during absence seizures and 2) investigate the dynamics of absence seizures.

The acquisition process of the data is explained in the following. Then, we briefly explain how the data are analyzed in different chapters to achieve our goals.

DATA ACQUISITION

The data were acquired in four GAERS rats [Danober et al. (1998)]. All experiments were performed in accordance with local Ethical Committee and European Union guidelines (directive 86/609/EEC), and every precaution was taken to minimize stress and the number of animals used in each series of experiments.

Animals were anesthetized (100 mg/kg ketamine, i.p. plus 10 mg/kg xylazine, i.p.) and placed into a stereotactic frame (see [Depaulis et al. (2016)] for a complete description of this preparation). One electrode (\varnothing : 0.125 mm, polyester isolated) with sixteen sensors ($E = 16$) was stereotaxically implanted at different layers of somatosensory cortex with the bregma as the reference [Paxinos and Watson (2009)], and extracellular field potentials were recorded. The distance between the sensors was $h = 150 \mu\text{m}$. Potentials were amplified through a miniature headstage preamplifier (MPA-8i, 8-channel single-ended amplifier with one common subtracting input for an indifferent electrode; voltage gain, x10; frequency band, DC to 5 kHz; Multi Channel Systems, Reutlingen, Germany) connected to a 32-channel programmable gain amplifier (PGA-32, voltage gain, x200 Multi Channel Systems) and sampled at 20 kHz (64 bit ADC). Recordings were collected on a personal computer via a CED interface (Cambridge Electronic Design, Cambridge, UK) using the Spike 2 software (Version 6.0). The implementation scheme and the raw data during a recorded absence seizure are respectively shown in Figs. 1.1 and 1.2.

In fact, we want to answer the following questions using the recorded

CHAPTER 1. PROBLEM SKETCH: ABSENCE EPILEPSY AND CHALLENGES

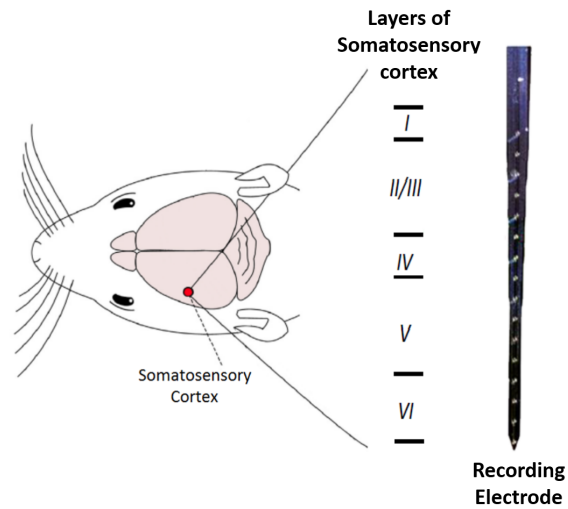


Figure 1.1: The axial view of implementation scheme in the data acquisition.

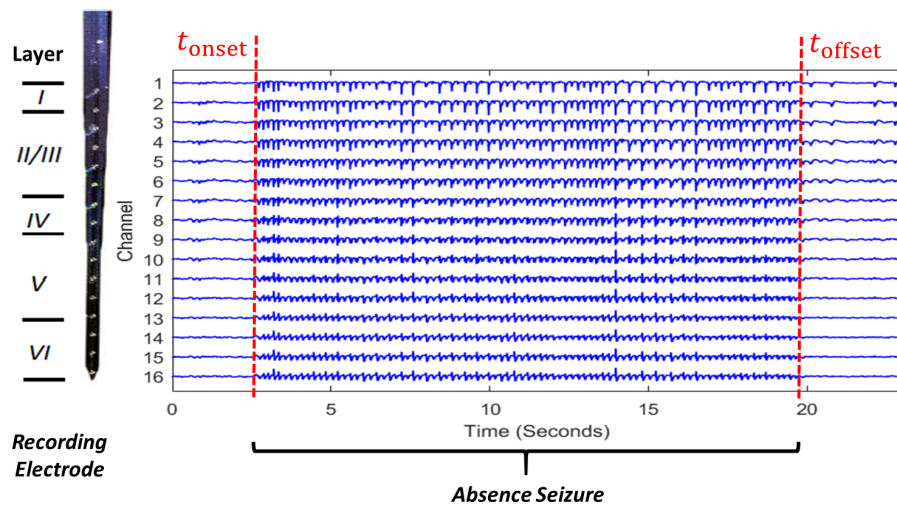


Figure 1.2: The recording electrode and a recorded absence seizure. The beginning and the end of the absence seizure are indicated by t_{onset} and t_{offset} , respectively.

absence seizures:

1) Are there some specific layers in somatosensory cortex which generate the absence seizures? or which layers have more activity during absence seizures? (spatial analysis)

2) Is there any specific pattern during absence seizures over time? or

how do the absence seizures change over time? (temporal analysis)

Answering these questions is difficult because if we look at the data, we find that the data are highly correlated in different channels, and the time delay between the channels is almost negligible. Therefore, we try to answer these questions throughout this thesis.

THESIS OVERVIEW

CHAPTER 2

Both localizing the active layers of somatosensory cortex (spatial analysis) and investigating the dynamics of recorded absence seizures (temporal analysis) are the goals of this chapter. During the recorded absence seizures, a characteristic spike waveform is repeatedly observed. We model these epileptic spike discharges using a generative spatio-temporal model. We assume that there are some hidden states under first-order Markovian model during absence seizures, and each spike is generated when the corresponding state is activated. We also assume that a few specific epileptic activities (or factors) exist in each state, that are linearly combined to form the observed spikes. Each epileptic activity is described by two important characteristics: 1) spatial topography which shows the organization of current sources and sinks in different layers of somatosensory cortex, and 2) temporal representation which illustrates the activation function of epileptic activity. We estimate parameters of the considered model, i.e., states and their epileptic activities, using a factor analysis method. Experimental results show that during absence seizures there are one dominant and one unstable state, with two epileptic activities in each. The interesting point is that one of the epileptic activities is common between the states, hence, it always participates in the generation of spikes. We also show that contributions of epileptic activities in the generation of spikes can be modeled by stationary random processes, and the top and bottom layers of somatosensory cortex are the most active

CHAPTER 1. PROBLEM SKETCH: ABSENCE EPILEPSY AND CHALLENGES

layers during absence seizures. After determination of the model parameters, generality of the proposed model in characterizing absence epileptic seizures is confirmed using a cross validation framework.

CHAPTER 3

In this chapter, the focus is on analyzing the dynamics of absence seizures using source separation methods. Based on the results obtained in chapter 2, we describe the recorded seizures by a linear superposition of static and dynamic sources. The static sources are stable and have a fixed structure, while the dynamic sources are unstable and highly non-stationary. The static sources play the role of background epileptic activities and the dynamic sources are complementary to the static sources in the generation of seizures. Retrieving the sources and their structures from the recorded seizures is the main goal of this chapter from the signal processing point of view which helps us achieve the desired analysis. Experimental results show existence of a static source and a few specific dynamic sources during the recorded seizures. Moreover, it is shown that the origins of the sources are the same in different absence epileptic rats. It is worth mentioning that the considered model and the proposed method in this chapter can be adapted to several applications such as radar or brain signals. Moreover, it can provide an interesting solution to the classical EEG denoising consisting in removing the EEG background activity and cleaning the EEG epileptic data.

CHAPTER 4

This chapter spatially and temporally investigates absence epileptic seizures which are highly noisy and cannot be analyzed using the methods proposed in chapters 2 and 3. We model these kinds of absence seizures by a linear superposition of a few epileptic activities which have spatio-temporal representations. The spatial representation shows the organization of the current sources and sinks generating the epileptic activity, and the temporal

CHAPTER 1. PROBLEM SKETCH: ABSENCE EPILEPSY AND CHALLENGES

representation displays the occurrence time and the activation function of the epileptic activity. Retrieving the epileptic activities from the recorded absence seizures which are noisy is the main target of this chapter which helps us localize the onset layers of somatosensory cortex and understand the temporal evolution of recorded absence seizures in a general form. The obtained results are in accordance with the results presented in chapters 2 and 3.

CHAPTER 5

In this chapter, we conclude the thesis, present the comprehensive analysis of absence epileptic seizures, and answer the scientific questions mentioned in the end of data acquisition section, based on the results obtained in previous chapters. We also state the perspectives and future works.

NOTATION

Throughout the paper, we use bold capital letters to show matrices (\mathbf{X}) and bold small letters to show vectors (\mathbf{x}). The i^{th} column and the $(i, j)^{th}$ entry of \mathbf{X} are shown by \mathbf{x}_i and x_{ij} , respectively. The i^{th} entry of \mathbf{x} is represented by $\mathbf{x}(i)$. We use $(\cdot)^T$, $(\cdot)^H$, and $(*)$ to denote transpose, conjugate transpose, and convolution operator, respectively. $diag(\mathbf{X})$ keeps the diagonal entries of \mathbf{X} , and $trace(\mathbf{X})$ shows the trace of \mathbf{X} . Finally, $\|\mathbf{X}\|_F$, $\|\mathbf{x}\|_2$ and $\|\mathbf{x}\|_0$ show the Frobenius, Euclidean, and l_0 norm, respectively.

2 SPATIO-TEMPORAL MODELING OF ABSENCE SEIZURES

Contents

2.1	Main Idea	10
2.2	Model Definition	11
2.2.1	CSD as a representation of LFP	11
2.2.2	Definition of Epileptic Activity	13
2.2.3	Model for Generation of Spikes	14
2.2.4	Model for Absence Seizure	15
2.3	Data Processing Pipeline	17
2.3.1	Reference Removal	17
2.3.2	LFP Extraction	18
2.3.3	CSD Extraction	18
2.3.4	Seizure Detection	20
2.3.5	Spike Detection	20
2.3.6	Aligning and Stacking Spikes	20
2.3.7	Parameters Estimation	21
2.3.8	Validation of Model	26
2.4	Results	28
2.4.1	Training Phase: Estimation of Parameters	28
2.4.2	Testing Phase: Validation of Model	39
2.5	Discussion	42
2.6	Conclusion	45

2.1 MAIN IDEA

In this chapter, we aim to: 1) estimate the onset layers of somatosensory cortex during absence seizures (spatial analysis), and 2) investigate the dynamics of absence seizures (temporal analysis).

Since the data were recorded locally, when one spike appears in one layer of somatosensory cortex during the absence seizures, we can consider a multisensor recording of a single spike, from hereon referred to as “spike”, as shown in Fig. 2.1 (in the green frame).

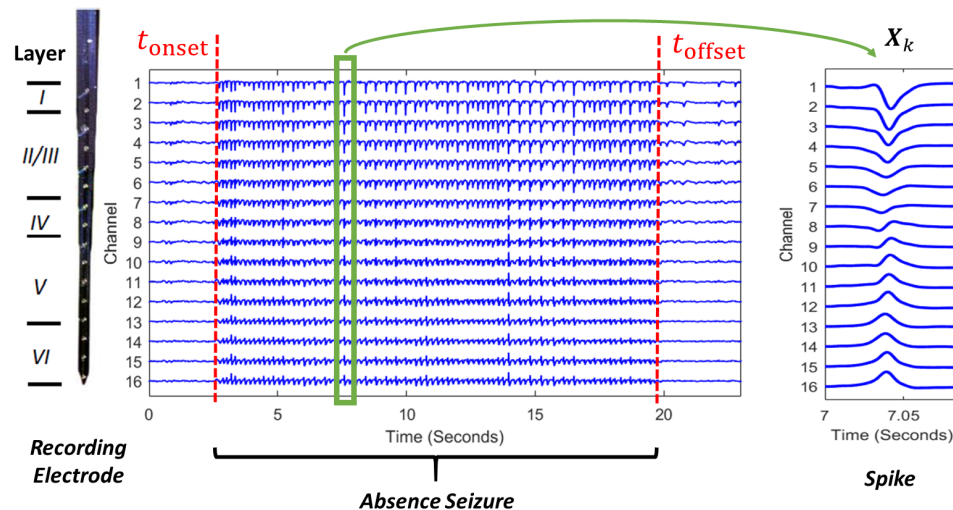


Figure 2.1: The recording electrode, an absence seizure and a spike (in the green frame) isolated from the raw data. The beginning and the end of the absence seizure are indicated by t_{onset} and t_{offset} , respectively.

We model the process by which these spikes are generated to achieve the mentioned targets. We assume that there are some hidden states which are activated under first-order Markovian model during an absence seizure, and each spike of an absence seizure is generated when one of these states is activated. Each state consists of a few specific epileptic activities which are linearly combined and generate the associated spikes. We call each of the epileptic activities as one factor. Each factor is described with two important characteristics. The first one is the spatial topography which shows the

distribution or the organization of current sources and sinks generating the factor, and the second one is the temporal representation which illustrates the activation function or the waveform of the factor. Estimating the explained states and their factors using factor analysis methods [Mulaik (2009)], and investigating the transition between the states help us find the most active layers of somatosensory cortex during absence seizures (spatial analysis) and analyze the dynamics of absence seizures (temporal analysis).

In the following, Section 2.2 explains the proposed model, and Section 2.3 presents the proposed framework for extracting the model parameters, and validation of the results. Section 2.4 is dedicated to the experimental results. The discussion and concluding remarks are reported in Section 2.5, and finally, Section 2.6 concludes this chapter.

2.2 MODEL DEFINITION

The factor model is based on factorization of multi-dimensional measurements of local field potentials (LFPs) into spatial factors and temporal loadings. The spatial factors get their full expressive power when they are given as current source densities (CSDs) which allow to describe the observed potentials as consequence of current sources and sinks. Hence, we first review the relation between LFP and CSD. Then, we define an epileptic activity (a factor) as the atomic element of our model. After that, the relation between a spike and the defined epileptic activity is explained, and finally, we introduce our complete model for an absence seizure.

2.2.1 CSD AS A REPRESENTATION OF LFP

Since the data consist of multichannel measurements of extracellular field potentials, using the concepts of LFP and CSD is a suitable solution for revealing the interaction of different layers of somatosensory cortex. The LFP is generated by transmembrane currents in the vicinity of the recording electrode, and provides valuable information like understanding cortical

functions that cannot be obtained by only measuring the spiking activity of a small population of neurons [Mazzoni et al. (2013); Einevoll et al. (2013)]. Mathematically, the LFP is obtained by low-pass filtering of the extracellular field potential recorded by the electrode [Mazzoni et al. (2013)]. The biophysical origin of LFP is well understood in the framework of volume conductor theory, and using CSD is a standard way for representing LFP. The CSD representation shows the current sources and sinks generating the LFPs. In fact, the information are sent and received among the sources and sinks. Fig. 2.2 schematically shows the relation between the CSD and the LFP at one specific instant in different layers of somatosensory cortex. The mathematical details for extracting CSD from LFP in this research would be explained later in 2.3.3.

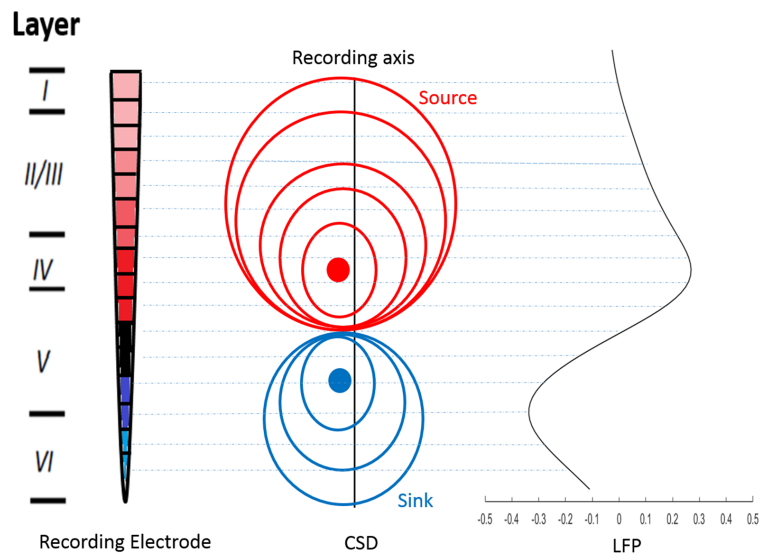


Figure 2.2: Interaction of current sources and sinks generating LFPs at one instant. The points and the curves in the middle plot respectively show the current source and sink, and the corresponding equipotential lines. We can assign a CSD vector to a LFP vector at every time point as explained in 2.3.3. CSD is shown by color coding to clearly show the organization of sources and sinks in different layers of somatosensory cortex.

As sketched in Fig. 2.2, and explained formally in 2.3.3, CSD clearly

exposes the equivalent current source and sink model for LFP. We can use the CSD representation to localize the current sources and sinks generating the measured potentials. Therefore, we define our model based on the CSD representation of the data.

2.2.2 DEFINITION OF EPILEPTIC ACTIVITY

We characterize an epileptic activity by a synchronous activity of current sources and sinks. Assume that there are a few current sources and sinks in the vicinity of the recording electrode which are well localized, i.e., they have a spatial localization, which does not move over time. If the amplitudes of the sources and sinks change according to a specific temporal function over time $0 \leq t \leq T$, we say an epileptic activity has been generated. An epileptic activity is schematically shown in Fig. 2.3.

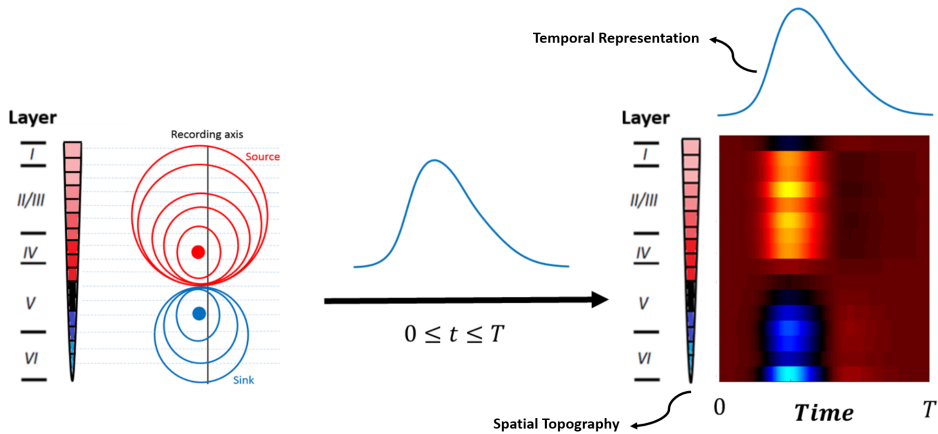


Figure 2.3: CSD representation of an epileptic activity. An epileptic activity is described by two characteristics, spatial topography and temporal representation. The CSD map over time ($0 \leq t \leq T$) is shown by color coding to clearly show the organization of sources and sinks in different layers of somatosensory cortex.

The main advantage of this definition is that the obtained CSD map over time ($0 \leq t \leq T$) can be described by only two characteristics. The first one is the spatial topography which shows the distribution or the organization of the current sources and sinks in different layers, and the second one is

the temporal representation which illustrates the temporal evolution of the current sources and sinks. Mathematically, we can say that an epileptic activity is produced by the vector multiplication of its spatial topography and temporal representation, hence, it is a rank-one factor.

2.2.3 MODEL FOR GENERATION OF SPIKES

Spikes are the most important epileptic discharges during the absence seizures because they are the spatial integration of potentials [Polack et al. (2007)]. Therefore, we analyze the absence seizures based on investigation of spikes. At the moment, we suppose that we have already accurately extracted the spikes from the data. The extraction method will be explained later. We assume that each spike is generated by a linear combination of J epileptic activities. Hence, we can consider the following rank- J factorization for each spike $\mathbf{X}_k \in \mathbb{R}^{E \times T}$, where E and T respectively show the number of sensors and samples in each spike.

$$\mathbf{X}_k = \sum_{j=1}^J c_{kj} \mathbf{a}_j \mathbf{b}_j^T \quad (2.1)$$

Based on this decomposition, if we assume that \mathbf{X}_k is generated by a linear superposition of J epileptic activities, and consider each epileptic activity as a factor, $c_{kj} \in \mathbb{R}$, $\mathbf{a}_j \in \mathbb{R}^E$ and $\mathbf{b}_j \in \mathbb{R}^T$ respectively show the contribution of the j^{th} factor in the generation of \mathbf{X}_k , the spatial topography, and the temporal representation of the j^{th} factor. In fact, \mathbf{a}_j shows the spatial distribution of the CSD in different layers of somatosensory cortex and \mathbf{b}_j informs temporal activation function of each factor.

For instance, Fig. 2.4 schematically shows that $J = 2$ different epileptic activities linearly contribute to the construction of the considered spike. It must be mentioned that linearity is a reasonable assumption because we process the low frequency content of the data (LFP or CSD) which does not include effects of capacity and induction. Therefore, there is no building up of charges and we can directly measure the fields [Reitz et al. (2008)].

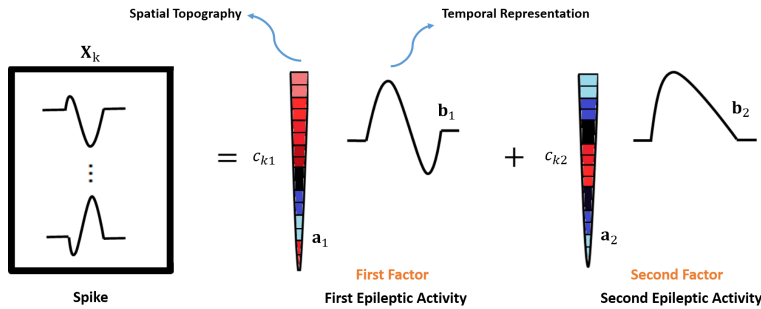


Figure 2.4: Proposed model for the generation of a spike. The considered spike is constructed by a linear superposition of $J = 2$ epileptic activities (or factors). Each epileptic activity is described by two characteristics; 1) the spatial topography (with colorcoded positive and negative values) and 2) the temporal representation.

2.2.4 MODEL FOR ABSENCE SEIZURE

We can consider each absence seizure as a train of spikes as shown in Fig. 2.1. Based on the similarity of spikes, meaning that they have temporal activation functions that are almost equal, we assume that there are a few hidden states (S) during an absence seizure, and each spike is generated when the corresponding state is activated. In order to model the dynamics of the state activations, we also assume the state activations are modeled by a first-order Markovian model with a fixed transition probability matrix $\mathbf{P} \in \mathbb{R}^{S \times S}$ for the state activations, where the $(i, j)^{th}$ entry of \mathbf{P} , or in other words, p_{ij} shows the probability of transition from state i to state j . The first-order Markovian model means that the activation of each state is only dependent on the previous active state. Generally, this assumption enables reasoning and computation with the data that would otherwise be intractable. Fig. 2.5 shows the considered model for the generation of a train of spikes, or in other words, an absence seizure assuming $S = 2$, i.e., when there are two states.

In fact, each state consists of a few specific factors (e.g., J factors) which participate in the generation of spikes. If we assume that there are K spikes during an absence seizure and stack them in a three dimensional tensor

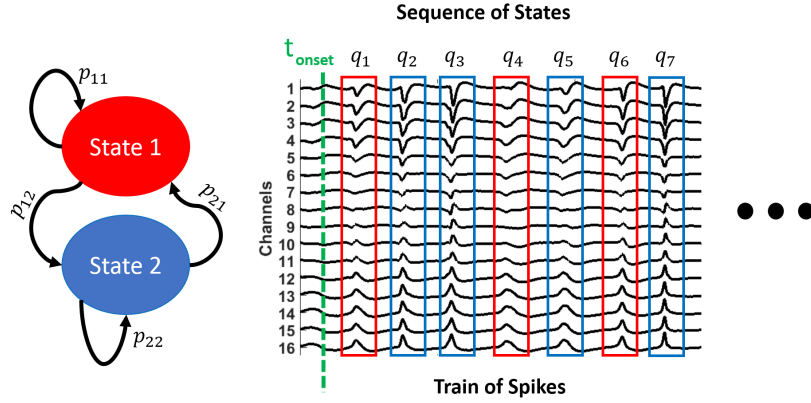


Figure 2.5: There are S states under first-order Markovian model during an absence seizure. Each spike, which is specified by a color rectangle, is generated when the corresponding state is activated. The activated state for the k^{th} spike is shown by $q_k \in \{1, 2, \dots, S\}$.

$\mathcal{T} \in \mathbb{R}^{E \times T \times K}$, where E and T respectively show the number of channels (sensors) and the length of each spike, Fig. 2.6 schematically shows the complete model for the generation of spikes assuming that there are $S = 2$ states and $J = 2$ factors in each state. It should be noted that S , J , and the factors are unknown, and Fig. 2.6 is just a schematic figure.

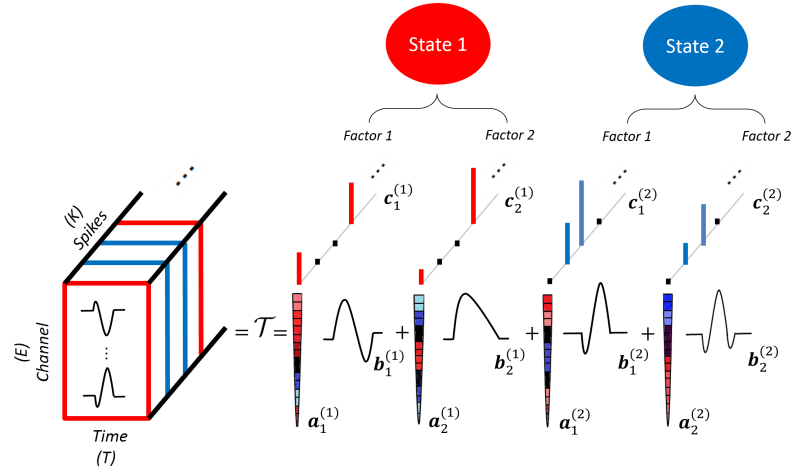


Figure 2.6: Proposed model for the generation of spikes during an absence seizure considering $S = 2$ states and $J = 2$ factors in each state.

It is worth noting that only one state can be active for each spike (see Fig. 2.6) which results in zeroing the factor loadings of all non-active states for that spike. Now that the model definition is complete, we propose a framework to extract the hidden states, their factors, and the transition probability matrix from the recorded absence seizures, and cross validate the obtained results.

2.3 DATA PROCESSING PIPELINE

The proposed data processing pipeline is shown in Fig. 2.7. There are three main stages in this pipeline: pre-processing, proposed method, and cross validation. In the first stage, the pre-processing steps are performed. The parameters of the model are extracted in the second stage, and finally, we cross validate the extracted results in the last stage. In the following, each block of the proposed pipeline is explained.

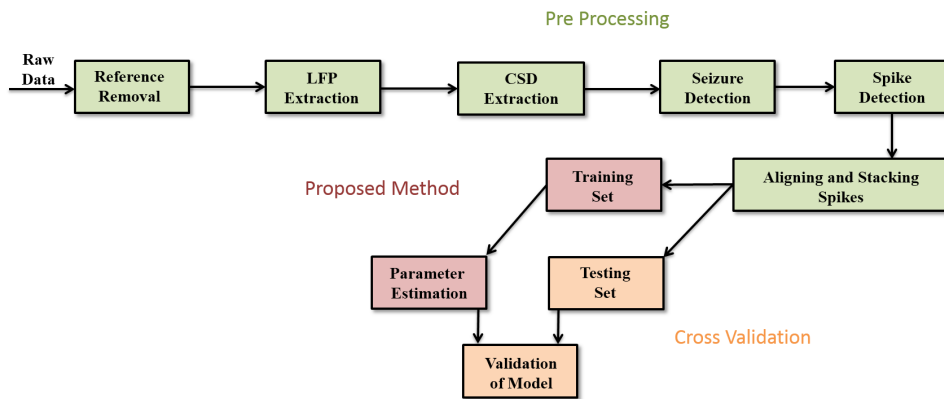


Figure 2.7: Block diagram of the proposed pipeline for 1) pre-processing the data, 2) estimating the unknown parameters of the model, and 3) validation of the results.

2.3.1 REFERENCE REMOVAL

Since the recorded raw data for each sensor is the potential difference between the tip of the sensor and a distant cortical site, the first pre-processing step

consists in removing the effect of reference point by subtracting each column of the data from its average. In fact, we re-reference to the average as a proxy of the unknown reference. The common information between all of the channels is removed by this subtraction. Subtraction of the common average has also been shown to be useful for other reasons [Ludwig et al. (2009)]. For instance, some sources of noise, especially those from non-physiological external sources, are removed by this pre-processing step because the sensors are located very close to each other.

2.3.2 LFP EXTRACTION

The LFP is obtained by low-pass filtering of the extracellular field potential recorded by the electrode [Mazzoni et al. (2013)]. Therefore, the recorded signal of each sensor (channel) is filtered by a 5th-order low pass Butterworth filter with a cutoff frequency equal to 100 Hz. In fact, the high-frequency content (above 100 Hz) of the data consists of action potentials and noise which are not of interest in this research. The main target of this pre-processing step is preparing the data for calculating the CSD.

2.3.3 CSD EXTRACTION

The biophysical origin of LFP is well understood in the framework of volume conductor theory, and CSD is one of the standard ways of representing LFP. In fact, the CSD representation shows the current sources and sinks generating the measured potentials. We use an inverse CSD (iCSD) [Pettersen et al. (2006)] method to extract the CSD from the LFP, as explained in the following.

In iCSD method, there is a linear relationship between LFPs ($\phi \in \mathbb{R}^E$) and CSDs ($\mu \in \mathbb{R}^E$) at each time instant by means of a coefficient matrix $\mathbf{F} \in \mathbb{R}^{E \times E}$ as follows:

$$\phi = \mathbf{F}\mu \tag{2.2}$$

where $E = 16$ shows the number of channels. If we assume the recording

electrode is located on the z axis, each entry of the coefficient matrix $f_{ij} = [\mathbf{F}]_{ij}$ is calculated as follow:

$$f_{ij} = \int_{z_i - \frac{h}{2}}^{z_i + \frac{h}{2}} \frac{1}{2\sigma} (\sqrt{(z_j - z)^2 + r^2} + |z_j - z|) dz \quad (2.3)$$

where z_i ($i = 1, 2, \dots, 16$) shows the positions of the sensors on the recording electrode and $h = 150 \mu m$ denotes the distance between the sensors. r represents the radius of the cylindrical volume around the sensors which consists of current sources and sinks as shown in Fig. 2.8, and it is considered equal to $r = 50 \mu m$ [Einevoll et al. (2013)] in this research. The value of σ , which shows the extracellular electrical conductivity, is not important here, and it is just a scaling factor. It should be noted that we assume the sensors are located in the homogeneous media. Therefore, the CSD vector in each time instant is extracted by $\boldsymbol{\mu} = \mathbf{F}^{-1}\boldsymbol{\phi}$.

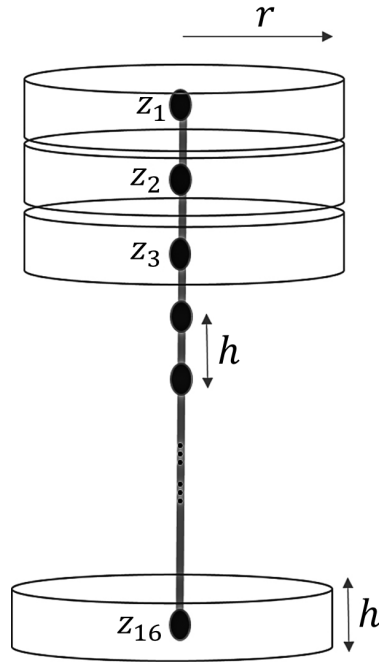


Figure 2.8: Considered cylinders for sources and sinks in iCSD method. z_i ($i = 1, 2, \dots, 16$) shows the positions of the sensors on the electrode.

2.3.4 SEIZURE DETECTION

We aim to investigate the absence seizures, therefore, we must separate them from the data. A good survey on seizure detection methods can be found in [Alotaiby et al. (2014)]. Since the amplitudes of the signals (now, the CSDs) change significantly in the beginning and end of absence seizures (as shown in Fig. 2.1), we identify absence seizures by simple thresholding. It is worth mentioning that after detecting the seizures, we also apply a median filtering on a window around each peak which its amplitude is greater than the half of the maximum absolute amplitude of the signals for the whole period of processing to remove the outliers and artifacts from the seizures. The length of moving median window is equal to 0.2 s with 70% overlap and the length of window around the peak is equal to 0.4 s [Amini et al. (2014)].

2.3.5 SPIKE DETECTION

Once the absence seizures are separated from the data, we detect the spikes. Following [Quiroga et al. (2004)], we again use thresholding to detect the spikes. Each spike is shown by $\mathbf{X}_k^{(t_k)} \in \mathbb{R}^{E \times T}$, where t_k denotes the starting time of the k^{th} spike, $E = 16$ shows the number of channels (sensors), and $T = 1750$ samples (87.5 ms) [Polack et al. (2007)] represents the length of each spike.

2.3.6 ALIGNING AND STACKING SPIKES

The alignment of spikes is a necessary step to obtain accurate results. We align the spikes using the improved version of Woody's method proposed in [Cabasson and Meste (2008)]. For this purpose, in an iteration loop, each spike $\mathbf{X}_k^{(t_k)}$ is aligned with the average of the other spikes until convergence of the algorithm. Considering \mathbf{X}_0 as the average of all spikes except $\mathbf{X}_k^{(t_k)}$, we shift the window of spike $\mathbf{X}_k^{(t_k)}$ until achieving the maximum cross correlation between $\mathbf{X}_k^{(t_k)}$ and \mathbf{X}_0 . Mathematically, the following calculations are

performed in each iteration:

$$\begin{aligned} \tau_k^* &= \underset{\tau_i}{\operatorname{argmax}} \quad \rho(\mathbf{X}_0, \mathbf{X}_k^{(t_k - \tau_k)}), \quad |\tau_k| < \frac{T}{2} \\ t_k &\leftarrow t_k - \tau_k^* \end{aligned} \quad (2.4)$$

The cross correlation coefficient is calculated as follows:

$$\rho(\mathbf{X}_0, \mathbf{X}_k^{(t_k - \tau_k)}) = \frac{\operatorname{Tr}\{\mathbf{X}_0^T \mathbf{X}_k^{(t_k - \tau_k)}\}}{\|\mathbf{X}_0\|_F \|\mathbf{X}_k^{(t_k - \tau_k)}\|_F} \quad (2.5)$$

where Tr and $\|\cdot\|_F$ denote the trace function and Frobenius norm, respectively. In fact, we repeat (2.4) for all spikes until the algorithm convergence.

After aligning the spikes, we drop the starting time of each spike and consider each one as \mathbf{X}_k . Once the spikes were aligned, we stack them in 3-way data tensor \mathcal{T} as shown in Fig. 2.6 to prepare the data for estimating the model parameters, i.e. the states, their factors, and the transition probability matrix.

As shown in the block diagram of the proposed framework (Fig. 2.7), we split the data into two groups of training set and testing set. \mathcal{T}_{train} consists of spikes of only an absence seizure and $\mathcal{T}_{test} = \{\mathcal{T}_{test}^{(1)}, \mathcal{T}_{test}^{(2)}, \dots, \mathcal{T}_{test}^{(M)}\}$ consists of spikes of M absence seizures. In the following, estimation of the model parameters using \mathcal{T}_{train} is explained.

2.3.7 PARAMETERS ESTIMATION

According to the proposed model and as shown in Fig. 2.6, the main idea for estimating the model parameters is factorizing $\mathcal{T}_{train} \in \mathbb{R}^{E \times T \times K}$, which is a cube of data, using tensor factorization. Hence, the desired factorization for \mathcal{T}_{train} is as follows:

$$\mathcal{T}_{train} \simeq \sum_{s=1}^S \sum_{j=1}^J \mathbf{a}_j^{(s)} \otimes \mathbf{b}_j^{(s)} \otimes \mathbf{c}_j^{(s)} \quad (2.6)$$

where E , T , K , S , and J are respectively the number of channels, samples in each spike, spikes, states, and factors. \otimes denotes the tensor product. $\mathbf{a}_j^{(s)} \in \mathbb{R}^E$, $\mathbf{b}_j^{(s)} \in \mathbb{R}^T$, and $\mathbf{c}_j^{(s)} \in \mathbb{R}^K$ show spatial topography of each factor,

temporal representation of each factor and contribution of each factor in the generation of spikes, respectively. This factorization is schematically shown in Fig. 2.6 assuming $S = J = 2$. We also consider the following constraints in this factorization:

1- According to the model, there is a first-order Markovian model in the activation of the states, i.e., the $(k + 1)^{th}$ state only depends on the k^{th} state. The transition probability matrix $\mathbf{P} \in \mathbb{R}^{S \times S}$, which shows the probability of activation of each state subject to knowing the previous activated state, must also be estimated during the factorization. It should be noted that if the considered absence seizure was almost noiseless, we could ignore the Markovian dependency between the spikes and estimate the parameters (see Appendix A).

2- In order to omit the scaling and a part of polarization ambiguities, $\mathbf{a}_j^{(s)}$ and $\mathbf{b}_j^{(s)}$ are considered unit norm vectors, and entries of $\mathbf{c}_j^{(s)}$ are considered positive for all of the factors [Comon and Jutten (2010)].

A noticeable point here is that we do not have any prior information about the number of states (S) and factors (J). However, we have to fix them to be able to extract the unknown parameters. Since we are looking for results which have biophysiological interpretation, at first we estimate the unknown parameters for different S and J , then, we select the one with the best biophysiological interpretation. We discuss more about this issue later.

We use the maximum likelihood estimator (MLE) and the expectation maximization (EM) to obtain the unknown parameters as explained in the following.

We consider the parameters of the s^{th} state in the matrices $\mathbf{A}^{(s)} \in \mathbb{R}^{E \times J}$, $\mathbf{B}^{(s)} \in \mathbb{R}^{T \times J}$ and $\mathbf{C}^{(s)} \in \mathbb{R}^{K \times J}$ as follows:

$$\begin{aligned} \mathbf{A}^{(s)} &= [\mathbf{a}_1^{(s)} \quad \mathbf{a}_2^{(s)} \quad \dots \quad \mathbf{a}_J^{(s)}] \\ \mathbf{B}^{(s)} &= [\mathbf{b}_1^{(s)} \quad \mathbf{b}_2^{(s)} \quad \dots \quad \mathbf{b}_J^{(s)}] \\ \mathbf{C}^{(s)} &= [\mathbf{c}_1^{(s)} \quad \mathbf{c}_2^{(s)} \quad \dots \quad \mathbf{c}_J^{(s)}], \quad [\mathbf{C}^{(s)}]_{kj} = c_{kj}^{(s)} \end{aligned} \quad (2.7)$$

Therefore, the set of unknown parameters is as follows:

$$\Theta = \{\mathbf{A}, \mathbf{B}, \mathbf{C}, \mathbf{P}\} \quad (2.8)$$

where $\mathbf{A} = [\mathbf{A}^{(1)} \dots \mathbf{A}^{(S)}] \in \mathbb{R}^{E \times JS}$, $\mathbf{B} = [\mathbf{B}^{(1)} \dots \mathbf{B}^{(S)}] \in \mathbb{R}^{T \times JS}$, $\mathbf{C} = [\mathbf{C}^{(1)} \dots \mathbf{C}^{(S)}] \in \mathbb{R}^{K \times JS}$, and $\mathbf{P} \in \mathbb{R}^{S \times S}$ shows the transition probability matrix.

We assume that the error of the measurement is modeled as an additive white Gaussian term. Hence, each recorded spike $\mathbf{X}_k \in \mathbb{R}^{E \times T}$ is expressed as:

$$\mathcal{H}_k^{(s)} : \mathbf{X}_k = \sum_{j=1}^J c_{kj}^{(s)} \mathbf{a}_j^{(s)} \mathbf{b}_j^{(s)T} + \mathbf{N}_k \quad (2.9)$$

where $\mathcal{H}_k^{(s)}$ ($s = 1, 2, \dots, S$) means that state s is active for generating the k^{th} spike. $c_{kj}^{(s)} \in \mathbb{R}^+$ shows the contribution of the j^{th} factor from the s^{th} state in the generation of \mathbf{X}_k . $\mathbf{a}_j^{(s)} \in \mathbb{R}^E$ and $\mathbf{b}_j^{(s)} \in \mathbb{R}^T$ respectively represent the spatial topography and the temporal representation of the j^{th} factor from the s^{th} state. Finally, $\mathbf{N}_k \in \mathbb{R}^{E \times T}$ is additive white Gaussian noise with independent and identically distributed (i.i.d.) entries, and each entry of this matrix has a normal distribution with zero mean and variance σ_0^2 . Therefore, we have:

$$f(\mathbf{X}_k | \mathcal{H}_k^{(s)}, \Theta) = \left(\frac{1}{\sqrt{2\pi\sigma_0^2}} \right)^{ET} \exp \left(- \frac{\|\mathbf{X}_k - \sum_{j=1}^J c_{kj}^{(s)} \mathbf{a}_j^{(s)} \mathbf{b}_j^{(s)T}\|_F^2}{2\sigma_0^2} \right) \quad (2.10)$$

It should be noted that since σ_0^2 is unknown, it is also added to the set of unknown parameters. Considering (2.10), we can use the maximum likelihood estimator (MLE) to find the set of unknown parameters, i.e.,

$$\Theta^* = \underset{\Theta}{\operatorname{argmax}} \log(f(\mathcal{T}_{train} | \Theta)) \quad (2.11)$$

where the superscript $*$ shows the optimum value of the parameter. Since the noise matrices \mathbf{N}_k ($k = 1, 2, \dots, K$) are independent, the observations \mathbf{X}_k for $k = 1, 2, \dots, K$ are also independent given Θ . Therefore, the objective

function can be expressed as follows:

$$\log(f(\mathcal{T}_{train}|\Theta)) = \sum_{k=1}^K \log(f(\mathbf{X}_k|\Theta)) = \sum_{k=1}^K \log \left\{ \sum_{s=1}^S p(\mathcal{H}_k^{(s)}) f(\mathbf{X}_k|\mathcal{H}_k^{(s)}, \Theta) \right\} \quad (2.12)$$

where $p(\mathcal{H}_k^{(s)})$ shows the probability of the activation of the s^{th} state in the generation of the k^{th} spike. Since $p(\mathcal{H}_k^{(s)})$ is unknown, and the summation over s in (2.12) is like an expectation operator, we solve this optimization problem using the expectation maximization (EM) method. This means that the following two steps are alternately performed to extract the unknown parameters (*E-step* and *M-step*).

2.3.7.1 Expectation Step (E-step)

In this step, we assume that the set of unknown parameters Θ and consequently $f(\mathbf{X}_k|\mathcal{H}_k^{(s)}, \Theta)$ are known, then, we estimate $p(\mathcal{H}_k^{(s)})$. This step is performed using a forward-backward procedure, which is explained in Appendix B. In this procedure, the probability of being in state m for the k^{th} spike and being in state n for the $(k+1)^{th}$ spike ($p(\mathcal{H}_k^{(m)}, \mathcal{H}_{k+1}^{(n)})$) is also calculated which is used in the *M-step* to extract the transition probability matrix.

2.3.7.2 Maximization Step (M-step)

Given $p(\mathcal{H}_k^{(s)})$ in the previous step, Θ is extracted in this step. The entries of the transition probability matrix are easily estimated using the following equation:

$$[\mathbf{P}]_{mn} = p_{mn} \rightarrow p_{mn}^* = \frac{\sum_{k=1}^{K-1} p(\mathcal{H}_k^{(m)}, \mathcal{H}_{k+1}^{(n)})}{\sum_{k=1}^{K-1} p(\mathcal{H}_k^{(m)})} \quad (2.13)$$

For extracting the other parameters, directly maximizing (2.12) is difficult because the log term ($\log \sum$) cannot be further reduced. Therefore, instead of maximizing this objective function, we consider its lower bound

using the Jensen's inequality (log-concavity):

$$\sum_{k=1}^K \log\left\{\sum_{s=1}^S p(\mathcal{H}_k^{(s)}) f(\mathbf{X}_k | \mathcal{H}_k^{(s)}, \Theta)\right\} \geq \underbrace{\sum_{k=1}^K \sum_{s=1}^S p(\mathcal{H}_k^{(s)}) \log\{f(\mathbf{X}_k | \mathcal{H}_k^{(s)}, \Theta)\}}_{Q(\Theta)} \quad (2.14)$$

In fact, hereafter, we solve the following optimization problem:

$$\Theta^* = \underset{\Theta}{\operatorname{argmax}} \quad Q(\Theta) \quad (2.15)$$

By substituting (2.10) in (2.15), and some simple calculations, we get:

$$Q(\Theta) = -\frac{ET}{2} \log(2\pi\sigma_0^2) - \frac{1}{2\sigma_0^2} \sum_{k=1}^K \sum_{s=1}^S p(\mathcal{H}_k^{(s)}) \|\mathbf{X}_k\|^2 - \sum_{j=1}^J c_{kj}^{(s)} \mathbf{a}_j^{(s)} \mathbf{b}_j^{(s)T} \Big\|_F^2 \quad (2.16)$$

It can be easily seen that maximizing this function is done by maximizing each of its independent terms, i.e., we can separate the parameters of each state in this optimization problem. Therefore, for each state, we have:

$$\{\mathbf{A}^{(s)*}, \mathbf{B}^{(s)*}, \mathbf{C}^{(s)*}\} = \underset{\mathbf{A}^{(s)}, \mathbf{B}^{(s)}, \mathbf{C}^{(s)}}{\operatorname{argmin}} \sum_{k=1}^K p(\mathcal{H}_k^{(s)}) \|\mathbf{X}_k\|^2 - \sum_{j=1}^J c_{kj}^{(s)} \mathbf{a}_j^{(s)} \mathbf{b}_j^{(s)T} \Big\|_F^2 \quad (2.17)$$

According to the constraints mentioned in 2.3.7, $\mathbf{a}_j^{(s)}$ and $\mathbf{b}_j^{(s)}$ are unit norm vectors and $c_{kj}^{(s)}$ is positive. Therefore, we must also consider the following constraints in this optimization:

$$\begin{aligned} \|\mathbf{a}_j^{(s)}\|_2 = 1, \quad \|\mathbf{b}_j^{(s)}\|_2 = 1, \quad c_{kj}^{(s)} > 0 \\ j = 1, 2, \dots, J \quad s = 1, 2, \dots, S \quad k = 1, 2, \dots, K \end{aligned} \quad (2.18)$$

Hence, the proposed optimization problem in (2.17) is a constrained weighted least square problems which can be solved using alternating least square method (ALS) [Boyd and Vandenberghe (2004)].

After solving (2.17) for all of the states, and hence determination of $\{\mathbf{A}^*, \mathbf{B}^*, \mathbf{C}^*\}$, by computing the first derivative of $Q(\Theta)$ with respect to σ_0^2 , it can

be shown that the variance of noise is estimated according to the following formula:

$$\sigma_0^{2*} = \frac{1}{ET} \sum_{k=1}^K \sum_{s=1}^S p(\mathcal{H}_k^{(s)}) \|\mathbf{X}_k - \sum_{j=1}^J c_{kj}^{(s)*} \mathbf{a}_j^{(s)*} \mathbf{b}_j^{(s)*T}\|_F^2 \quad (2.19)$$

The final set of unknown parameters are extracted by alternately performing the *E-step* and the *M-step* until convergence of the parameters.

After the parameter estimation, we must assign one state to each spike, and determine the sequence of states during the training absence seizure. For this purpose, since we have found all characteristics of the states, the sequence of states can be determined using the Viterbi algorithm [Rabiner (1989)].

After determination of the sequence of states, we must apply one minor modification on matrix \mathbf{C} to get the optimal parameters for the obtained sequence. In each row of \mathbf{C} , we must just have non-zero entries for a single state because only one state is active for each spike. Therefore, we keep the entries of the corresponding activated state (factors), and make the other entries zero. Now, all of the unknown parameters $\Theta^* = \{\mathbf{A}^*, \mathbf{B}^*, \mathbf{C}^*, \mathbf{P}^*, \sigma_0^{2*}\}$ are determined.

Finally, in order to show that the proposed model is adapted to the training data, we must have good reconstruction using the estimated parameters. This means that the following relative reconstruction error must be small:

$$Er_{train} = \frac{\|\mathcal{T}_{train} - \sum_{s=1}^S \sum_{j=1}^J \mathbf{a}_j^{(s)*} \otimes \mathbf{b}_j^{(s)*} \otimes \mathbf{c}_j^{(s)*}\|_F^2}{\|\mathcal{T}_{train}\|_F^2} \quad (2.20)$$

where $\|\cdot\|_F$ denotes the Frobenius norm. $\mathbf{a}_j^{(s)*}$, $\mathbf{b}_j^{(s)*}$ and $\mathbf{c}_j^{(s)*}$ show spatial topography, temporal representation, and contribution of each factor estimated from the training absence seizure. In fact, we check this error to evaluate the goodness of fit of the proposed model to the training data.

2.3.8 VALIDATION OF MODEL

The last block of the proposed framework is cross-validation. We must check the compatibility of the obtained parameters from \mathcal{T}_{train} with each of the ab-

sence seizures in the testing set, i.e., $\mathcal{T}_{test}^{(m)}$ for $m = 1, 2, \dots, M$. For this purpose, we suppose that the main parameters of the proposed model including the spatial topography of the factors ($\mathbf{a}_j^{(s)*}$), the temporal representation of the factors ($\mathbf{b}_j^{(s)*}$), and the transition probability matrix (\mathbf{P}^*) are common for all of the absence seizures. Therefore, we just estimate the contribution of the factors ($\mathbf{c}_j^{(s)}$) in the generation of $\mathcal{T}_{test}^{(m)}$ and calculate the relative reconstruction error. In fact, we assume that the main parameters of the model are independent of absence seizures, hence the only free parameters that need to be estimated are the contributions of the factors in the construction of $\mathcal{T}_{test}^{(m)}$. The estimation procedure of $\mathbf{c}_j^{(s)}$ is explained in the following.

There is a state corresponding to each spike, therefore, we can assign a sequence of states to each absence seizure as shown in Fig. 2.5. Since all of the model parameters except $\mathbf{c}_j^{(s)}$ are determined, and there is a first-order Markovian model in the activation of the states, we can extract the sequence of states for testing absence seizure $\mathcal{T}_{test}^{(m)}$ using Viterbi algorithm [Rabiner (1989)] and following the proposed method in the previous section. Once the sequence of states is determined, we project each spike of the testing absence seizure on the corresponding state (factor) and find $\mathbf{c}_j^{(s)*}$. Positivity of the coefficients must be considered in this decomposition.

Finally, we calculate the following relative reconstruction error to evaluate the goodness of fit of the proposed model to the unseen testing data.

$$Er_{test}^{(m)} = \frac{\|\mathcal{T}_{test}^{(m)} - \sum_{s=1}^S \sum_{j=1}^J \mathbf{a}_j^{(s)*} \otimes \mathbf{b}_j^{(s)*} \otimes \mathbf{c}_j^{(s)*}\|_F^2}{\|\mathcal{T}_{test}^{(m)}\|_F^2} \quad (2.21)$$

An important point must be discussed before presenting the results obtained from the neural dataset. The data used in this study were acquired from somatosensory cortex using an electrode with $E = 16$ sensors. The distance between the first and the last sensor is 2.5 mm which shows that the data were recorded from a very small area of the brain. Hence, the time lag between the channels is negligible and we can consider each 16 spikes recorded in different channels as a unique spike time window, and apply the proposed approach on these spike time windows. In fact, the proposed ap-

proach can be applied on any databases in which the time delay between the signals recorded in different channels is negligible, or in other words, on any database which has been acquired from a very small area of the brain. Hence, the proposed approach cannot be employed for investigating different brain regions to find the spatial origin of an absence seizure.

2.4 RESULTS

In this section, we present the results. The discussion and the interpretation of the results are brought with details in Section 2.5.

2.4.1 TRAINING PHASE: ESTIMATION OF PARAMETERS

We consider one of the absence seizures of the first rat which consists of $K = 390$ spikes as the training data $\mathcal{T}_{train} \in \mathbb{R}^{16 \times 1750 \times 390}$. In fact, each spike consists of the data of $E = 16$ channels for $T = 1750$ samples (87.5 ms). Since we do not have any information about the number of states (S) and factors (J), we apply the proposed method on \mathcal{T}_{train} with different S and J . Then, we select the best model order by considering the following:

- 1- According to (2.20), the relative reconstruction error must be small.
- 2- Assuming that the seizures follow the same structural model for all the rats, we enforce the values of J and S to be the same both for different seizures of the same rat, and for different rats.

Considering the above two points, the best results are obtained using two states ($S = 2$) and two factors in each state ($J = 2$) with $Er_{train} = 0.05$. The probability of transition between the states (transition probability matrix), the spatial topography, and the temporal representation of the factors are shown in Fig. 2.9. It should be noted that the first factors of both states are similar, and the first state is unstable because the probability of remaining in the first state ($p_{11} = 0.01$) is very low with respect to the probability of

transition to the second state ($p_{12} = 0.99$).

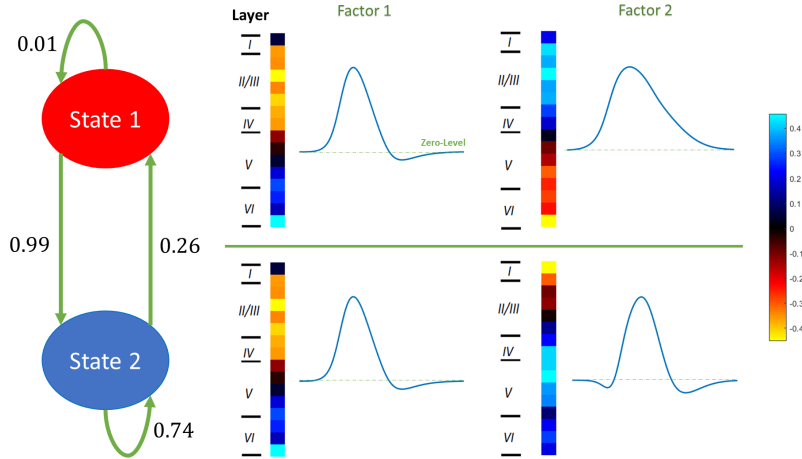


Figure 2.9: Estimated parameters of the considered model for the training absence seizure. The probability of transition between the states is shown in the left plot. The obtained factors associated with the first and second states are respectively shown in the first and second rows of the right plot.

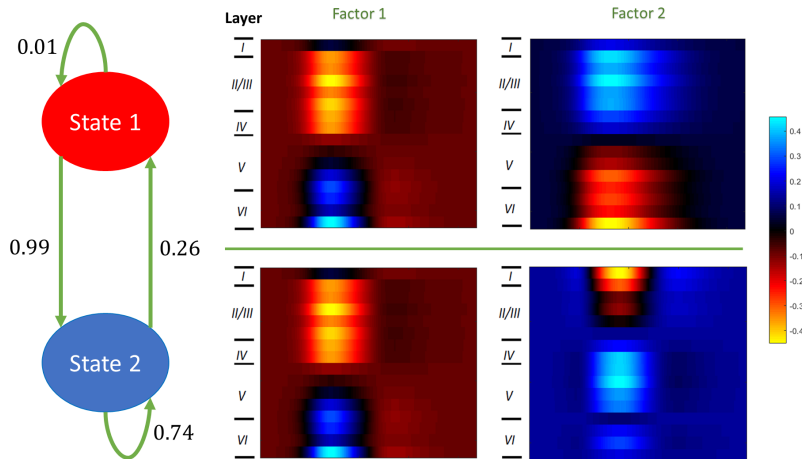


Figure 2.10: The CSD maps of the factors for the training absence seizure. The probability of transition between the states is shown in the left plot. The CSD maps of the obtained factors associated with the first and second states are respectively shown in the first and second rows of the right plot.

For each factor, we can also obtain a CSD map by vector multiplication of the spatial topography and the temporal representation. These maps are

shown in Fig. 2.10.

The sequence of states for the training absence seizure is shown in Fig. 2.11. It seems that there is no specific pattern in the activation of the states during the training absence seizure. Moreover, both states are unstable for some time intervals. However, on average, state 2 is more stable than state 1 during the training absence seizure.

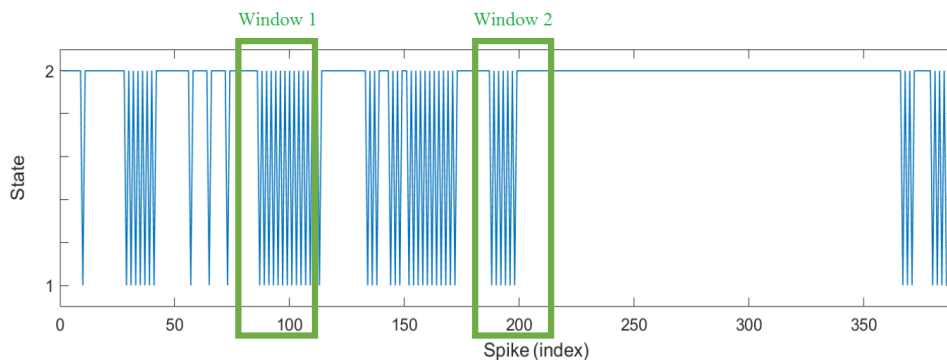
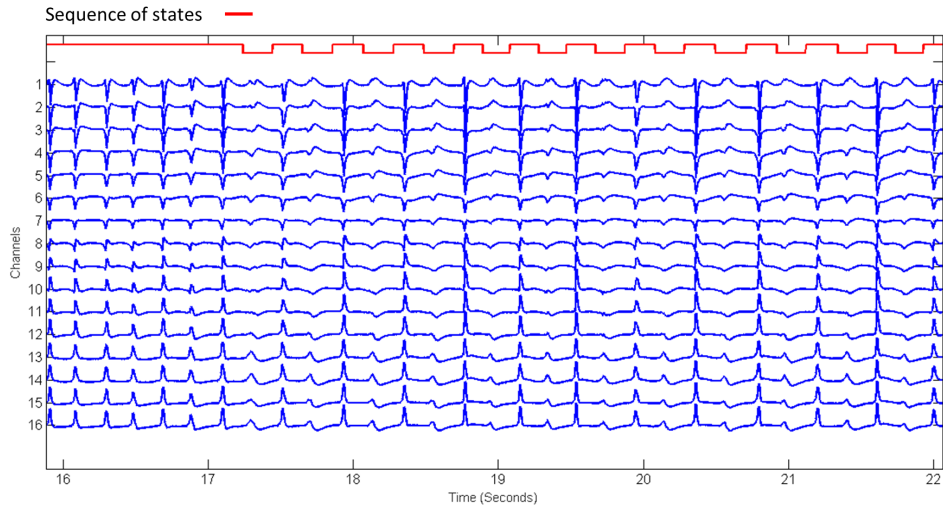


Figure 2.11: Sequence of states for the training absence seizure consisting of $K = 390$ spikes.

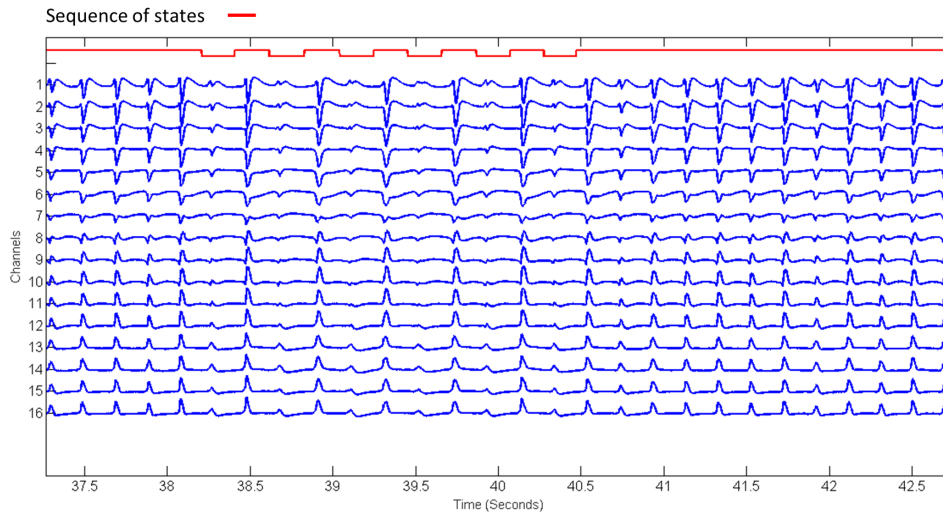
To investigate the behavior of spikes and their corresponding states during the training absence seizure, two windows have been specified in Fig. 2.11. The spikes and their states in these windows are shown in Fig. 2.12.

During the training absence seizure, $k_1 = 94$ and $k_2 = 296$ spikes ($K = k_1 + k_2 = 390$) respectively belong to the first and second states. The spikes in each state are generated by a linear combination of $J = 2$ fixed factors. The only difference among the spikes in a state, is the contribution of the factors $(\mathbf{c}_j^{(s)})$ in the generation of spikes. In fact, the factors $(\mathbf{a}_j^{(s)}, \mathbf{b}_j^{(s)})$ show the stationary part, and $\mathbf{c}_j^{(s)}$ represents the dynamic part of the model for absence seizures.

The contribution of the factors in the generation of spikes for the training absence seizure data is shown in part (a) of Fig. 2.13. To better show the dynamics of the spikes, we have removed the entries of $\mathbf{c}_j^{(s)}$ which are equal to zero. It should be noted that the factors of a single state are only activated for each spike (see Fig. 2.6). In fact, we respectively have $\mathbf{c}_j^{(1)} \in \mathbb{R}^{k_1}$ and



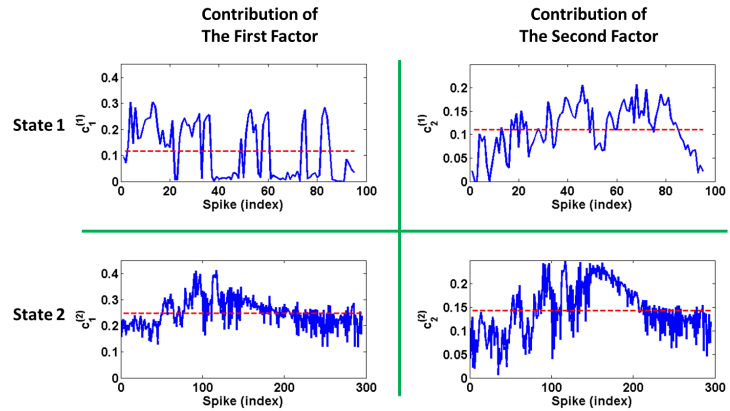
(a) Spikes and their states in window 1.



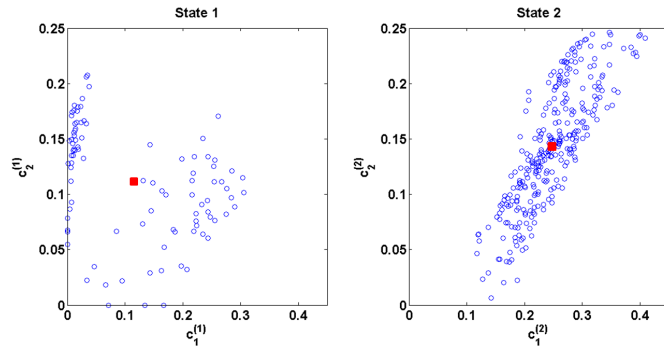
(b) Spikes and their states in window 2.

Figure 2.12: Spikes and their states during the windows specified in Fig. 2.11.

$\mathbf{c}_j^{(2)} \in \mathbb{R}^{k_2}$ for the first and second states in part (a) of Fig. 2.13. The joint distribution of the contribution of the factors in each state is also shown in part (b) of Fig. 2.13. The average of components of $\mathbf{c}_j^{(s)}$ ($\bar{c}_j^{(s)} \in \mathbb{R}$) is shown by red color in Fig. 2.13. These values are $\bar{c}_1^{(1)} = 0.11$, $\bar{c}_2^{(1)} = 0.11$, $\bar{c}_1^{(2)} = 0.24$ and $\bar{c}_2^{(2)} = 0.14$.



(a) Contribution of factors in the generation of spikes.



(b) Joint distribution of the contributions of the factors in each state.

Figure 2.13: (a) Contributions of factors and (b) their joint distribution in each state for the training absence seizure. The average of $\mathbf{c}_j^{(s)}$ is shown by red dashed line in (a) and the average of each joint distribution is shown by a red square in (b).

As shown in part (b) of Fig. 2.13, the contribution of the factors in the second state are dependent because their joint distribution almost has a linear form, while in the first state, there is no such dependency. It is also observed that for some of the spikes in the first state, the contribution of the second factor is much greater than the contribution of the first factor. With regards to part (a) of Fig. 2.13, it seems that this phenomenon occurs randomly, and there is no specific pattern in the appearance of this kind of spikes.

In order to show the behavior of current sources and sinks during the spikes in state 1 and state 2, we individually compute the average of the CSD representations of the spikes in each state as shown in Fig. 2.14. We respectively show these average CSD maps by $\mathbf{M}^{(1)} \in \mathbb{R}^{E \times T}$ and $\mathbf{M}^{(2)} \in \mathbb{R}^{E \times T}$ for the first and second states. Since the relative reconstruction error is very small for the training absence seizure ($Er_{train} = 0.05$), mathematically, these average CSD maps can be approximately expressed as follows:

$$\begin{aligned} \mathbf{M}^{(1)} &\simeq \bar{c}_1^{(1)} \mathbf{a}_1^{(1)} \mathbf{b}_1^{(1)T} + \bar{c}_2^{(1)} \mathbf{a}_2^{(1)} \mathbf{b}_2^{(1)T} \\ \mathbf{M}^{(2)} &\simeq \bar{c}_1^{(2)} \mathbf{a}_1^{(2)} \mathbf{b}_1^{(2)T} + \bar{c}_2^{(2)} \mathbf{a}_2^{(2)} \mathbf{b}_2^{(2)T} \end{aligned} \quad (2.22)$$

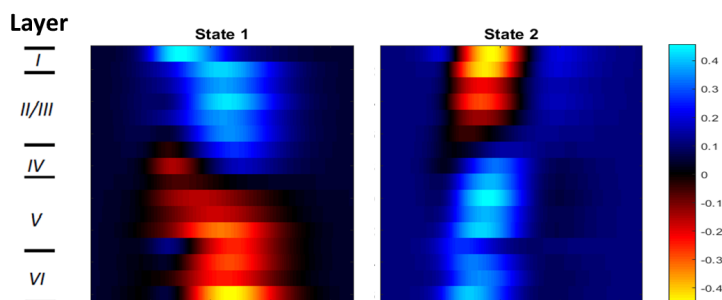


Figure 2.14: The average of the CSD representations of the spikes in each state.

2.4.1.1 Other Absence Seizures of The First Rat

The same results are obtained if we consider other absence seizures of the first rat in the training phase. This means that the spatial topography and the temporal representation of the factors, and the transition probability matrix are similar to Figs. 2.9 and 2.10. The obtained relative reconstruction error (Er_{train}) for four absence seizures of the first rat, which consist of $K_1 = 87$, $K_2 = 94$, $K_3 = 95$, and $K_4 = 88$ spikes are respectively equal to 0.04, 0.07, 0.07 and 0.09.

The sequence of states for the mentioned absence seizures is shown in Fig. 2.15. Similar to the training absence seizure, it seems that there is no specific pattern in the activation of the states during these absence seizures,

and for some time intervals, both states are unstable. However, on average, state 2 is more stable than state 1 during these absence seizures.

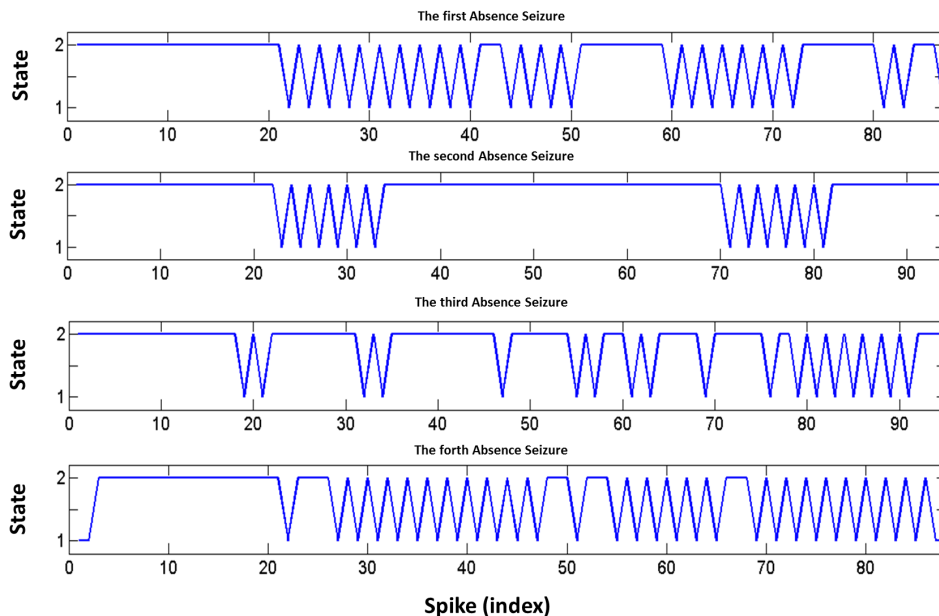
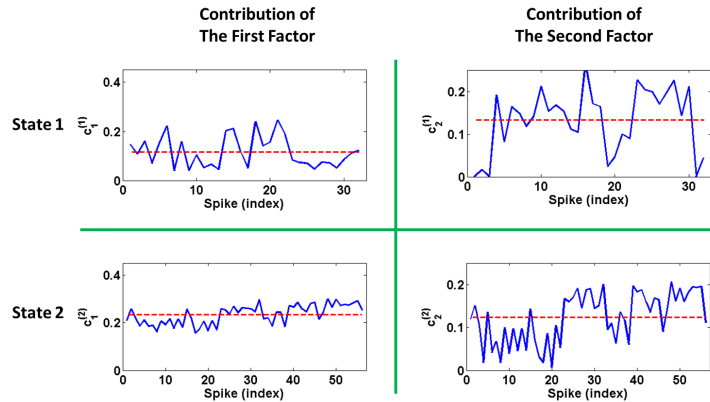


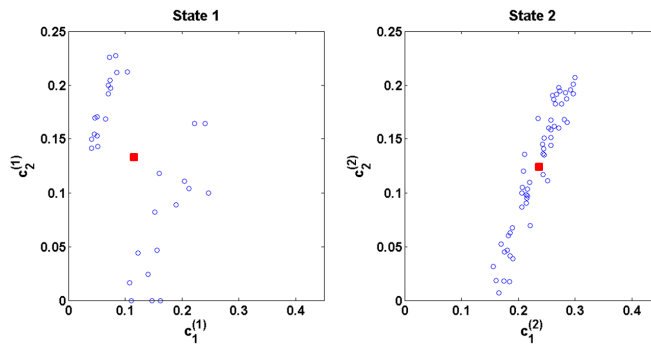
Figure 2.15: The sequence of states for four absence seizures of the first rat which consist of $K_1 = 87$, $K_2 = 94$, $K_3 = 95$ and $K_4 = 88$ spikes, respectively.

To see the dynamic part of the model for the new absence seizures, i.e., the contribution of the factors in the generation of spikes, $\mathbf{c}_j^{(s)}$ for the fourth absence seizure is shown in part (a) of Fig. 2.16. The joint distribution of the contribution of the factors in each state is also shown in part (b) of Fig. 2.16. $k_1 = 32$ and $k_2 = 56$ spikes ($K_4 = k_1 + k_2 = 88$) respectively belong to the first and second states during the considered absence seizure.

Since the number of spikes in the considered absence seizure and the training absence seizure in the previous section are different, comparison of $\mathbf{c}_j^{(s)}$ over time in these two absence seizures is not possible, but it can be seen that the joint distribution of the contribution of the factors is similar in these two absence seizures (compare Fig. 2.16 with Fig. 2.13). Hence, all of the mentioned remarks in the previous section regarding the contribution of the factors are again valid for the new absence seizure. Moreover, the average values of $\mathbf{c}_j^{(s)}$ ($\bar{c}_j^{(s)}$) are equal to $\bar{c}_1^{(1)} = 0.11$, $\bar{c}_2^{(1)} = 0.13$, $\bar{c}_1^{(2)} = 0.23$



(a) Contribution of factors in the generation of spikes.



(b) Joint distribution of the contributions of the factors in each state.

Figure 2.16: (a) The contributions of factors and (b) their joint distribution in each state for the fourth absence seizure of the first rat. The average of $\mathbf{c}_j^{(s)}$ is shown by red dashed line in (a), and the average of each joint distribution is shown by a red square in (b).

and $\bar{c}_2^{(2)} = 0.12$ for the considered absence seizure, which are very close to the obtained results for the training absence seizure in the previous section. Similar results are obtained if we consider other absence seizures of the first rat.

Since the average values of $\mathbf{c}_j^{(s)}$ and the factors $(\mathbf{a}_j^{(s)}, \mathbf{b}_j^{(s)})$ in the new absence seizures are similar to the results of the training absence seizure in the previous section, the average of the CSD representations of the spikes in each state is also similar to Fig. 2.14. This means that on average, the

current sources and sinks in each state have similar behavior in different absence seizures of the first rat.

2.4.1.2 Other Rats

The best results are again obtained by considering two states ($S = 2$) and two factors ($J = 2$) for the absence seizures of other rats. Also, the spatial topography of the factors and the transition probability matrix are similar to the first rat, one of the factors of the states is again similar, and one of the states is unstable. However, the temporal representation of the factors are different.

For instance, the obtained factors and transition probability matrix for one of the absence seizures of the second rat, which consists of $K = 146$ spikes, are shown in Fig. 2.17 (compare with Fig. 2.9). Also, the corresponding CSD maps of the factors are shown in Fig. 2.18. The reconstruction error for this absence seizure is $Er_{train} = 0.09$.

It can be seen that the first factors of both states are similar, and the first state is unstable because the probability of remaining in the first state ($p_{11} = 0.08$) is very low with respect to the probability of transition to the second state ($p_{12} = 0.92$).

The sequence of states for this absence seizure is shown in Fig. 2.19. During the absence seizure, $k_1 = 54$ and $k_2 = 92$ spikes ($K = k_1 + k_2 = 146$) respectively belong to the first and second states.

Similar to the sequence of states for the absence seizures of the first rat, it seems that there is no specific pattern in the states activation during this absence seizure, and for some time intervals, both states are unstable. However, on average, state 2 is more stable than state 1 during this absence seizure.

The contribution of the factors ($\mathbf{c}_j^{(s)}$) in the generation of spikes and their joint distribution in each state are shown in Fig. 2.20. With regards to part (b) of Fig. 2.20, it can be observed that the joint distributions of the factors are different from the obtained results in the absence seizures of the first rat

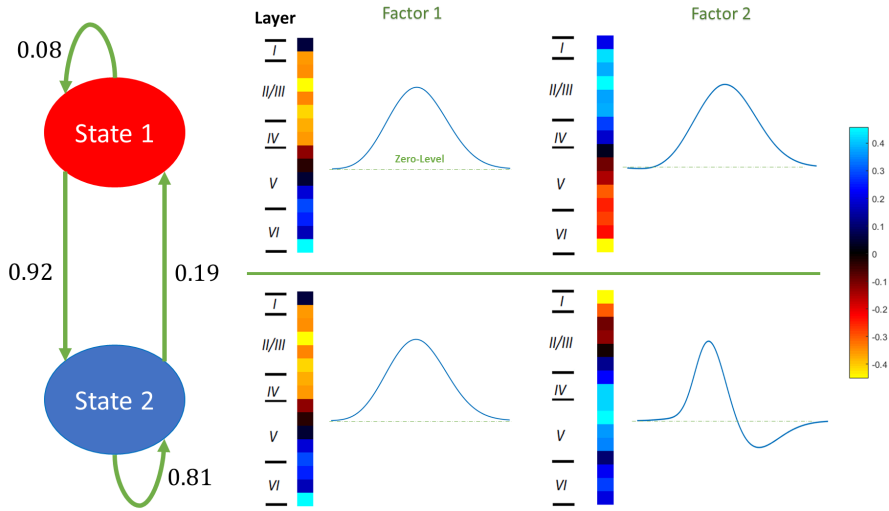


Figure 2.17: Estimated parameters of the proposed model for an absence seizure of the second rat. The probability of transition between the states is shown in the left plot. The obtained factors associated with the first and second states are respectively shown in the first and second rows of the right plot.

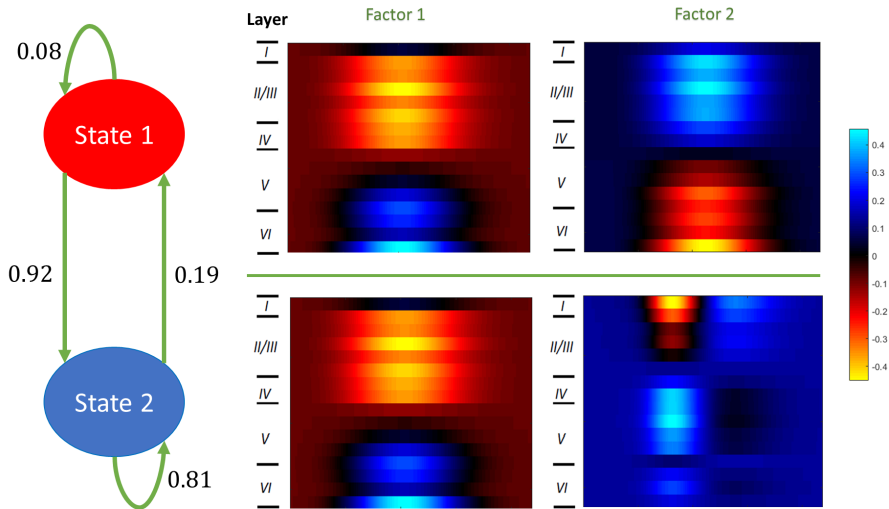


Figure 2.18: The CSD maps of the factors for an absence seizure of the second rat. The probability of transition between the states is shown in the left plot. The CSD maps of the obtained factors associated with the first and second states are respectively shown in the first and second rows of the right plot.

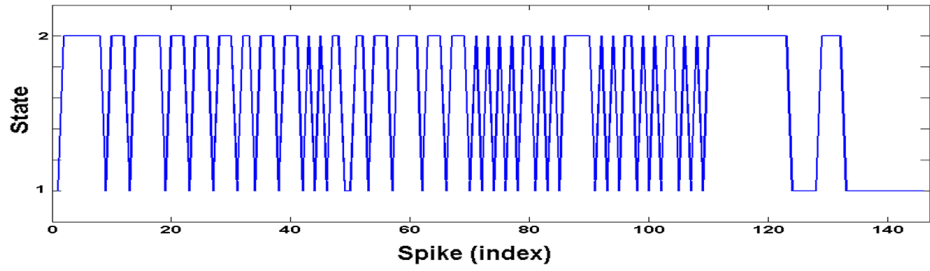
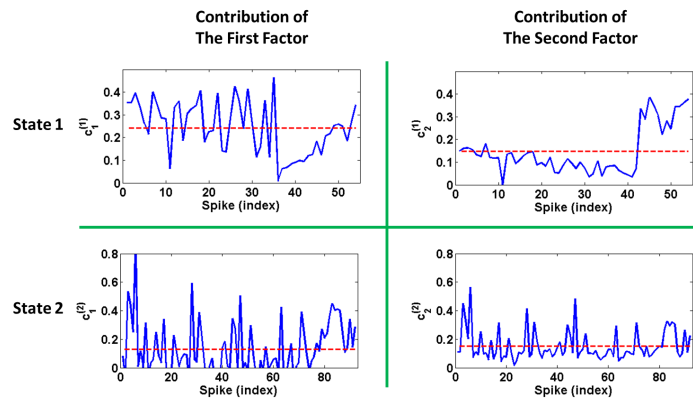
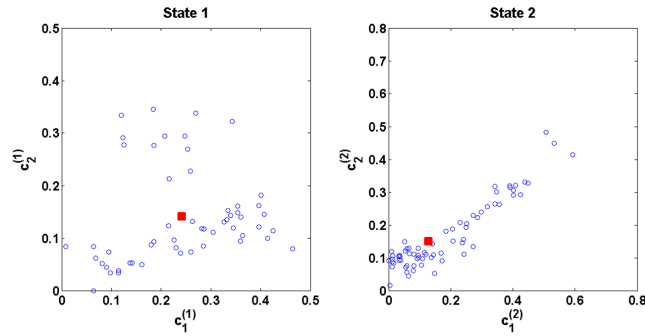


Figure 2.19: The sequence of states for an absence seizure of the second rat.



(a) Contribution of factors in the generation of spikes.



(b) Joint distribution of the contributions of the factors in each state.

Figure 2.20: (a) The contributions of factors and (b) their joint distribution in each state for an absence seizure of the second rat. The average of $\mathbf{c}_j^{(s)}$ is shown by red dashed line in (a) and the average of each joint distribution is shown by a red square in (b).

(compare Fig. 2.20 with Fig. 2.13 or Fig. 2.16). Moreover, the average values of $\mathbf{c}_j^{(s)}$ ($\bar{c}_j^{(s)}$) are equal to $\bar{c}_1^{(1)} = 0.24$, $\bar{c}_2^{(1)} = 0.14$, $\bar{c}_1^{(2)} = 0.12$ and $\bar{c}_2^{(2)} = 0.15$ for the absence seizure, which are not similar to the results of the first rat. Based on these results, it seems that there is no similarity in dynamics of the absence seizures in different rats.

The average of the CSD representations of the spikes in each state for the considered absence seizure is also shown in Fig. 2.21. Since the temporal representation of the factors and the values of $\bar{c}_j^{(s)}$ are different from the results of the first rat, the obtained CSD maps are also different.

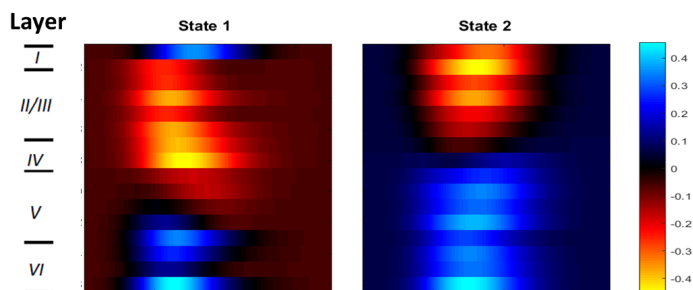


Figure 2.21: The average of the CSD representations of the spikes in each state for an absence seizure of the second rat.

2.4.2 TESTING PHASE: VALIDATION OF MODEL

For the absence seizures of the first rat used in 2.4.1 and 2.4.1.1, the relative reconstruction errors are reported in Table 2.1. The absence seizures consist of $K_1 = 87$, $K_2 = 94$, $K_3 = 95$, $K_4 = 88$, and $K_5 = 390$ spikes. The last one was used in 2.4.1, and the others were used in 2.4.1.1. In Table 2.1, $\mathcal{T}_{train}^{(m)}$ and $\mathcal{T}_{test}^{(m)}$ for $m \in \{1, 2, \dots, 5\}$ are associated with the tensor of spikes of the m^{th} absence seizure. The diagonal and non-diagonal entries of the table respectively show Er_{train} and Er_{test} .

These results show the accuracy and generality of the proposed model and the obtained results for the recorded absence seizures from the first rat. For other rats, the relative reconstruction errors have the same order of magnitudes as the first rat. For instance, the relative reconstruction errors

CHAPTER 2. SPATIO-TEMPORAL MODELING OF ABSENCE SEIZURES

Table 2.1: Relative reconstruction error for five absence seizures of the first rat, which consist of $K_1 = 87$, $K_2 = 94$, $K_3 = 95$, $K_4 = 88$, and $K_5 = 390$ spikes. The diagonal and non-diagonal entries of the table respectively show Er_{train} and Er_{test} .

Training on \ Testing on	$\mathcal{T}_{test}^{(1)}$	$\mathcal{T}_{test}^{(2)}$	$\mathcal{T}_{test}^{(3)}$	$\mathcal{T}_{test}^{(4)}$	$\mathcal{T}_{test}^{(5)}$
$\mathcal{T}_{train}^{(1)}$	0.04	0.13	0.14	0.13	0.09
$\mathcal{T}_{train}^{(2)}$	0.08	0.07	0.11	0.10	0.10
$\mathcal{T}_{train}^{(3)}$	0.10	0.12	0.07	0.11	0.10
$\mathcal{T}_{train}^{(4)}$	0.12	0.10	0.12	0.09	0.11
$\mathcal{T}_{train}^{(5)}$	0.11	0.11	0.12	0.13	0.05

Table 2.2: Relative reconstruction error for four absence seizures of the second rat which consist of $K_1 = 181$, $K_2 = 300$, $K_3 = 350$, $K_4 = 260$ and $K_5 = 146$ spikes. The diagonal and non-diagonal entries of the table respectively show Er_{train} and Er_{test} .

Training on \ Testing on	$\mathcal{T}_{test}^{(1)}$	$\mathcal{T}_{test}^{(2)}$	$\mathcal{T}_{test}^{(3)}$	$\mathcal{T}_{test}^{(4)}$	$\mathcal{T}_{test}^{(5)}$
$\mathcal{T}_{train}^{(1)}$	0.04	0.06	0.12	0.08	0.13
$\mathcal{T}_{train}^{(2)}$	0.07	0.04	0.09	0.10	0.11
$\mathcal{T}_{train}^{(3)}$	0.12	0.13	0.08	0.12	0.11
$\mathcal{T}_{train}^{(4)}$	0.09	0.09	0.10	0.07	0.14
$\mathcal{T}_{train}^{(5)}$	0.11	0.12	0.11	0.13	0.09

for five absence seizures of the second rat which consist of $K_1 = 181$, $K_2 = 300$, $K_3 = 350$, $K_4 = 260$ and $K_5 = 146$ spikes are reported in Table 2.2. The last one is the absence seizure discussed in 2.4.1.2.

Based on the results presented in Table 2.2 (and also Table 2.1), we find that the model estimated on any seizure of one rat can be used for modeling any other seizure of the same rat.

We can also cross validate the results obtained from two different rats. For instance, we consider the absence seizures of the first (in Table 2.1) and second (in Table 2.2) rat as the training and testing data, respectively. The relative reconstruction errors are reported in Table 2.3.

CHAPTER 2. SPATIO-TEMPORAL MODELING OF ABSENCE SEIZURES

Table 2.3: Relative reconstruction error by considering the absence seizures of the first and second rat as the training and testing data, respectively. The bad results are due to the high inter-rats variability, and consequently, it is not possible to use the parameters learned from one rat for the other rats.

Training on \ Testing on	$\mathcal{T}_{test}^{(1)}$	$\mathcal{T}_{test}^{(2)}$	$\mathcal{T}_{test}^{(3)}$	$\mathcal{T}_{test}^{(4)}$	$\mathcal{T}_{test}^{(5)}$
$\mathcal{T}_{train}^{(1)}$	0.38	0.37	0.28	0.33	0.41
$\mathcal{T}_{train}^{(2)}$	0.36	0.32	0.39	0.46	0.37
$\mathcal{T}_{train}^{(3)}$	0.27	0.32	0.36	0.34	0.41
$\mathcal{T}_{train}^{(4)}$	0.23	0.34	0.31	0.37	0.35
$\mathcal{T}_{train}^{(5)}$	0.36	0.37	0.34	0.44	0.38

Table 2.4: The cross correlation coefficient between the spatial topographies of the atoms obtained from the first and second rat.

First Rat	Second Rat			
	$\mathbf{a}_1^{(1)}$	$\mathbf{a}_2^{(1)}$	$\mathbf{a}_1^{(2)}$	$\mathbf{a}_2^{(2)}$
$\mathbf{a}_1^{(1)}$	0.97	-0.78	0.96	0.65
$\mathbf{a}_2^{(1)}$	-0.77	0.94	-0.78	-0.83
$\mathbf{a}_1^{(2)}$	0.96	-0.79	0.98	0.66
$\mathbf{a}_2^{(2)}$	0.64	-0.81	0.65	0.96

These results show that the inter-rat variability is important, therefore, we cannot use the data from one rat for training the model, and then testing on the other rats. In fact, since the temporal representation of the factors are not similar in different rats (compare Fig. 2.9 with Fig. 2.17), the results of cross validation among the absence seizures from different rats are inferior to the results of cross validation among the absence seizures of the same rat.

It is worth mentioning that based on the results presented in Fig. 2.9 with Fig. 2.17, the spatial topographies of the factors are similar in different rats. To show the correctness of this remark quantitatively, we calculate the cross correlation coefficient between the spatial topographies of the factors obtained from the two rats. The cross correlation coefficients between the

spatial topographies of the factors obtained from the first and second rat are reported in Table 2.4. As reported, the diagonal entries of Table 2.4 are close to one meaning that the spatial topographies of the atoms are similar in the rats, i.e. the localization of atomic epileptic activities are not rat-dependent.

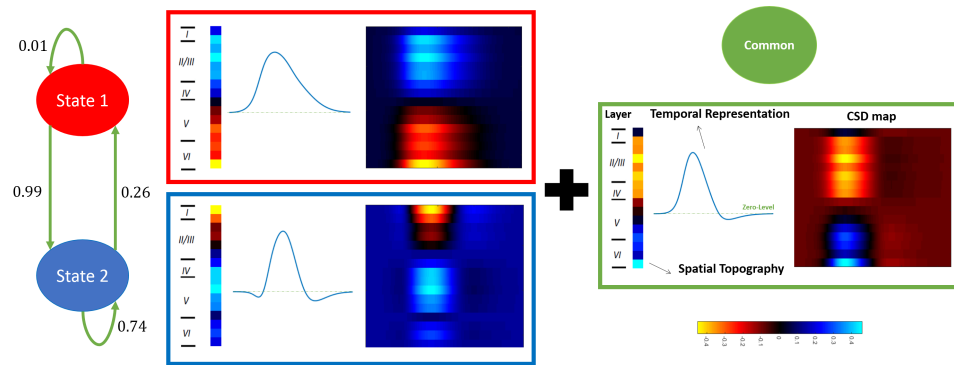
2.5 DISCUSSION

In this section, we present the spatial and temporal analysis of the absence seizures recorded from different layers of somatosensory cortex of GAERS based on the results obtained in the previous section.

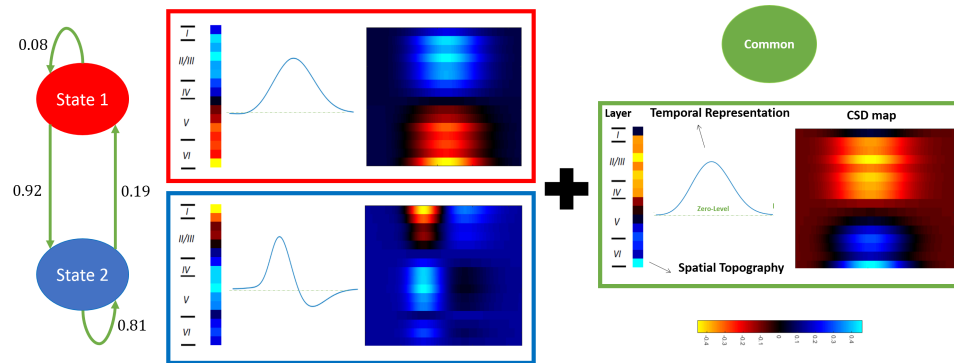
Obtained spatio-temporal model: As shown in Figs. 2.9 and 2.17, there are $S = 2$ hidden states under first-order Markovian model during the absence seizures. Each state consists of $J = 2$ epileptic activities (factors) which are linearly combined and construct the spikes of absence seizures.

Existence of a common epileptic activity (temporal analysis): An interesting point about the characterizations of the states is that the first factors of the states are similar. This means that there is a factor which always participate in the generation of spikes. We call this factor as a common epileptic activity (factor). Based on this observation, we can upgrade the proposed model for the absence seizures. We can say that during the absence seizures, there is a common epileptic activity, and there are $S = 2$ states under the first-order Markovian model with $J = 1$ factor (epileptic activity) in each one. The new model for the generation of spikes during the absence seizures of the first and second rats is shown in Fig. 2.22.

Unstable and dominant states (temporal analysis): Based on the obtained results for the transition probability matrix, on average, we can say that state 1 is an unstable state during the absence seizures because p_{11} , the probability to stay on state 1 when state 1 is active, is very small. Moreover, state 2 more occurs than state 1, or in other words, state 2 is the dominant state because p_{12} and p_{22} are respectively larger than p_{11} and p_{21} . These results can also be seen in the sequence of states for the absence seizures in



(a) Model for the first rat.



(b) Model for the second rat.

Figure 2.22: Final spatio-temporal model for the generation of spikes during absence seizures of the first and second rats.

Figs. 2.11, 2.15, and 2.19. It should be noted that for some time intervals, both states are unstable.

Similarity of spatial topographies in GAERS (spatial analysis):

As shown in Fig. 2.22 and reported in Table 2.4, although the temporal representations of the corresponding factors in the first and second rats are different, the corresponding spatial topographies are similar. Therefore, the organization of current sources and sinks in the corresponding factors (epileptic activities) are the same in different rats. Based on the estimated spatial topographies, we can say:

1- For the epileptic activity in the first state, the current sources and sinks are located in the vicinity of layers VI and II/III. In fact, the information

are sent and received among these layers for this epileptic activity. It should be noted that due to the polarization ambiguity, we cannot exactly specify which layer sends or receives information.

2- For the epileptic activity in the second state, the current sources and sinks are located in the vicinity of layers I and V.

3- For the common epileptic activity, the current sources and sinks are located in the vicinity of layers II/III and VI.

Contribution of epileptic activities in generation of spikes (temporal analysis): The characterization of the factors are fixed during the absence seizure, while their contribution in generation of spikes changes over time. In fact, the factors and their contribution show the stationary and dynamic part of the model, respectively. Here, we discuss about the dynamic part of the model.

As shown in Figs. 2.13 and 2.16, the distributions of the contribution of factors and their averages are similar in different absence seizures of the same rat. This means that we can consider a stationary random process with fixed distribution for contribution of each factor in generation of spikes. In fact, different absence seizures of a rat can be considered as different trials for these random processes.

To show the stationarity of these random processes for different absence seizures of a rat quantitatively, for instance, the average and variance of the contribution of each factor in the generation of spikes, based on the upgraded model (Fig. 2.22), for five absence seizures of the first rat are reported in Table 2.5. k_s , \bar{c}_s and $\sigma_{c_s}^2$ for $s = \{1, 2\}$ show the number of spikes corresponding to the s^{th} state, the average of the contribution of the factor corresponding to the s^{th} state in the generation of spikes and the corresponding variance, respectively. Moreover, k_c , \bar{c}_c and $\sigma_{c_c}^2$ are associated with the common factor.

As shown here, the averages and variances are similar in different absence seizures of the first rat verifying the assumption that the contributions of the factors in generating spikes can be considered as stationary random

CHAPTER 2. SPATIO-TEMPORAL MODELING OF ABSENCE SEIZURES

Table 2.5: The average and variance of the contribution of each factor in the generation of spikes for five absence seizures of the first rat. k_s , \bar{c}_s and $\sigma_{c_s}^2$ for $s = \{1, 2\}$ respectively show the number of spikes, the average and variance of the contribution of each factor corresponding to the s^{th} state. Also, k_c , \bar{c}_c and $\sigma_{c_c}^2$ are corresponded to the common factor.

Parameters	k_1	\bar{c}_1	$\sigma_{c_1}^2$	k_2	\bar{c}_2	$\sigma_{c_2}^2$	k_c	\bar{c}_c	$\sigma_{c_c}^2$
Seizure 1	24	0.13	33×10^{-4}	63	0.13	38×10^{-4}	87	0.21	55×10^{-4}
Seizure 2	12	0.14	29×10^{-4}	82	0.15	31×10^{-4}	94	0.22	49×10^{-4}
Seizure 3	18	0.12	36×10^{-4}	77	0.12	35×10^{-4}	95	0.20	61×10^{-4}
Seizure 4	32	0.13	41×10^{-4}	56	0.12	39×10^{-4}	88	0.19	57×10^{-4}
Seizure 5	94	0.11	32×10^{-4}	296	0.14	33×10^{-4}	390	0.21	84×10^{-4}

processes. The same results are obtained in the other rats. Since the corresponding random processes have the same averages in different absence seizures of a rat, and also the factors are similar, we can say that on average, the current sources and sinks have similar behavior in each state during the absence seizures of a rat. This average behaviors is respectively shown in Figs. 2.14 and 2.21 for the first and second rats.

2.6 CONCLUSION

In this chapter, we considered a spatio-temporal model for the generation of spikes which are the most important epileptic events during absence seizures. We assumed that there were some hidden states under the first-order Markovian model during the absence seizures, and each spike of the absence seizures, consisting of spikes of different layers of somatosensory cortex, was generated when one of the states was activated. Each state consisted of a few epileptic activities (factors) which were linearly combined, and generated the spikes. Each epileptic activity had two important features. The first one was the spatial topography which helped us recognize the distribution of current sources and sinks for the epileptic activity, and the

second one was the temporal representation which showed us the temporal activation function or waveform for the epileptic activity. We extracted the model parameters using a specific factor analysis method, and confirmed the generality of the proposed model and the obtained results using cross validation. The final results showed that there were a dominant and an unstable state (with an epileptic activity in each one), and a common epileptic activity during the recorded absence seizures (temporal analysis). It was shown that the organization of current sources and sinks in the obtained epileptic activities was the same in different GAERS, and they were located in the vicinity of top (layers I, II/III) and bottom (layers V, VI) of somatosensory cortex (spatial analysis). It was also shown that the contribution of epileptic activities in generating spikes were stationary random processes, with fixed distributions for the absence seizures of each GAERS (temporal analysis).

The most interesting result of this chapter is that there is a background or common epileptic activity during the recorded absence seizures. This result motivates us to propose a new model for analyzing the absence seizures as explained in Chapter 3.

On the other hand, the drawback of the proposed model in this chapter is that the model is based on investigation of spikes. The segmentation of an absence seizure to several spike time windows is not always possible because the data may contain some noise which makes the spike detection step very difficult. In Chapter 4, we propose a method for solving this issue.

3 STATIC AND DYNAMIC MODELING OF ABSENCE SEIZURES

Contents

3.1	Main Idea	47
3.2	Model Definition	49
3.3	Problem Formulation	51
3.4	Proposed Method	54
3.4.1	Extraction of The Static Structure and The Number of Dynamic Sources	54
3.4.2	Extraction of Dynamic Sources	57
3.4.3	Extraction of Static Sources and Dynamic Structure	58
3.5	Simulation and Experimental Results	59
3.5.1	Simulations	59
3.5.2	Depth Recordings	62
3.6	Conclusion	74

3.1 MAIN IDEA

In this chapter, another model is considered for the recorded absence seizures, and the main focus is on analyzing the dynamics of recorded absence seizures using source separation methods (temporal analysis). For this purpose, we describe the recorded absence seizures by a linear combination of few specific sources. Based on the results obtained in the previous chapter, we assume

that there are two kinds of sources during absence seizures, 1) static and 2) dynamic sources. Static sources play the role of common or background epileptic activities and dynamic sources are complementary to static sources in the generation of absence seizures. In other words, if we segment one absence seizure into non-overlapped time windows as shown in Fig. 3.1, the static sources participate in the generation of the data in all of the time windows, while the dynamic sources exist in some of the time windows. The static sources are stable and always on, while the dynamic sources are unstable and they may be off for several time windows. We propose a method to retrieve the static and dynamic sources and their structures from the recorded absence seizures. Then, we analyze the dynamics of recorded absence seizures using the obtained results.

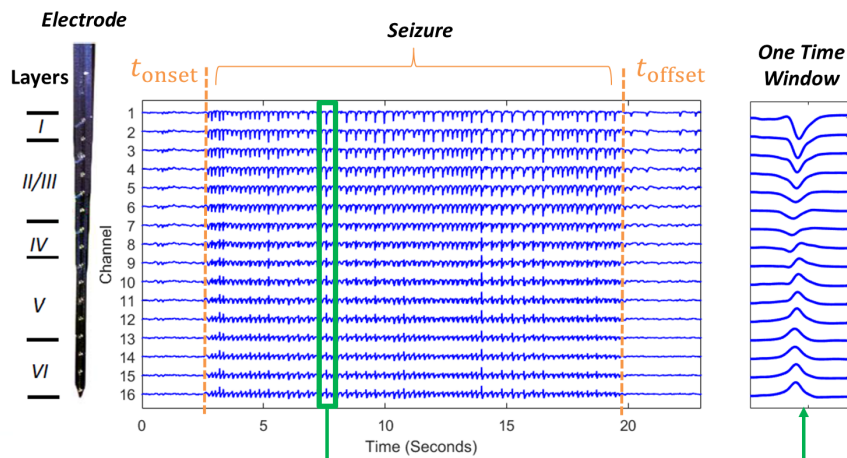


Figure 3.1: From left to right, the recording electrode, an absence seizure and a time window (length of 87.5 ms) which consists of $n = 16$ spikes from different channels. The absence seizure onset and the end of the absence seizure are indicated by t_{onset} and t_{offset} , respectively.

It should be noted that the considered model and the proposed method in this chapter can be adapted to several applications such as radar signals [Zhu et al. (2018); Dai et al. (2015)], brain images or signals like functional magnetic resonance imaging (fMRI) or electroencephalography (EEG) [Gonzalez-Navarro et al. (2017); Becker et al. (2012)], and target tracking in

videos [Hu et al. (2017); Du et al. (2017)]. For instance, in radar signals, the clutters like mountains and earth act as static sources, and the targets in the sky perform like the dynamic sources [Wang et al. (2018)]. As another example, in brain signals like EEG, the static sources can play the role of background brain activities such as neural activities corresponded to breathing, and the dynamic sources can act as temporary activities such as neural activities corresponded to blinking or eye movements [Boudet et al. (2007)].

The rest of this chapter is organized as follows. section 3.2 introduces the considered model for absence seizures. Problem formulation and considered assumptions are stated in section 3.3. The proposed method for estimating the model parameters is explained in section 3.4, while section 3.5 is dedicated to simulations and experimental results. Finally, the discussion and concluding remarks are reported in section 3.6.

3.2 MODEL DEFINITION

We assume that some physical activities or phenomena are taking place during the absence seizures and the sensors on the electrode record the instantaneous linear combination of the signals (extracellular field potentials) produced by the mentioned sources. The mixture of the signals is considered linear and instantaneous due to the quasi-static assumption of Maxwell's laws. We assume that there are two kinds of sources during the absence seizures, static and dynamic sources.

Static sources are located in fixed positions and have a static structure. They always contribute in generation of the signals, and their number is fixed and equal to m ($m < n$). Unlike static sources, dynamic sources are highly non-stationary. They sometimes appear and after a short time disappear. A few of them are activated in each time window and their number is unknown. In fact, there is much more variability in dynamic sources than static sources.

Schematic diagrams of the considered model for three time windows are shown in Fig. 3.2. All of the sources and their structures in different time

windows are unknown and we should retrieve them from the recorded absence seizures. In the following, we explain how the time windows are considered for an absence seizure.

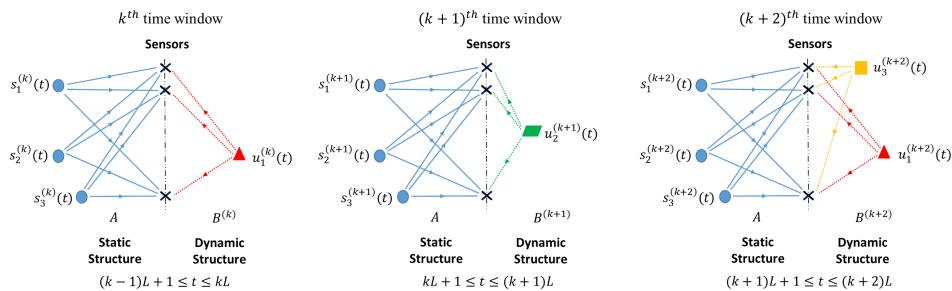


Figure 3.2: Static and dynamic sources for three consecutive time windows. The static sources (\mathbf{s}_1 , \mathbf{s}_2 , \mathbf{s}_3) and the dynamic sources (\mathbf{u}_1 , \mathbf{u}_2 , \mathbf{u}_3) are shown in the left and right sides of the sensors, respectively.

Time Windows of Absence Seizures: Appearance of spikes in absence epileptic seizures is the most important indication of this syndrome. In the recorded data, the spikes appear in different channels simultaneously during the absence seizures because the data have been acquired very locally. Hence, we consider each $n = 16$ spikes (at the same time) as one time window as shown in Fig. 3.1. For this purpose, we must at first separate the absence seizures from the data, and then, detect the spikes during the absence seizures. The same procedure as explained in the previous chapter is employed to perform these preprocessing steps. This means that since the amplitude of the signals changes significantly at the beginning and at the end of the absence seizures, we separate the absence seizures from the data by simple thresholding. Once the absence seizures were separated from the data, we detect the spikes for each absence seizure individually, following the proposed method in [Quiroga et al. (2004)] and construct the time windows (each of length 87.5 ms , $L = 1750$ samples). The length of the time windows is chosen according to the length of the spikes during absence seizures [Polack et al. (2007)]. We also align the time windows using improved version of Woody’s method proposed in [Cabasson and Meste (2008)] to achieve higher

correlation among the time windows, and get accurate results. Finally, the time windows are consecutively placed for each absence seizure separately. Thus, an absence seizure constituted by K spikes, is represented by the concatenation of its K elementary time windows. Hence, we remove the part of the recordings, which are not directly related to spikes. Now, we define our problem on the time windows of an absence seizure for estimating the model parameters.

3.3 PROBLEM FORMULATION

Assume that the considered absence seizure has K elementary time windows (each of length L). The data for the k^{th} time window at time instant t ($(k-1)L+1 \leq t \leq kL$) can be expressed as:

$$\mathbf{y}_t^{(k)} = \mathbf{A}\mathbf{s}_t^{(k)} + \mathbf{B}^{(k)}\mathbf{u}_t^{(k)} + \mathbf{n}_t^{(k)} \quad (3.1)$$

where $\mathbf{y}_t^{(k)} = [y_1^{(k)}(t), \dots, y_n^{(k)}(t)]^T \in \mathbb{R}^n$, $\mathbf{A} \in \mathbb{R}^{n \times m}$ and $\mathbf{s}_t^{(k)} = [s_1^{(k)}(t), \dots, s_m^{(k)}(t)]^T \in \mathbb{R}^m$ represent the recorded signals on the sensors, the static structure and the static sources, respectively. If we assume that the total number of activated dynamic sources in the time window k is equal to r_k , $\mathbf{B}^{(k)} \in \mathbb{R}^{n \times r_k}$ and $\mathbf{u}_t^{(k)} = [u_1^{(k)}(t), \dots, u_{r_k}^{(k)}(t)]^T \in \mathbb{R}^{r_k}$ show the dynamic structure and the dynamic sources, respectively. Finally, $\mathbf{n}_t^{(k)} = [n_1^{(k)}(t), \dots, n_n^{(k)}(t)]^T \in \mathbb{R}^n$ is an independent and identically distributed (i.i.d.) noise vector at different sensors, which is considered to be a zero-mean Gaussian noise with an unknown covariance matrix $\boldsymbol{\Sigma}_N \in \mathbb{R}^{n \times n}$.

For each time window k ($k = 1, 2, \dots, K$), if we concatenate the L vectors (samples) of the recorded signals, the static sources, the dynamic sources and the noise, we obtain the matrices $\mathbf{Y}^{(k)} \in \mathbb{R}^{n \times L}$, $\mathbf{S}^{(k)} \in \mathbb{R}^{m \times L}$, $\mathbf{U}^{(k)} \in \mathbb{R}^{r_k \times L}$ and $\mathbf{N}^{(k)} \in \mathbb{R}^{n \times L}$. Therefore, (3.1) can be written as:

$$\mathbf{Y}^{(k)} = \mathbf{A}\mathbf{S}^{(k)} + \mathbf{B}^{(k)}\mathbf{U}^{(k)} + \mathbf{N}^{(k)} \quad (3.2)$$

Hence, the set of unknown parameters (Θ) can be expressed as

$$\Theta = \left\{ \mathbf{A}, \bigcup_{k=1}^K \{ \mathbf{S}^{(k)}, r_k, \mathbf{B}^{(k)}, \mathbf{U}^{(k)} \} \right\} \quad (3.3)$$

We aim to extract Θ using recorded signals in all of the time windows, i.e., $\mathbf{Y}^{(k)}$ for $k = 1, 2, \dots, K$.

Known Characteristics of The System: The following assumptions are considered in the procedure of parameters extraction:

(A1) The number of static sources (m) is a constant for all the seizures, and it is determined by physiological reasons.

Neuroscientists have spatially and temporally explored the spike and wave discharges generating the seizures, and they have shown that these spike and wave discharges are similar in different seizures of a specific rat [Meeren et al. (2002); Polack et al. (2007)]. In other words, there is intra-rat similarity between the seizures. We use this suitable physiological information to obtain m . In fact, we expect to obtain results with intra-rat similarity. For this purpose, we extract the model parameters by considering different m . Then, the number of static sources which leads to the results with better intra-rat similarity is considered as the optimum number of static sources. It is worth mentioning that the similarity between results can be measured by the cross correlation coefficient.

(A2) The total number of static and dynamic sources ($m + r_k$) is less than the number of sensors (n) in each time window.

Consider (3.2) without presence of noise:

$$\mathbf{Y}^{(k)} = [\mathbf{A} \ \mathbf{B}^{(k)}] \begin{bmatrix} \mathbf{S}^{(k)} \\ \mathbf{U}^{(k)} \end{bmatrix} \quad (3.4)$$

If we assume $[\mathbf{A} \ \mathbf{B}^{(k)}] \in \mathbb{R}^{n \times (m+r_k)}$ is known, it is needed to compute the inverse of $[\mathbf{A} \ \mathbf{B}^{(k)}]$ for estimating the sources. Therefore, $m + r_k \leq n$ and $[\mathbf{A} \ \mathbf{B}^{(k)}]$ must be a full column rank matrix.

(A3) The columns of \mathbf{A} are unit norm.

To omit the scaling ambiguity problem in separation of the static sources, the columns of \mathbf{A} are considered unit norm vectors [Comon and Jutten (2010)].

(A4) Static sources and dynamic sources are considered uncorrelated in each time window.

When the sources are considered uncorrelated, it means that there is no linear relationship between them. In fact, we assume that all of the sources have their own specific origins. Mathematically, we can write:

$$\begin{aligned} \sum_{t=(k-1)L+1}^{kL} \mathbf{s}_t^{(k)} \mathbf{u}_t^{(k)T} &= \mathbf{0} \in \mathbb{R}^{m \times r_k} \\ \frac{1}{L} \sum_{t=(k-1)L+1}^{kL} \mathbf{s}_t^{(k)} \mathbf{s}_t^{(k)T} &= \mathbf{\Lambda}_s^{(k)} \in \mathbb{R}^{m \times m} \\ \frac{1}{L} \sum_{t=(k-1)L+1}^{kL} \mathbf{u}_t^{(k)} \mathbf{u}_t^{(k)T} &= \mathbf{\Lambda}_u^{(k)} = \mathbf{I} \in \mathbb{R}^{r_k \times r_k} \end{aligned} \quad (3.5)$$

where $\mathbf{\Lambda}_s^{(k)}$ is the auto-correlation matrix of the static sources in the k^{th} time window and unknown. It is a diagonal matrix with positive entries which are not necessarily constant during different time windows. Auto-correlation matrix of dynamic sources ($\mathbf{\Lambda}_u^{(k)}$) is considered equal to identity matrix (\mathbf{I}) in order to omit the scaling ambiguity problem in separation of dynamic sources [Comon and Jutten (2010)].

(A5) The dynamic sources are considered statistically independent in each time window.

There is no synchronization between the dynamic sources, and they may randomly activate in each time window. Hence, we assume that they are statistically independent. It should be noted that two random variables (X, Y) are independent when their joint probability distribution is the product of their marginal probability distributions, i.e.,

$$p_{X,Y}(x, y) = p_X(x) p_Y(y) \quad (3.6)$$

If X and Y are independent, then, they are also uncorrelated because

$$E_{X,Y}(xy) = E_X(x) E_Y(y) \quad (3.7)$$

However, the reverse of this remark is not correct. This means that if X and Y are uncorrelated, then they are not essentially independent. Hence, independency is a stronger condition than uncorrelatedness [Comon and Jutten (2010)].

(A6) The noise is uncorrelated with all of the sources in each time window.

Since the noise is zero-mean and independent of the sources, it is uncorrelated with all of the sources in each time window, i.e.,

$$\begin{aligned} \sum_{t=(k-1)L+1}^{kL} \mathbf{s}_t^{(k)} \mathbf{n}_t^{(k)T} &= \mathbf{0} \in \mathbb{R}^{m \times n} \\ \sum_{t=(k-1)L+1}^{kL} \mathbf{u}_t^{(k)} \mathbf{n}_t^{(k)T} &= \mathbf{0} \in \mathbb{R}^{r_k \times n} \end{aligned} \quad (3.8)$$

Now, the problem statement is complete and the goal is estimating the set of unknown parameters (Θ) from the time windows of a recorded absence seizure ($\mathbf{Y}^{(k)}$ for $k = 1, 2, \dots, K$) based on the known characteristics of the model.

3.4 PROPOSED METHOD

At first, we estimate the static structure (\mathbf{A}) and the number of dynamic sources in each time window (r_k). Then, the dynamic sources ($\mathbf{U}^{(k)}$) are obtained in each time window. Finally, we estimate the static sources ($\mathbf{S}^{(k)}$) and the dynamic structure ($\mathbf{B}^{(k)}$) in each time window.

3.4.1 EXTRACTION OF THE STATIC STRUCTURE AND THE NUMBER OF DYNAMIC SOURCES

We follow the proposed method in [Yeredor (2002)], regarding the joint diagonalization of a set of target matrices, to estimate the static structure and the number of dynamic sources in each time window. Since the sources are

uncorrelated according to (A4), we solve the following optimization problem:

$$\begin{aligned} \Theta_1^* &= \underset{\Theta_1}{\operatorname{argmin}} g(\Theta_1) \\ \Theta_1 &= \{\mathbf{A}, \bigcup_{k=1}^K \{\boldsymbol{\Lambda}_s^{(k)}, r_k, \mathbf{R}_B^{(k)}\}\} \\ g(\Theta_1) &= \sum_{k=1}^K \|\mathbf{R}_y^{(k)} - \mathbf{A}\boldsymbol{\Lambda}_s^{(k)}\mathbf{A}^T - \underbrace{\mathbf{B}^{(k)} \overbrace{\boldsymbol{\Lambda}_u^{(k)}}^{\mathbf{I}} \mathbf{B}^{(k)T}}_{\mathbf{R}_B^{(k)}}\|_F^2 \end{aligned} \quad (3.9)$$

where $\|\cdot\|_F$ denotes the Frobenius norm, and the auto-correlation matrix of recorded signals $(\mathbf{R}_y^{(k)} \in \mathbb{R}^{n \times n})$ in the k^{th} time window is calculated as follows:

$$\mathbf{R}_y^{(k)} = \frac{1}{L} \sum_{t=(k-1)L+1}^{kL} \mathbf{y}_t^{(k)} \mathbf{y}_t^{(k)T} \quad (3.10)$$

It should be mentioned that $\boldsymbol{\Lambda}_s^{(k)}$ is not an important parameter, but it must be estimated during the optimization. The other noticeable point is that the rank of $\mathbf{R}_B^{(k)}$ is equal to r_k , and since $r_k < n$, it is a low-rank matrix. We use this information to extract the number of dynamic sources (r_k) in each time window.

The following constraints must also be considered in the optimization:

- c₁) The columns of \mathbf{A} are unit norms.
- c₂) $\boldsymbol{\Lambda}_s^{(k)}$ is diagonal with positive entries.
- c₃) $\mathbf{R}_B^{(k)}$ is a low-rank and positive semidefinite matrix ($\mathbf{R}_B^{(k)} \succeq 0$).

We use alternating least square (ALS) method to solve the optimization problem. We consider some feasible initial values for Θ_1 , then, we alternately perform the following steps until the convergence of the parameters.

Step 1. Assuming $\boldsymbol{\Lambda}_s^{(k)}$ and $\mathbf{R}_B^{(k)}$ for $k = 1, 2, \dots, K$ are fixed, we have:

$$\begin{aligned} \mathbf{A}^* &= \underset{\mathbf{A}}{\operatorname{argmin}} \sum_{k=1}^K \|\mathbf{R}_y^{(k)} - \mathbf{A}\boldsymbol{\Lambda}_s^{(k)}\mathbf{A}^T - \mathbf{R}_B^{(k)}\|_F^2 \\ &s.t. \quad \operatorname{diag}(\mathbf{A}^T \mathbf{A}) = \mathbf{I} \end{aligned} \quad (3.11)$$

where $diag(\mathbf{X})$ keeps the diagonal entries of \mathbf{X} , and makes the other entries equal to zero. This constrained optimization problem can easily be solved using gradient-projection (GP) method [Kelley (1999)] (see Appendix C.1).

Step 2. Assuming \mathbf{A} and $\mathbf{R}_B^{(k)}$ are fixed, we have:

$$\begin{aligned} \Lambda_s^{(k)*} &= \underset{\Lambda_s^{(k)}}{\operatorname{argmin}} \|\mathbf{R}_y^{(k)} - \mathbf{A}\Lambda_s^{(k)}\mathbf{A}^T - \mathbf{R}_B^{(k)}\|_F^2 \\ \text{s.t. } \Lambda_s^{(k)} &= \operatorname{diag}(\Lambda_s^{(k)}), \Lambda_s^{(k)} \succeq 0 \end{aligned} \quad (3.12)$$

This optimization problem is solved using non-negative least square (NNLS) method if we consider the vectorization form of all matrices in the optimization (see Appendix C.2). This step must be performed for all of the time windows ($k = 1, 2, \dots, K$) separately.

Step 3. Assuming \mathbf{A} and $\Lambda_s^{(k)}$ are fixed, we have:

$$\begin{aligned} \mathbf{R}_B^{(k)*} &= \underset{\mathbf{R}_B^{(k)}}{\operatorname{argmin}} \|\mathbf{R}_y^{(k)} - \mathbf{A}\Lambda_s^{(k)}\mathbf{A}^T - \mathbf{R}_B^{(k)}\|_F \\ \text{s.t. } \mathbf{R}_B^{(k)} &\succeq 0, \mathbf{R}_B^{(k)} \text{ is low-rank.} \end{aligned} \quad (3.13)$$

This step must also be performed for all of the time windows ($k = 1, 2, \dots, K$) separately. We will explain later why we remove the power two in the objective function. Since we must impose $\mathbf{R}_B^{(k)}$ to be a low-rank matrix, we use a penalty parameter ($\lambda^{(k)}$) to minimize both the objective function and the rank of $\mathbf{R}_B^{(k)}$. Hence, we have:

$$\begin{aligned} \mathbf{R}_B^{(k)*} &= \underset{\mathbf{R}_B^{(k)}}{\operatorname{argmin}} \|\mathbf{R}_y^{(k)} - \mathbf{A}\Lambda_s^{(k)}\mathbf{A}^T - \mathbf{R}_B^{(k)}\|_F + \lambda^{(k)} \operatorname{rank}(\mathbf{R}_B^{(k)}) \\ \text{s.t. } \mathbf{R}_B^{(k)} &\succeq 0 \end{aligned} \quad (3.14)$$

where $\lambda^{(k)}$ is a penalty parameter which helps to minimize the rank of $\mathbf{R}_B^{(k)}$. Since minimization of rank function is an NP-hard problem [Recht et al. (2010)], we approximate $\operatorname{rank}(\mathbf{R}_B^{(k)})$ with $\operatorname{Tr}\{\mathbf{R}_B^{(k)}\}$ which is a well-known convex relaxation for this function [Candes and Plan (2010); Malek-Mohammadi et al. (2015)]. The obtained optimization problem is very similar to the square root LASSO problem [Belloni et al. (2011); Koochakzadeh

et al. (2015)], and it can be converted to a semidefinite programming (SDP) as shown in Appendix C.3. The main advantage of the square-root LASSO is that the penalty parameter can be obtained independently from variance of the noise. In fact, we dropped the power of two in the objective function considered in (3.13) to solve the problem similar to the square-root LASSO problem. The final optimization problem can be solved using well known solvers like `sdpt3` and `cvx` [Toh et al. (1999)].

By performing a few iterations between these three steps, the static structure (\mathbf{A}^*), the auto-correlation matrix of static sources ($\mathbf{\Lambda}_s^{(k)*}$) and $\mathbf{R}_B^{(k)*}$ for $k = 1, 2, \dots, K$ are estimated. Finally, the number of dynamic sources in each time window is obtained as follows:

$$r_k^* = \text{rank}(\mathbf{R}_B^{(k)*}) \quad (3.15)$$

3.4.2 EXTRACTION OF DYNAMIC SOURCES

Consider the singular value decomposition (SVD) of the static structure as follows:

$$\begin{aligned} \mathbf{A} &= \mathbf{V} \mathbf{\Sigma} \mathbf{Q}^T \\ \mathbf{V} &= [\underbrace{\mathbf{v}_1 \dots \mathbf{v}_m}_{\mathbf{V}_1} \underbrace{\mathbf{v}_{m+1} \dots \mathbf{v}_n}_{\mathbf{V}_2}] \end{aligned} \quad (3.16)$$

where $\mathbf{V}_1 \in \mathbb{R}^{n \times m}$ is an orthonormal basis for columns of \mathbf{A} and $\mathbf{V}_2 \in \mathbb{R}^{n \times (n-m)}$ spans the null space of \mathbf{A} because we know that $\text{rank}(\mathbf{A}) = m$. Hence, if we left multiply both sides of (3.2) by \mathbf{V}_2^T , we can omit the contribution of the static sources in each time window:

$$\underbrace{\mathbf{V}_2^T \mathbf{Y}^{(k)}}_{\mathbf{Y}'^{(k)}} = \underbrace{\mathbf{V}_2^T \mathbf{A} \mathbf{S}^{(k)}}_0 + \underbrace{\mathbf{V}_2^T \mathbf{B}^{(k)}}_{\mathbf{B}'^{(k)}} \mathbf{U}^{(k)} + \underbrace{\mathbf{V}_2^T \mathbf{N}^{(k)}}_{\mathbf{N}'^{(k)}} \quad (3.17)$$

where $\mathbf{Y}'^{(k)} \in \mathbb{R}^{(n-m) \times L}$, $\mathbf{B}'^{(k)} \in \mathbb{R}^{(n-m) \times r_k}$ and $\mathbf{N}'^{(k)} \in \mathbb{R}^{(n-m) \times L}$ are respectively the new data, the new dynamic structure and the new noise in the k^{th} time window. The distribution of each column of the new noise is $\mathcal{N}(\mathbf{0}, \mathbf{V}_2^T \mathbf{\Sigma}_N \mathbf{V}_2)$. The important point here is that we must be sure that

$\mathbf{B}'^{(k)}$ is not equal to zero because the dynamic sources must be kept. According to (A2), since we assumed that $[\mathbf{A} \ \mathbf{B}^{(k)}] \in \mathbb{R}^{n \times (m+r_k)}$ is a full rank matrix, each column of $\mathbf{B}^{(k)}$ certainly exists in the space of \mathbf{V}_2 , and hence, $\mathbf{B}'^{(k)}$ would not be equal to zero. Now, we can extract the dynamic sources in each time window.

According to (A5), since we assumed that the dynamic sources are statistically independent, we are faced with an overdetermined BSS problem in the presence of noise. Hence, independent component analysis (ICA) can be applied to extract the dynamic sources ($\mathbf{U}^{(k)}$) from nosiy measurements [Arora et al. (2015)]. We use JADE algorithm to extract the dynamic sources [Cardoso and Souloumiac (1993)]. Since we have estimated the number of dynamic sources (r_k) in the previous part, the dimension of the separating matrix $\mathbf{W}^{(k)} \in \mathbb{R}^{r_k \times (n-m)}$ is known, and regarding (3.17), we get:

$$\mathbf{W}^{(k)} \mathbf{Y}'^{(k)} = \mathbf{W}^{(k)} \mathbf{B}'^{(k)} \mathbf{U}^{(k)} + \mathbf{W}^{(k)} \mathbf{N}'^{(k)} \quad (3.18)$$

In fact, ICA tries to make the rows of $\mathbf{W}^{(k)} \mathbf{Y}'^{(k)}$ as much independent as possible. After applying ICA, the dynamic sources ($\mathbf{U}^{(k)*}$) are determined.

For each time window, the explained procedure must be applied to retrieve the dynamic sources in all of the time windows.

3.4.3 EXTRACTION OF STATIC SOURCES AND DYNAMIC STRUCTURE

When the static structure (\mathbf{A}) and the dynamic sources ($\mathbf{U}^{(k)}$) are determined, we can extract the static sources ($\mathbf{S}^{(k)}$) and the dynamic structure ($\mathbf{B}^{(k)}$) in each time window using the maximum log-likelihood estimator (MLE). It can be shown that minimizing the following objective function leads to finding the MLE solution of the parameters:

$$q(\mathbf{S}^{(k)}, \mathbf{B}^{(k)}) = \|(\mathbf{Y}^{(k)} - \mathbf{A}\mathbf{S}^{(k)} - \mathbf{B}^{(k)}\mathbf{U}^{(k)})\|_F^2 \quad (3.19)$$

This objective function can simply be minimized using alternation minimization. For each time window, (3.19) must be minimized to retrieve the static

sources ($\mathbf{S}^{(k)*}$) and the dynamic structures ($\mathbf{B}^{(k)*}$) in all of the time windows.

By determination of the static sources and the dynamic structure in all of the time windows, all parameters of the model are determined.

3.5 SIMULATION AND EXPERIMENTAL RESULTS

In this section, we first show the efficiency of the proposed method using simulated data. Then, the results obtained from depth recordings are presented.

3.5.1 SIMULATIONS

3.5.1.1 Data Generation

We generate the data according to (3.1) for each time window. We consider $K = 50$ time windows (each of length $L = 100$), $n = 10$ sensors, $m = 5$ static sources, and at most $n - m = 5$ dynamic sources in each time window. The number of dynamic sources (r_k) are chosen randomly between 1 and 5 in each time window. Then, we generate the static structure \mathbf{A} by a random matrix of size 10×5 with zero-mean and unit-variance i.i.d. Gaussian entries, followed by normalizing the columns. In each time window, the static sources are considered sine signals with different frequencies as follows:

$$\begin{aligned} s_i^{(k)}(t) &= \alpha_{ik} \sin(2\pi(2^{i-1} f_0) t) \\ i &= 1, 2, \dots, 5 \\ k &= 1, 2, \dots, 50 \\ (k-1)100 + 1 &\leq t \leq k 100 \end{aligned} \tag{3.20}$$

where $f_0 = \frac{1}{L} = 0.01$. The amplitude of each static source in each time window (α_{ik}) is uniformly distributed between 0 and 1. The static sources are not stationary because their amplitudes change in different time windows, and according to (A4), they are uncorrelated with each other because they have different frequencies in each time window. The entries of the dynamic

structure in each time window $\mathbf{B}^{(k)} \in \mathbb{R}^{10 \times r_k}$ are independently chosen from zero-mean and unit-variance Gaussian distribution. The dynamic sources in each time window are again considered sine signals as follows:

$$\begin{aligned} u_i^{(k)}(t) &= \sqrt{2L} \sin(2\pi(2^{i+4} f_0) t) \\ i &= 1, \dots, r_k \\ k &= 1, 2, \dots, 50 \\ (k-1)100 + 1 &\leq t \leq k100 \end{aligned} \quad (3.21)$$

where $\sqrt{2L}$ is equal to $\sqrt{200}$ in order to have unit norm dynamic sources. According to (A4) and (A5), the frequencies are selected such that the dynamic sources are mutually independent and uncorrelated with the static sources. Finally, each column of the noise $\mathbf{N}^{(k)}$ is generated from Gaussian distribution with zero-mean and covariance matrix $\sigma_0^2 \mathbf{I} \in \mathbb{R}^{10 \times 10}$ for all of the time windows. We also use the following criteria to evaluate the performance of the proposed method in estimation of the parameters:

$$\begin{aligned} Er_S &= \mathop{\text{mean}}_k \frac{\|S^{(k)} - S^{(k)*}\|_F^2}{\|S^{(k)}\|_F^2}, \quad Er_U = \mathop{\text{mean}}_{k: r_k=r_k^*} \frac{\|U^{(k)} - U^{(k)*}\|_F^2}{\|U^{(k)}\|_F^2} \\ Er_A &= \frac{\|A - A^*\|_F^2}{\|A\|_F^2}, \quad Er_r = \mathop{\text{mean}}_k \frac{|r_k - r_k^*|}{r_k}, \quad Er_B = \mathop{\text{mean}}_{k: r_k=r_k^*} \frac{\|B^{(k)} - B^{(k)*}\|_F^2}{\|B^{(k)}\|_F^2} \end{aligned} \quad (3.22)$$

It should be noted that Er_r is not squared. We also consider the signal to noise (SNR) ratio as follows for the simulations:

$$\text{SNR} = 10 \log\left(\frac{1}{K} \sum_{k=1}^K \frac{\|Y^{(k)} - N^{(k)}\|_F^2}{\|N^{(k)}\|_F^2}\right) \quad (3.23)$$

3.5.1.2 Results

It is worth noting that we assume that the number of static sources ($m = 5$) is known during the simulations.

First Simulation: In this simulation, we consider σ_0^2 such that $\text{SNR} = 20 \text{ dB}$. The values of the criteria introduced in (3.22) are reported in the fifth

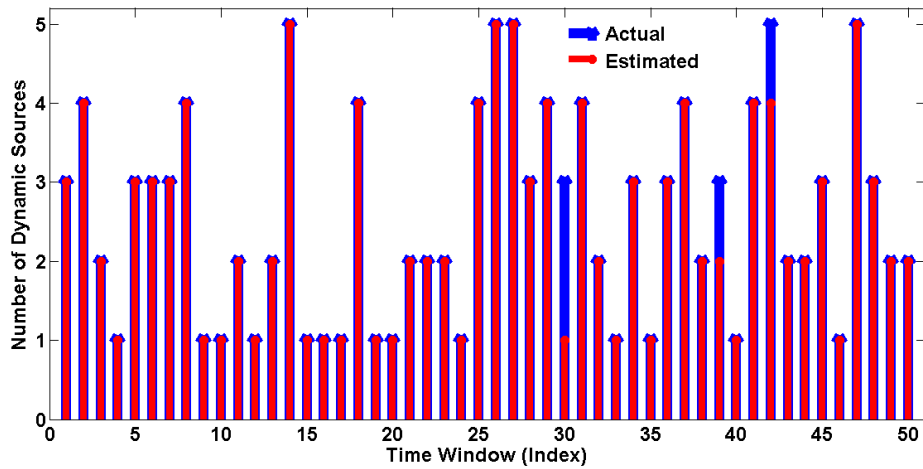


Figure 3.3: The actual and estimated number of dynamic sources in different time windows (SNR = 20 dB).

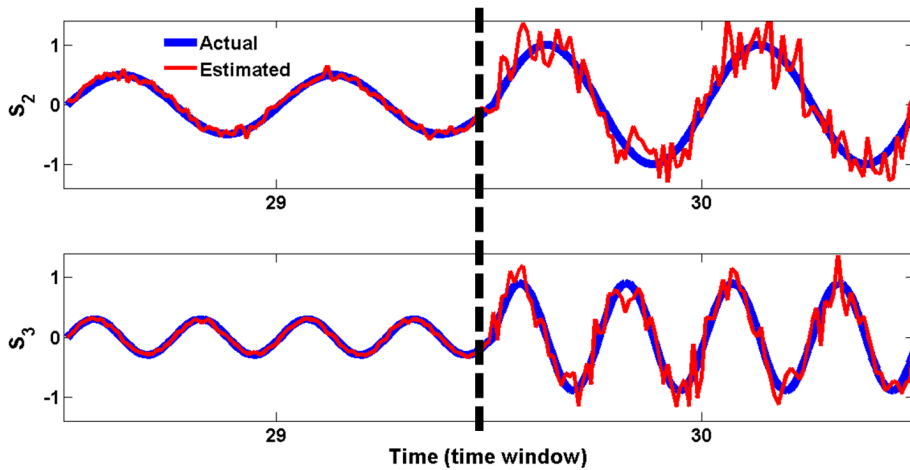


Figure 3.4: The actual and estimated static sources in the marked region of Fig. 3.3. The vertical dashed line shows the boundary of the time windows.

row of Table 3.1. Moreover, the actual and estimated number of dynamic sources in each time window are shown in Fig. 3.3.

As shown in Fig 3.3, the estimated number of dynamic sources is often equal to the actual number. To see the behavior of the actual and estimated sources, the second and third static sources and their estimations during the 29th and 30th time window are zoomed in Fig. 3.4.

The normalized squared error ($\|S^{(k)} - S^{(k)*}\|_F^2 / \|S^{(k)}\|_F^2$) for the static sources in these time windows are 0.026 and 0.157, respectively. The quality of the estimation is not good during the 30th time window because the number of dynamic sources was not estimated correctly in this time window (see Fig. 3.3).

Second Simulation: In this simulation, we repeat the first simulation for different SNR. The values of the criteria introduced in (3.22) are reported in Table 3.1.

Table 3.1: Performance of the proposed method in different SNR.

SNR (dB)	Er_A	Er_S	Er_U	Er_B	Er_r
5	0.155	0.216	0.196	0.131	0.148
10	0.041	0.124	0.102	0.111	0.091
15	0.003	0.083	0.073	0.086	0.045
20	0.001	0.031	0.027	0.041	0.024
25	≤ 0.001	0.008	≤ 0.001	≤ 0.001	0.004

In a specific time window in which the number of dynamic sources was obtained correctly in different SNR, the estimated signals for the first static source are shown in Fig. 3.5.

These results confirm the efficiency of the proposed method in retrieving the model parameters.

3.5.2 DEPTH RECORDINGS

We recall that the data set was acquired from four absence epileptic rats using an electrode with $n = 16$ sensors. The recorded data from each rat consisted of few absence seizures, and each absence seizure was a train of spike time windows. We apply the proposed method on time windows of an absence seizure to extract the static and dynamic sources and their structures.

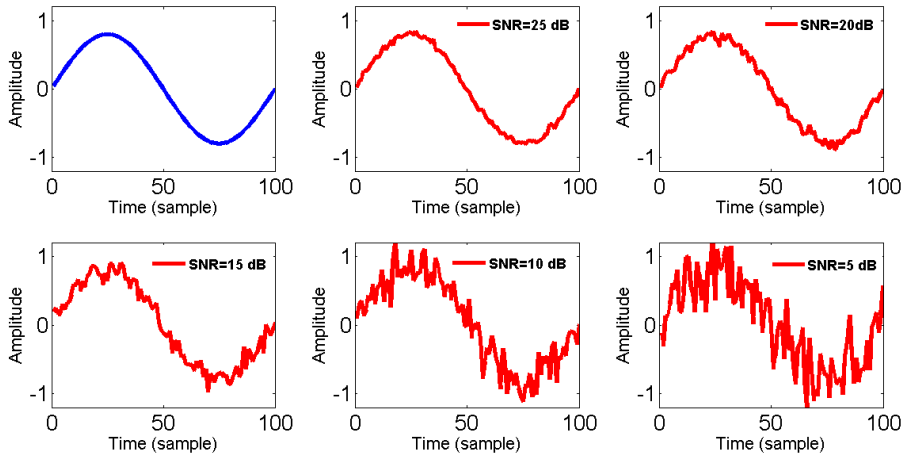


Figure 3.5: The actual and estimated signals for the first static source in a specific time window in different SNR. The top left figure shows the actual static source.

3.5.2.1 Parameter Extraction (Training Phase)

Since there is no prior information about the number of static sources (m), we apply the proposed method on the seizures for different m and select the one which has suitable biophysiological interpretation. As explained in (A1), the suitable model order must lead to results with intra-rat similarity. In other words, the results should be similar in different seizures of a GAERS rat. Considering this point, the best result is obtained by considering $m = 1$ for all of the absence seizures. In fact, when we consider $m > 1$, some of the sources become non-smooth and incomprehensible. Since a single static source is sufficient ($m = 1$), the static structure $\mathbf{A} \in \mathbb{R}^{n \times m}$ reduces to a simple vector with $n = 16$ entries. We consider one of the absence seizures of the first rat which consists of $K = 390$ time windows as the training absence seizure to show the results.

The obtained static structure (A) and static sources ($s_1^{(k)}(t)$) in different time windows for the training absence seizure are shown in Fig. 3.6 (for better representation, we normalized the static sources). It can be observed that the static sources in different time windows are similar, hence, we can consider them as one cluster. The average of this cluster is shown in red.

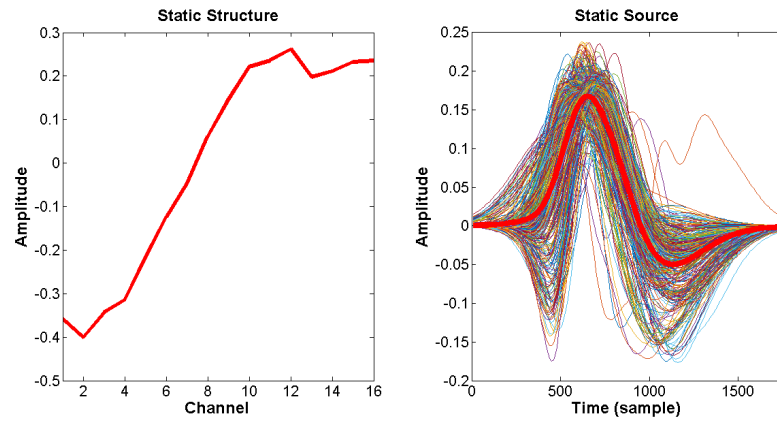


Figure 3.6: The estimated static structure (left) and the estimated static source in different time windows (right) for the training absence seizure. To better show the static sources, they are normalized. The average of the static sources is shown in red.

The estimated number of dynamic sources is also equal to one ($r_k = 1$) in all of the time windows of the training absence seizure. The extracted dynamic structure ($\mathbf{B}^{(k)}$) and source ($u_1^{(k)}(t)$) in different time windows of the training absence seizure are shown in Fig. 3.7 (for better representation, the dynamic structures are normalized).

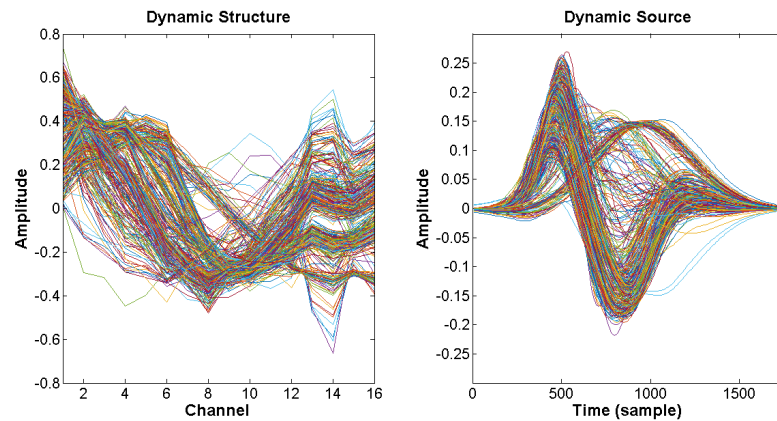


Figure 3.7: The estimated dynamic structure (left) and the estimated dynamic source in different time windows (right) for the training absence seizure. To better show the dynamic structures, they are normalized.

By observing the estimated dynamic sources, it can be understood that there are a few kinds of dynamic sources in the training absence seizure. Therefore, we partition the estimated dynamic sources using *k-means* clustering. The obtained results are shown in the right side of Fig. 3.8. As shown in Fig. 3.8, there are three clusters in the dynamic sources. After determination of the clusters, we also separate their corresponding dynamic structures, which are shown in the left side of Fig. 3.8. The red curves show the average of the clusters.

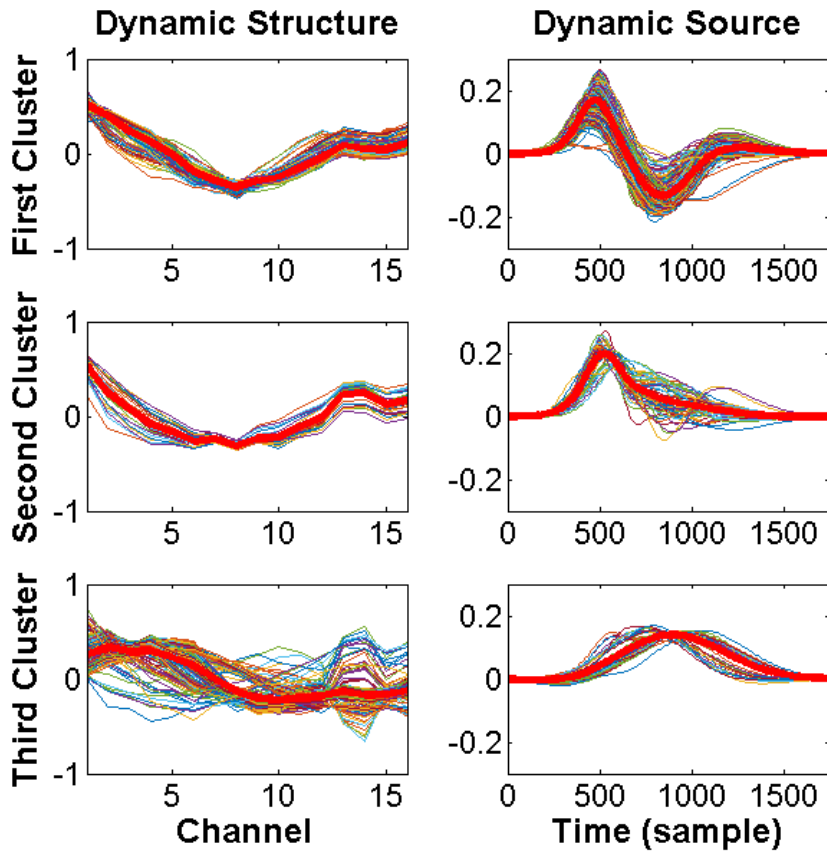


Figure 3.8: There are three clusters in the dynamic sources. The average of each cluster is shown in red.

Based on the obtained results, we can conclude that there is one static source (background activity), and there are three kinds of dynamic sources during the training absence seizure. A linear superposition of the background

activity and a dynamic source generates the data in each time window of the training absence seizure. This conclusion is illustrated in Fig. 3.9.

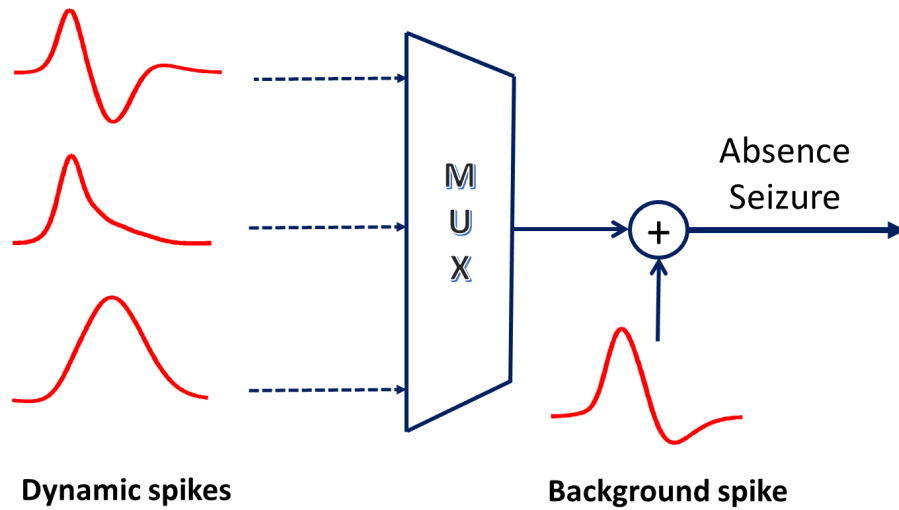


Figure 3.9: One kind of the dynamic spikes (sources) is added to the background spike (static source) to generate the spike time windows during the training absence seizure. MUX stands for multiplexer which only allows one dynamic spike to pass in each time window.

Since one kind of dynamic sources participate in the generation of the data in each time windows, we can assign a cluster to each time window. The sequence of clusters for the training absence seizure is shown in Fig. 3.10.

As shown, all kinds of dynamic sources participate in generation of the data in the beginning of the training absence seizure, while in the end of the training absence seizure, the first and the third dynamic sources just participate in the generation of data. This phenomenon can be corresponded to the fact that the performance of the existing circuit between somatosensory cortex and thalamus changes in the end of the absence seizures [Meeren et al. (2002); Polack et al. (2007)].

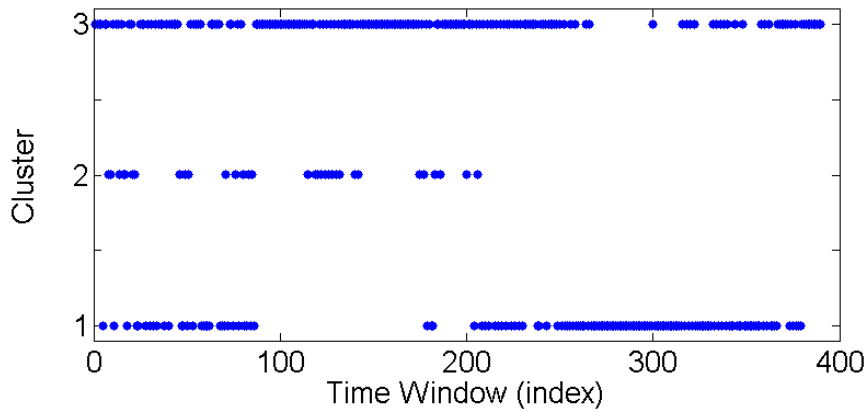


Figure 3.10: Sequence of clusters for the training absence seizure.

3.5.2.2 Results For Other Absence Seizures of The First Rat

The same results are obtained for other absence seizures of the first rat. In fact, we have intra-rat similarity between the results obtained from the absence seizures of the first rat. This means that the extracted average of the clusters are similar to the results obtained from the training absence seizure. The sequence of the clusters for one of the absence seizures which consists of $K = 88$ time windows is shown in Fig. 3.11. As shown, again, at the end of the absence seizure, the first and the third dynamic sources only participate in the generation of the absence seizure.

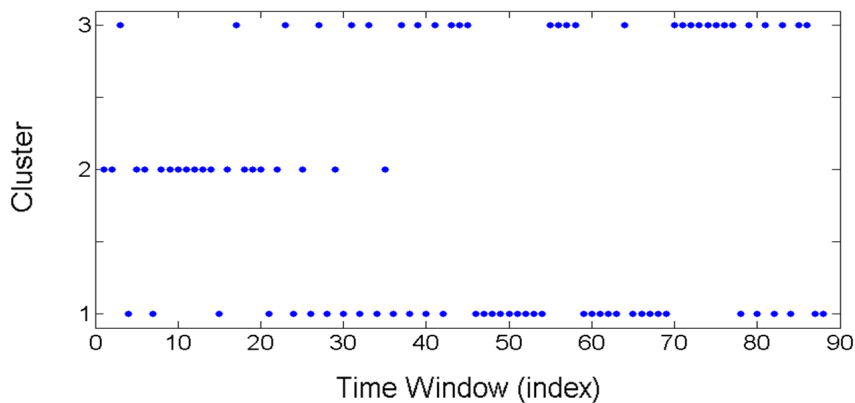


Figure 3.11: Sequence of clusters for one of the absence seizures from the first rat which consists of $K = 88$ spike time windows.

3.5.2.3 Results For Other Rats

For other rats, when we extract the model parameters, the best results are again obtained by considering one static source ($m = 1$). The estimated number of dynamic sources is also equal to one ($r_k = 1$) in each time window. Moreover, the same model as Fig. 3.6 and Fig. 3.8 can be considered after clustering the sources, i.e., there are three kinds of dynamic sources and a static source. Furthermore, one kind of dynamic sources completely disappears towards the end of the absence seizures similar to results of the first rat.

For instance, the results obtained from one of the absence seizures of the second rat are shown in Fig. 3.12 and 3.13. Moreover, the obtained linear model and the sequence of clusters are respectively shown in 3.14 and Fig. 3.15.

The noticeable point is that the obtained sources in the second rat are different from the ones in the first rat, however, the obtained static structure and averages of clusters for the dynamic structures are similar to ones in the first rat. Since the structures show the arrangement of the sources around the sensors, we can conclude that the origins of the sources are similar in these two rats. The same results are obtained in other rats.

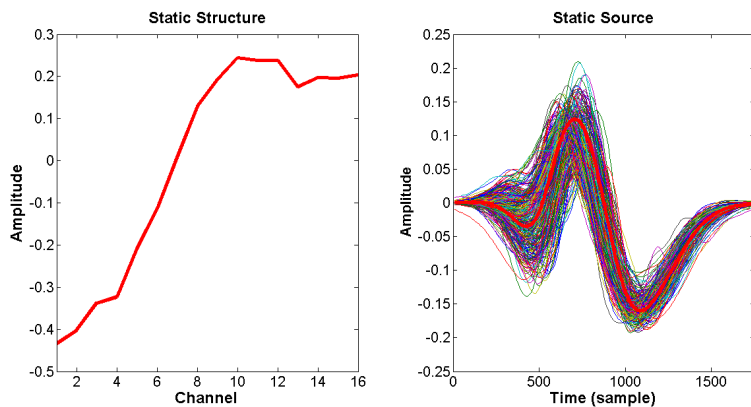


Figure 3.12: The static structure (left) and sources (right) obtained from one of the absence seizures of the second rat with $K = 560$ time windows.

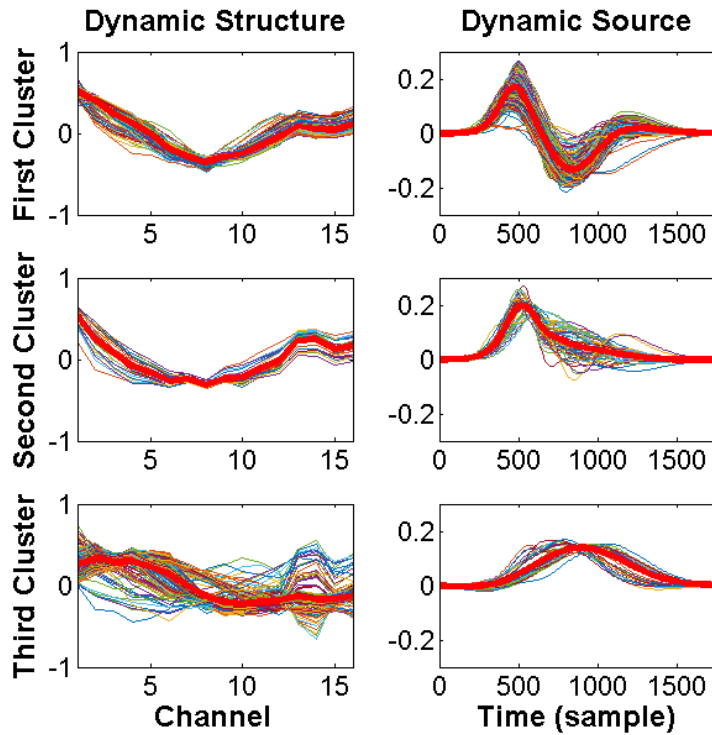


Figure 3.13: The dynamic structures (left) and sources (right) obtained from one of the absence seizures of the second rat with $K = 560$ time windows.

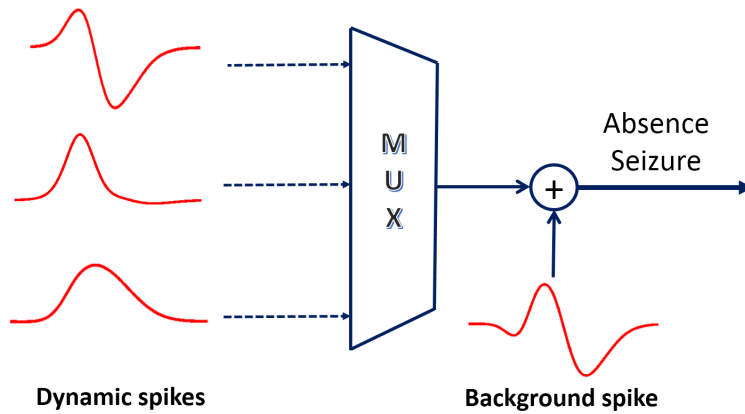


Figure 3.14: The obtained average of clusters for the dynamic and static sources in the second rat. One kind of the dynamic spikes (sources) is added to the background spike (static source) to generate the spike time windows during the absence seizures.

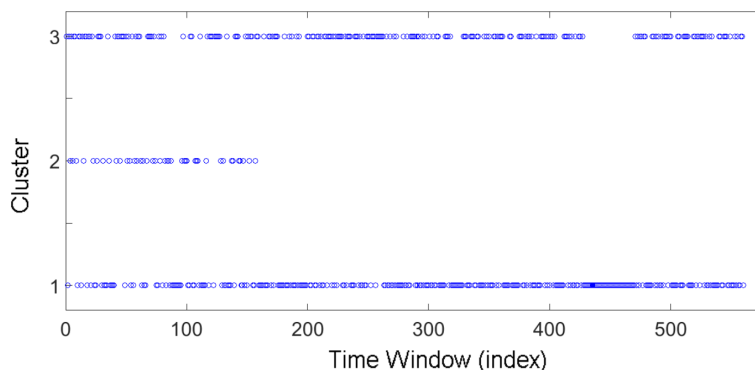


Figure 3.15: Sequence of clusters for one of the absence seizures of the second rat which consists of $K = 560$ time windows.

3.5.2.4 Adaptation of The Average of Clusters to The Training Absence Seizure

Now, we want to check if the results of clustering (averages of clusters) are adapted to the training absence seizure or not. For this purpose, we calculate the reconstruction error as explained in the following.

By considering the obtained static structure, the average of the normalized static sources, the average of the normalized dynamic structures, and the average of the dynamic sources respectively as \mathbf{a} , \mathbf{s} , \mathbf{b}_j ($j = 1, 2, 3$) and \mathbf{u}_j ($j = 1, 2, 3$), each time window of the training absence seizure ($\mathbf{Y}^{(k)}$) and its reconstruction ($\widehat{\mathbf{Y}}^{(k)}$) can be expressed as:

$$\mathbf{Y}^{(k)} = \underbrace{\alpha^{(k)} \mathbf{a} \mathbf{s}^T + \sum_{j=1}^3 \beta_j^{(k)} \mathbf{b}_j \mathbf{u}_j^T}_{\widehat{\mathbf{Y}}^{(k)}} + \mathbf{N}^{(k)} \quad (3.24)$$

where $\alpha^{(k)}$ and $\beta_j^{(k)}$ are the scaling coefficients because we have normalized the parameters of the model. One of $\beta_j^{(k)}$ ($j = 1, 2, 3$) is non-zero, and two of them are zero for each time window. Since we already clustered the dynamic sources and structures, the zero entries are known. It can be shown that the MLE solution of $\alpha^{(k)}$ and non-zero $\beta_j^{(k)}$ are as follows:

$$\alpha^{(k)*} = Tr\{\mathbf{Y}^{(k)} \mathbf{s} \mathbf{a}^T\}, \quad \beta_j^{(k)*} = Tr\{\mathbf{Y}^{(k)} \mathbf{u}_j \mathbf{b}_j^T\} \quad (3.25)$$

Now, we can define the reconstruction error as follows:

$$Er_{train} = \frac{1}{K} \sum_{k=1}^K \frac{\|\mathbf{Y}^{(k)} - \widehat{\mathbf{Y}}^{(k)}\|_F^2}{\|\mathbf{Y}^{(k)}\|_F^2} \quad (3.26)$$

This error is equal to 0.03 for the training absence seizure indicating that the obtained results of clustering are compatible with the training absence seizure. Now, we want to check if the results of clustering (average of clusters) are also adapted to the other absence seizures or not.

3.5.2.5 Cross-Validation (Testing Phase)

Since the sources are not similar in different rats, the cross-validation between two absence seizures from two different rats is meaningless. Hence, we perform the cross-validation for the absence seizures of the same rat.

We consider one of the absence seizures as the testing absence seizure. Then, using the obtained parameters from the training absence seizure and regarding (3.24), we estimate the best kind of dynamic source and structure, and scaling coefficients for each time window of the testing absence seizure. If we again employ the MLE method, we get:

$$\{j^*, \alpha^{(k)*}, \beta_j^{(k)*}\} = \underset{j, \alpha^{(k)}, \beta_j^{(k)}}{\operatorname{argmin}} \|\mathbf{Y}^{(k)} - \alpha^{(k)} \mathbf{a} \mathbf{s}^T - \beta_j^{(k)} \mathbf{b}_j \mathbf{u}_j^T\|_F^2 \quad (3.27)$$

By determination of the parameters, the reconstructed time window is calculated as follows:

$$\widehat{\mathbf{Y}}^{(k)} = \alpha^{(k)*} \mathbf{a} \mathbf{s}^T + \beta_{j^*}^{(k)*} \mathbf{b}_{j^*} \mathbf{u}_{j^*}^T \quad (3.28)$$

Now, we calculate the reconstruction error as follows to check the compatibility of the parameters, obtained from the training absence seizure, with the testing absence seizure:

$$Er_{test} = \frac{1}{K_{test}} \sum_{k=1}^{K_{test}} \frac{\|\mathbf{Y}^{(k)} - \widehat{\mathbf{Y}}^{(k)}\|_F^2}{\|\mathbf{Y}^{(k)}\|_F^2} \quad (3.29)$$

where K_{test} shows the number of time windows in the considered testing absence seizure. We perform the proposed training and testing phase on

five absence seizures of the first rat. The last absence seizure is the absence seizure considered in the previous part. The results of the reconstruction are reported in Table 3.2.

Table 3.2: Reconstruction error for 5 different absence seizures of the first rat. The absence seizures respectively consist of $K_1 = 87$, $K_2 = 94$, $K_3 = 95$, $K_4 = 88$ and $K_5 = 390$ time windows. The diagonal and non-diagonal entries of the table respectively show Er_{train} and Er_{test} .

Training on	Testing on				
seizure	1	2	3	4	5
1	0.05	0.11	0.13	0.12	0.09
2	0.07	0.06	0.10	0.09	0.08
3	0.08	0.11	0.06	0.10	0.09
4	0.10	0.09	0.10	0.08	0.10
5	0.09	0.10	0.11	0.12	0.03

These results show the intra-rat similarity between absence seizures, in the sense that the static and dynamic sources and structures trained on one absence seizure, provide an accurate estimation of signals in other absence seizures. For other rats, the reconstruction errors have the same order of magnitude as the first rat which show the generality of the results of clustering and proposed model for the recorded absence seizures.

Since there is no inter-rat similarity between the sources, the aforementioned cross-validation framework between two seizures from two different rats is meaningless. Hence, we calculate the cross correlation coefficient between the results obtained from the two rats. Tables 3.3 and 3.4 respectively show the cross correlation coefficient between the obtained structures and sources from the first and second rat.

As reported in Table 3.3, since the cross correlation coefficients between the structures obtained from two seizures of different rats are close to one, we find that the structures in all seizures and all rats are similar, or in other words, they have inter-rat similarity. Since the structures are corresponding

CHAPTER 3. STATIC AND DYNAMIC MODELING OF ABSENCE SEIZURES

Table 3.3: The cross correlation coefficient between the obtained structures from the first and second rat.

First Rat	Second Rat			
	a	b₁	b₂	b₃
a	0.97	-0.61	-0.54	-0.72
b₁	-0.58	0.94	0.78	0.36
b₂	-0.46	0.77	0.98	0.27
b₃	-0.77	0.35	0.32	0.96

Table 3.4: The cross correlation coefficient between the obtained sources from the first and second rat.

First Rat	Second Rat			
	s	u₁	u₂	u₃
s	0.83	0.86	0.65	0.53
u₁	0.78	0.81	0.64	0.58
u₂	0.49	0.46	0.88	0.71
u₃	0.63	0.66	0.73	0.79

to the spatial topography of the sources, we can conclude that the spatial locations of the sources are similar in different rats.

Moreover, as reported in Table 3.4, since the cross correlation coefficients between the sources obtained from two seizures of different rats are not close to one, we find that the sources do not have inter-rat similarity. Since the sources show the temporal activation functions of their origins, we can conclude that the propagated signals from the origins are not similar in different rats.

We recall that the dataset consists of the data recorded from four GAERS rats, and the data of each rat consist of several seizures. We extracted the sources and their structures from all of the seizures in all of the rats. In summary, the obtained results show that:

- 1) The structures in all seizures and all rats are similar. In fact, the

structures have both intra-rat and inter-rat similarities.

2) The sources in all seizures of a specific rat are similar, but the sources obtained from the seizures of different rats are not similar. In fact, the sources have intra-rat similarity, but they do not have inter-rat similarity.

The results presented in Tables 3.2, 3.3, 3.4 confirm the above conclusions.

3.6 CONCLUSION

In this chapter, we proposed a method to retrieve the static and dynamic sources which generate the absence seizures to analyze the dynamics of absence seizures. We also extracted the structures of the sources. The considered scenario in this chapter can be employed in several applications such as radar and brain signals. It was shown that there are one background activity (a static source) and three kinds of dynamic sources during absence seizures. The dynamic sources randomly appear and disappear during the absence seizures, however, one kind of dynamic sources completely disappears towards the end of the absence seizures perhaps due to the performance of the existing circuit between somatosensory cortex and thalamus. These results were extracted from all of the rats and confirmed using a cross-validation framework. The main difference between the results of different rats was in the shapes of the sources. For example, the shapes of the sources for the first and second rats are shown in Figs. 3.9 and 3.14, respectively. The interesting point is that the obtained structures were the same in different rats which show that the origins of the sources are the same in different rats. This point is in accordance with the result obtained in the previous chapter regarding the spatial analysis of absence seizures.

Similar to the previous chapter, the drawback of the model proposed in this chapter is that it is based on exploration of spike time windows. In the next chapter, we propose a model in which we do not need to detect the spikes for analyzing the absence seizures.

4 CHARACTERIZING ABSENCE SEIZURES USING BLIND DECONVOLUTION

Contents

4.1	Main Idea	75
4.2	Model and Problem Definition	77
4.3	Proposed Method	79
4.4	Experimental Results	80
4.4.1	Simulation	80
4.4.2	Neural Recording	84
4.5	Conclusion	89

4.1 MAIN IDEA

In the previous chapters, we explored absence seizures by segmenting them into several spike time windows. This segmentation is not always possible because detection of spikes is sometimes difficult when the data is noisy. For instance, the noisy and clean data, recorded in channel 1, during two of the absence seizures of the first rat are respectively shown in the left and right sides of Fig. 4.1. As shown here, the spike detection in the noisy data is much more difficult than in the clean data. It should be noted that more than % 90 of absence seizures were clean during the recorded data.

In this chapter, we propose a generalized method for analyzing the absence seizures which can even be employed for absence seizures in which

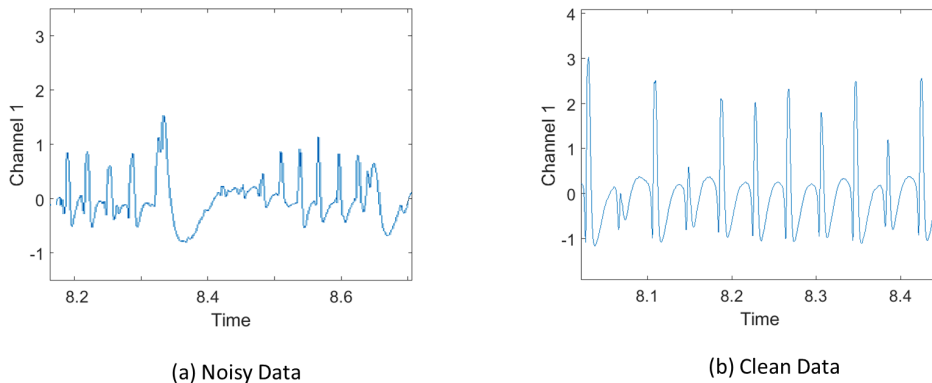


Figure 4.1: (a) the noisy data where the spike detection is difficult, and (b) the clean data where the spike detection can be easily performed.

performing the spike detection step is not easy. Similar to chapter 2, we aim to localize the onset layers of somatosensory cortex during absence seizures (spatial analysis) and investigate the dynamics of absence seizures (temporal analysis). Hence, all of the pre-processing steps explained in chapter 2 are again employed except detection and alignment of spikes.

To achieve our spatio-temporal targets, we model the recorded absence seizures by a linear combination of a few (R) epileptic activities. Each epileptic activity is represented using a spatio-temporal representation. The spatial representation shows the pattern of current sources and sinks generating the epileptic activity, while the temporal representation specifies the waveform and the occurrence time of the epileptic activity. Extracting the defined epileptic activities from the recorded absence seizures help us to find the onset layers of somatosensory cortex (spatial analysis) and investigate the temporal evolution of recorded absence seizures (temporal analysis).

The rest of this chapter is organized as follows. Section 4.2 is dedicated to the model and problem definition. We explain the proposed method for estimating the parameters in section 4.3. The results are reported in section 4.4, and finally, section 4.5 concludes the chapter.

4.2 MODEL AND PROBLEM DEFINITION

We assume that the linear superposition of a few (R) epileptic activities generates an absence seizure as shown in Fig. 4.2. We consider three characteristics for each epileptic activity; 1) the CSD, 2) the spike, and 3) the time series. These characteristics respectively show the pattern of current sources and sinks producing the epileptic activity, the activation function of the epileptic activity, and the firing times and the corresponding amplitudes of the epileptic activity during an absence seizure.

In fact, each epileptic activity has a spatio-temporal representation. The CSD is the spatial representation of an epileptic activity, and the convolution of the spike and the time series is the temporal representation of an epileptic activity. The considered model for an absence seizure is schematically shown in Fig. 4.2. We extract the epileptic activities and their characteristics from the absence seizures to figure out the onset layers of somatosensory cortex, and investigate the temporal evolution of absence seizures.

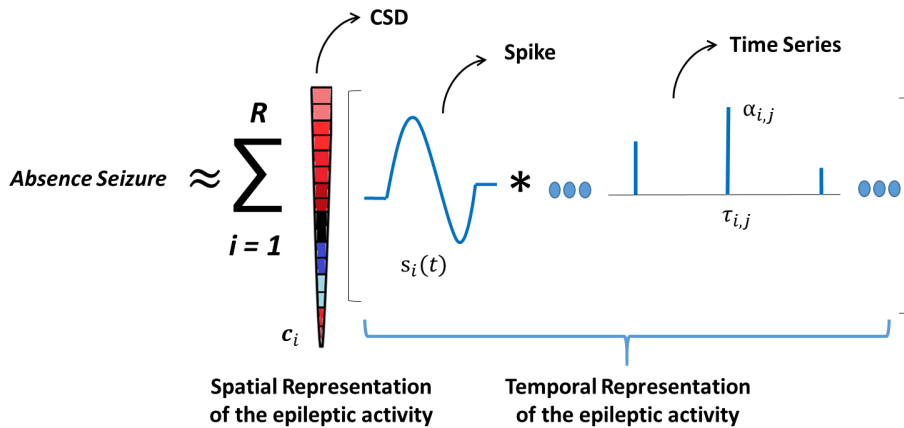


Figure 4.2: An absence seizure is modeled by a linear combination of R epileptic activities which have spatio-temporal representations.

As shown in Fig. 4.2, the absence seizure at time instant t ($\mathbf{x}(t) \in \mathbb{R}^E$)

can be expressed as:

$$\mathbf{x}(t) = \sum_{i=1}^R \mathbf{c}_i \sum_{j=1}^{L_i} \alpha_{i,j} s_i(t - \tau_{i,j}) + \mathbf{n}(t) \quad (4.1)$$

where R denotes the number of epileptic activities. For the i^{th} epileptic activity, $\mathbf{c}_i \in \mathbb{R}^E$, L_i , $s_i(t)$, $\tau_{i,j}$ and $\alpha_{i,j}$ show the CSD, the number of occurrences of the epileptic activity, the spike signal at time instant t , the occurrence time and the corresponding amplitude, respectively. The noise vector $\mathbf{n}(t) \in \mathbb{R}^E$ is considered zero-mean Gaussian with i.i.d. entries. It should be noted that the spike signal $s_i(t)$ has T samples, and it can be shown by $\mathbf{s}_i \in \mathbb{R}^T$ in the vector notation. T is considered equal to 1750 samples (87.5 ms) in this study as stated by [Polack et al. (2007)].

According to (4.1) and Fig. 4.2, estimating the parameters from an absence seizure is similar to solving a multi-channel blind deconvolution problem, which is in general ill-posed [Chi (2016)]. Therefore, we must consider some additional constraints for the problem. The identifiability of this problem for different scenarios is discussed in [Li et al. (2016)]. We consider the following constraints for the epileptic activities:

(\mathcal{C}_1) The times series are sparse signals (i.e., $L_i \leq L_{max}$). In fact, we assume that each epileptic activity happens at most L_{max} times.

(\mathcal{C}_2) The CSDs and the spikes are unit norm (i.e., $\|\mathbf{c}_i\|_2 = \|\mathbf{s}_i\|_2 = 1$), and the amplitudes of the spikes are positive (i.e., $\alpha_{i,j} > 0$). These assumptions are considered to omit the scaling and polarization ambiguities [Comon and Jutten (2010)].

(\mathcal{C}_3) The epileptic activities are synchronized. As explained in chapter 2, since the data was recorded very locally, we expect the instantaneous appearance of spikes in different layers of somatosensory cortex. Therefore, we assume that the occurrence time of the epileptic activities are similar. Hence, $\tau_{i,j}$ and L_i are respectively replaced by τ_j and L for all of the epileptic activities.

Now, the problem definition is complete. The set of unknown parameters $\Theta = \left\{ R, L, \bigcup_{i=1}^R \{\mathbf{c}_i, \mathbf{s}_i, \bigcup_{j=1}^L \{\alpha_{i,j}\}\}, \bigcup_{j=1}^L \{\tau_j\} \right\}$ must be estimated based on the

observed absence seizure and the considered constraints.

4.3 PROPOSED METHOD

Since there is no prior information about the number of epileptic activities (R), we estimate the results for different R . Then, we select the one which has the best biophysiological interpretation. Therefore, we assume that R is fixed and known. It can be easily shown that minimizing the following objective function leads to the maximum likelihood estimation (MLE) of the unknown parameters.

$$\tilde{f}(\Theta) = \sum_t \|\mathbf{x}(t) - \sum_{i=1}^R \mathbf{c}_i \sum_{j=1}^L \alpha_{i,j} s_i(t - \tau_j)\|_2^2 \quad (4.2)$$

Due to the presence of τ_j , it is more convenient to deal with this objective function in the Fourier domain. Therefore, we express the objective function as follows:

$$f(\Theta) = \sum_f \|\hat{\mathbf{x}}(f) - \sum_{i=1}^R \mathbf{c}_i \hat{s}_i(f) \sum_{j=1}^L \alpha_{i,j} e^{-j2\pi f \tau_j}\|_2^2 \quad (4.3)$$

where $\hat{\mathbf{x}}(f)$ and $\hat{s}_i(f)$ respectively show the Fourier transform of the data and $s_i(t)$ at frequency f . We can state (4.3) in the matrix notation as:

$$f(\Theta) = \|\hat{\mathbf{X}} - \mathbf{C}(\hat{\mathbf{S}} \odot \hat{\mathbf{A}})\|_F^2 \quad (4.4)$$

where \odot and $\|\cdot\|_F$ denote the element-wise product and the Frobenius norm, respectively. The columns of $\hat{\mathbf{X}}$, \mathbf{C} and $\hat{\mathbf{S}}$ are corresponding to $\hat{\mathbf{x}}(f)$ in different frequencies, the CSDs and the Fourier transform of the spikes in different epileptic activities, respectively. Also, the $(f, i)^{th}$ entry of $\hat{\mathbf{A}}$ is:

$$\hat{a}_i^f = \sum_{j=1}^L \alpha_{i,j} e^{-j2\pi f \tau_j} \quad (4.5)$$

The stated objective function in (4.4) and the considered assumptions in (\mathcal{C}_1) , (\mathcal{C}_2) , and (\mathcal{C}_3) form a constrained optimization problem. We use alternating minimization to solve the problem. Some initial values are considered

for Θ , then, the following three optimization problems are alternately solved until the parameters convergence.

$$\begin{aligned} \mathbf{C}_{opt} &= \underset{\mathbf{C}}{\operatorname{argmin}} \|\hat{\mathbf{X}} - \mathbf{C}(\hat{\mathbf{S}} \odot \hat{\mathbf{A}})\|_F^2 \\ \text{s.t. } & \operatorname{diag}(\mathbf{C}^T \mathbf{C}) = \mathbf{I} \end{aligned} \quad (4.6)$$

$$\begin{aligned} \hat{\mathbf{S}}_{opt} &= \underset{\hat{\mathbf{S}}}{\operatorname{argmin}} \|\hat{\mathbf{X}} - \mathbf{C}(\hat{\mathbf{S}} \odot \hat{\mathbf{A}})\|_F^2 \\ \text{s.t. } & \operatorname{diag}(\hat{\mathbf{S}}^H \hat{\mathbf{S}}) = \mathbf{I}, \quad \hat{s}_i(-f) = \hat{s}_i^*(f), \quad i = 1, 2, \dots, R \end{aligned} \quad (4.7)$$

$$\begin{aligned} \hat{\mathbf{A}}_{opt} &= \underset{\hat{\mathbf{A}}}{\operatorname{argmin}} \|\hat{\mathbf{X}} - \mathbf{C}(\hat{\mathbf{S}} \odot \hat{\mathbf{A}})\|_F^2 \\ \text{s.t. } & L \leq L_{max}, \quad \alpha_{i,j} > 0, \quad i = 1, 2, \dots, R, \quad j = 1, 2, \dots, L \end{aligned} \quad (4.8)$$

where the operator $\operatorname{diag}(\cdot)$ keeps the diagonal entries of a matrix. The new added constraint in (4.7) forces the spikes to be real signals in the time domain. The first and the second optimization problems can be solved using Lagrangian multipliers, and any of the spectral estimation methods such as MUSIC, ESPRIT or beamforming techniques can be employed to solve the last optimization problem [Li et al. (2016)]. Once the parameters were found, we easily convert them back to the time domain.

4.4 EXPERIMENTAL RESULTS

4.4.1 SIMULATION

4.4.1.1 Data Generation

We assume that there are $E = 3$ sensors which record the data from $R = 2$ activities for 2000 samples. The characteristics of the first and the second activity are shown in the top and the bottom of Fig. 4.3, respectively.

We select the entries of the CSDs from zero-mean and unit-variance i.i.d. Gaussian distribution, then, we normalize the CSD of each activity. The

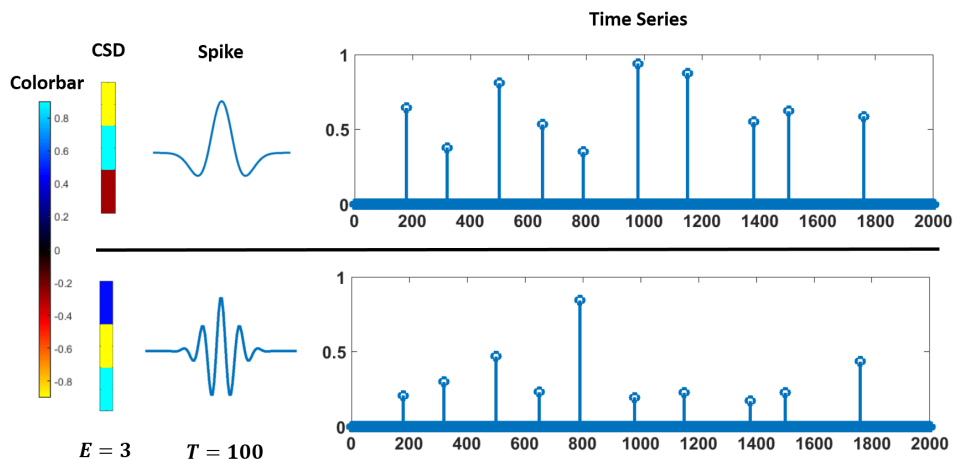


Figure 4.3: Characteristics of the activities generating the simulated data. The top and the bottom figures show the characteristics of the first and the second activity, respectively.

spike of the first and the second activities are considered a normalized Mexican hat and Morlet signal, respectively. The length of the spikes is equal to $T = 100$ samples. It should be noted that the MATLAB functions *Mexican* and *Morlet* can be employed to generate the spikes. The positions of the non-zero entries of the time series (τ_j) are randomly chosen, and their values ($\alpha_{i,j}$) are uniformly distributed between $[0 \ 1]$. We consider $L = 10$ non-zero entries for each time series.

The data is constructed according to the following expression:

$$\mathbf{x}(t) = \sum_{i=1}^R \mathbf{c}_i \sum_{j=1}^L \alpha_{i,j} s_i(t - \tau_j) + \mathbf{n}(t) \quad (4.9)$$

where the entries of noise ($\mathbf{n}(t)$) are i.i.d., and have zero-mean Gaussian distributions with variance σ_0^2 . Fig. 4.4 shows the generated data for $\sigma_0^2 = 0$.

4.4.1.2 Evaluation Criteria

We use the mean squared error (MSE) for the CSDs, spikes, and time series to evaluate the performance of the proposed method in the estimation of the

parameters. For instance, the MSE for the CSDs is defined as follows:

$$MSE_{CSDs} = \frac{1}{R} \sum_{i=1}^R \frac{\|\mathbf{a}_i - \mathbf{a}_i^*\|_2}{\|\mathbf{a}_i\|_2}, \quad (4.10)$$

The MSE for the spikes and time series are defined similar to the CSDs. The signal to noise ratio (SNR) of the simulations is also defined as:

$$SNR = 10 \log(E_t \left\{ \frac{\|\mathbf{x}(t) - \mathbf{n}(t)\|_2^2}{\|\mathbf{n}(t)\|_2^2} \right\}) \quad (4.11)$$

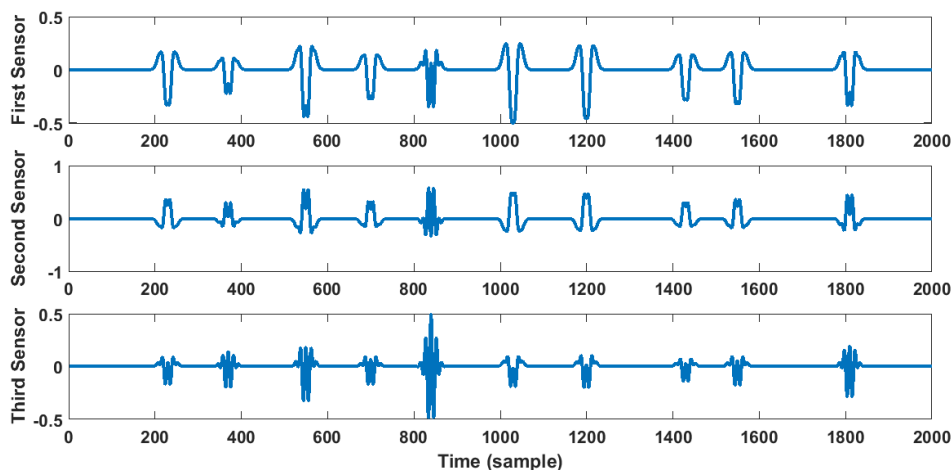


Figure 4.4: The simulated data in the noise-free model. The data is generated by a linear superposition of two activities.

4.4.1.3 Simulation Results

We apply the proposed method on the simulated data in different SNR to estimate the parameters. The obtained MSE for CSDs, spikes, and time series in different SNR are reported in Table 4.1. Moreover, the estimated spikes of the first and second activities in different SNR are respectively shown in Fig. 4.5 and Fig. 4.6. These results show the accuracy of the proposed method for retrieving the unknown parameters in the considered scenario.

CHAPTER 4. CHARACTERIZING ABSENCE SEIZURES USING
BLIND DECONVOLUTION

Table 4.1: Performance of the proposed method in different SNR.

SNR	MSE_{CSDs}	MSE_{spikes}	$MSE_{time\ series}$
5	0.321	0.343	0.349
10	0.127	0.161	0.186
15	0.038	0.049	0.048
20	0.011	0.015	0.018
25	0.002	0.004	0.005

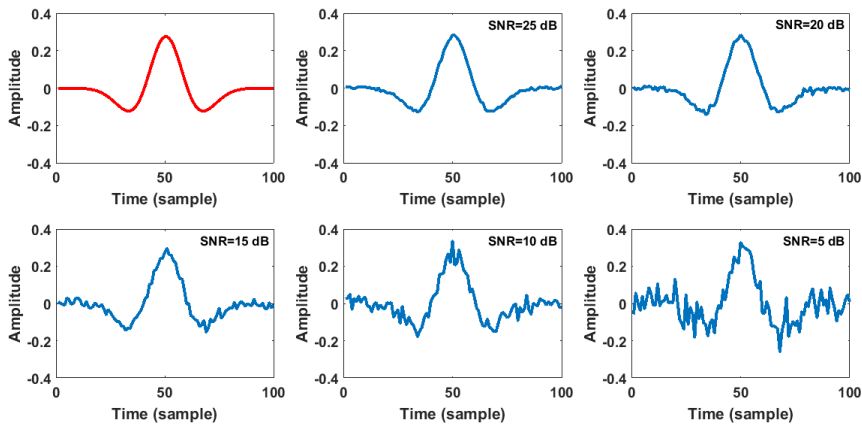


Figure 4.5: The estimated spikes of the first activity in different SNR. The top left figure shows the original spike.

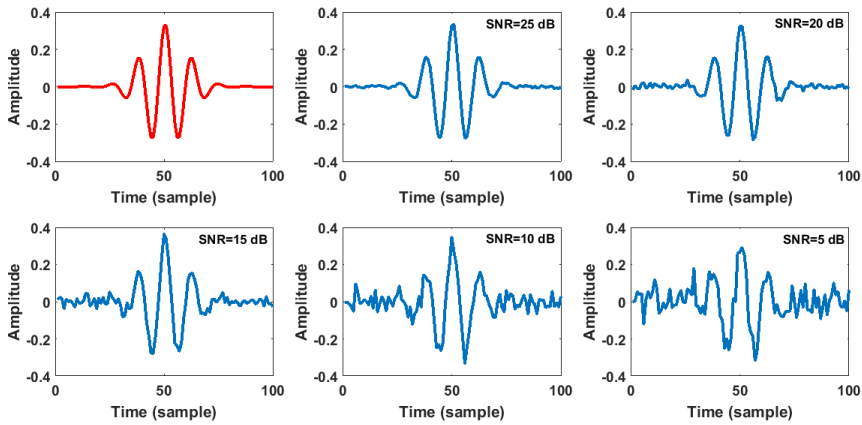


Figure 4.6: The estimated spikes of the second activity in different SNR. The top left figure shows the original spike.

4.4.2 NEURAL RECORDING

We apply the proposed method on the absence seizures for different number of epileptic activities (R). The best results are extracted by considering three epileptic activities in all of the absence seizures. When we consider $R > 3$, some of the spikes of the epileptic activities become non-smooth and incomprehensible, and when we consider $R < 3$, the reconstruction error severely increases. We will define the reconstruction error later. Therefore, we consider $R = 3$ to estimate the parameters.

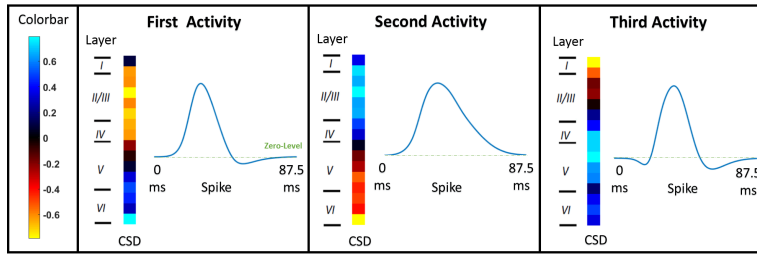
4.4.2.1 Training Phase

An absence seizure with the length of 19.3 sec from the first rat is considered to present the results. The characteristics of the estimated epileptic activities, i.e., the CSDs, the spikes, a part of the time series and the corresponding absence seizure are shown in Fig. 4.7.

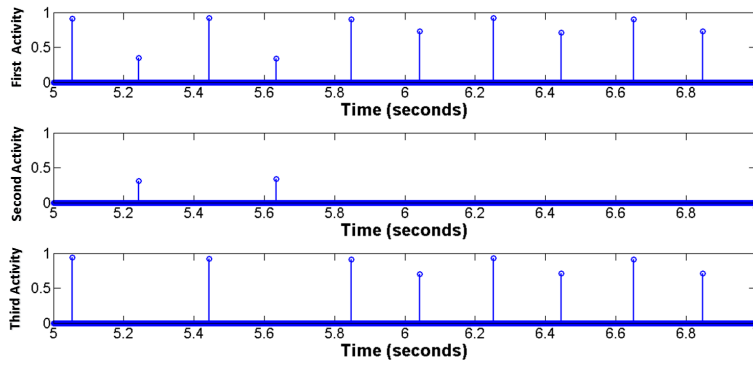
With regards to the obtained CSDs, the sources and sinks are distributed in layers II/III and VI for the first and the second epileptic activities, and in layers I and V for the third epileptic activity. Therefore, the top and the bottom layers of somatosensory cortex are the most active layers during the absence seizure similar to the results presented in chapter 2.

Moreover, based on the obtained time series, the first epileptic activity is the dominant activity during the absence seizure because it has more non-zero entries than the other epileptic activities. Also, the amplitude of the second or the third epileptic activity is equal to zero when the epileptic activities are activated. In fact, it seems that the second and the third epileptic activities are two differential activities which are randomly activated and act as a first-order correction for the first epileptic activity. Similar behavior is observed in the other parts of the absence seizure. For the considered absence seizure, the time series of the epileptic activities have $l_1 = 94$, $l_2 = 12$ and $l_3 = 82$ non-zero entries, respectively. The average and the variance (m_i, σ_i^2) of these non-zero values are respectively equal to

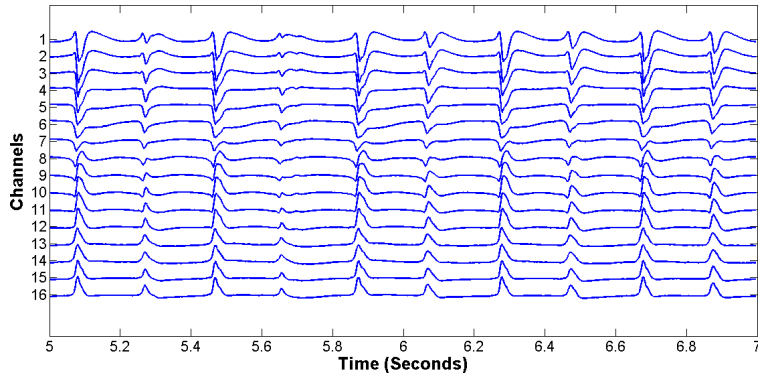
CHAPTER 4. CHARACTERIZING ABSENCE SEIZURES USING
BLIND DECONVOLUTION



(a)



(b)



(c)

Figure 4.7: (a) The CSDs and the spikes of the epileptic activities generating the absence seizure. (b) Two seconds of the time series of the epileptic activities, and (c) the corresponding absence seizure.

$(m_1 = 0.22, \sigma_1^2 = 49 \times 10^{-4})$, $(m_2 = 0.14, \sigma_2^2 = 29 \times 10^{-4})$, and $(m_3 = 0.15, \sigma_3^2 = 31 \times 10^{-4})$ for the epileptic activities.

4.4.2.2 Other Absence Seizures of The First Rat

The same results are obtained when we apply the proposed method on the other absence seizures of the first rat. It means that the estimated CSDs and spikes are similar to the illustrated results in Fig. 4.7. The first epileptic activity is the dominant epileptic activity, and the second and the third epileptic activities randomly activate with the first epileptic activity during the absence seizures. The noticeable point is that the average and the variance of the non-zero entries of the time series are very close to the previous results meaning that they can be considered as stationary random processes. For instance, these values for four absence seizures of the first rat are reported in Table 4.2.

Table 4.2: The average and variance of the non-zero entries of the time series in four absence seizures of the first rat. l_i shows the number of non-zero entries of the i^{th} time series, and m_i and σ_i^2 represent the corresponding average and variance.

Seizure	l_1	m_1	$\frac{\sigma_1^2}{10^{-2}}$	l_2	m_2	$\frac{\sigma_2^2}{10^{-2}}$	l_3	m_3	$\frac{\sigma_3^2}{10^{-2}}$
1	87	0.21	0.55	24	0.13	0.33	63	0.13	0.38
2	91	0.20	0.58	14	0.15	0.35	77	0.14	0.37
3	95	0.20	0.61	18	0.12	0.36	77	0.12	0.35
4	88	0.19	0.57	32	0.13	0.41	56	0.12	0.39

4.4.2.3 Other Rats

For other rats, the CSDs of the epileptic activities are similar to ones obtained in the first rat. Also, there is a dominant epileptic activity during absence seizures, and the non-zero entries of the time series can be considered as stationary random processes for different absence seizures of a rat. But the spikes are different from the obtained results in the first rat. For instance, the obtained CSDs and spikes for the epileptic activities generating the absence seizures of the second rat are shown in Fig. 4.8. Since the CSDs of the epileptic activities are similar but the spikes are different in the rats, we can conclude that the distribution of current sources and sinks, or in other

words, the origins of the epileptic activities are the same in the rats, but the propagated signals from the origins are different.

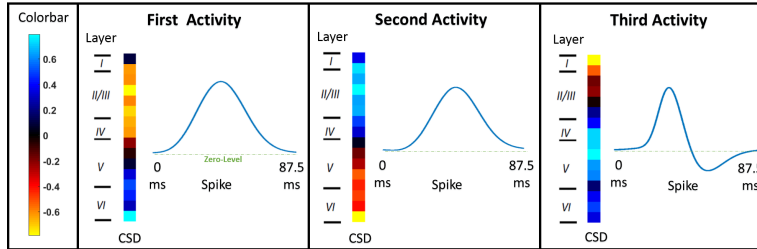


Figure 4.8: The CSDs and the spikes of the epileptic activities in the second rat.

4.4.2.4 Cross Validation

We also validate and cross validate the obtained results by computing the cross correlation of the obtained results in different absence seizures to show the accuracy and generality of the considered model. It should be noted that since the absence seizures considered in this chapter are noisy, the reconstruction error is not a suitable criterion for performing the cross validation.

As an example, the cross correlation coefficient between the obtained CSDs in two absence seizures of the first rat are reported in Table 4.3.

Table 4.3: The cross correlation coefficient between the obtained CSDs from two absence seizures of the first rat whose lengths are 19.3 *sec* and 18.5 *sec*, respectively.

First Absence Seizure	Second Absence Seizure		
	c_1	c_2	c_3
c_1	0.96	-0.25	0.59
c_2	-0.27	0.99	-0.43
c_3	0.61	-0.42	0.97

Moreover, the cross correlation coefficient between the obtained spikes in these two absence seizures are reported in Table 4.4.

As reported, at least one of the values are close to one in each column of the tables which shows that the obtained results are similar in the considered absence seizures.

CHAPTER 4. CHARACTERIZING ABSENCE SEIZURES USING
BLIND DECONVOLUTION

Table 4.4: The cross correlation coefficient between the obtained spikes from two absence seizures of the first rat whose lengths are 19.3 *sec* and 18.5 *sec*, respectively.

First Absence Seizure	Second Absence Seizure		
	s_1	s_2	s_3
s_1	0.95	0.82	0.74
s_2	0.80	0.98	0.83
s_3	0.72	0.86	0.97

The same results are obtained by considering other absence seizures of the first rat. These results show the accuracy of the obtained results in modeling the absence seizures.

We can also perform the proposed cross validation framework on absence seizures recorded from two different rats. For instance, the cross correlation coefficient between the obtained CSDs in an absence seizure recorded from the first rat and an absence seizure recorded from the second rat are reported in Table 4.5.

Table 4.5: The cross correlation coefficient between the obtained CSDs from two absence seizures recorded from the first and second rats whose lengths are 19.3 *sec* and 21.4 *sec*, respectively.

First Absence Seizure	Second Absence Seizure		
	c_1	c_2	c_3
c_1	0.93	-0.27	0.62
c_2	-0.31	0.97	-0.48
c_3	0.55	-0.43	0.98

As reported, the CSDs are similar in these absence seizures meaning that the origins of the epileptic activities are the same in the rats. The cross correlation coefficients between the obtained spikes in these two absence seizures are also reported in Table 4.6. Since the spikes of the epileptic activities are not similar in different rats, the reported coefficients are not close to one.

CHAPTER 4. CHARACTERIZING ABSENCE SEIZURES USING
BLIND DECONVOLUTION

Table 4.6: The cross correlation coefficient between the obtained spikes from two absence seizures recorded from the first and second rats whose lengths are 19.3 *sec* and 21.4 *sec*, respectively.

First Absence Seizure	Second Absence Seizure		
	\mathbf{s}_1	\mathbf{s}_2	\mathbf{s}_3
\mathbf{s}_1	0.72	0.76	0.84
\mathbf{s}_2	0.81	0.87	0.71
\mathbf{s}_3	0.67	0.71	0.78

4.5 CONCLUSION

In this chapter, we proposed a generalized method for analyzing absence seizures. We described the absence seizures by the linear superposition of a few epileptic activities which have spatio-temporal representations. Then, we proposed a blind deconvolution method to estimate the epileptic activities. The obtained results show that there are three epileptic activities during the absence seizures. One of the epileptic activities is dominant, and the other epileptic activities randomly activate with the dominant epileptic activity. It was shown that the origins of the epileptic activities, which are located in the top and the bottom layers of somatosensory cortex, are similar in the GAERS rats, but the propagated spikes from the origins are different.

5 CONCLUSION AND PERSPECTIVES

We explored absence epileptic seizures using the data recorded from different layers of somatosensory cortex of four GAERS to answer the following scientific questions:

1) Are there some specific layers in somatosensory cortex which generate the absence seizures? or which layers have more activity during absence seizures? (spatial analysis)

2) Is there any specific pattern during absence seizures over time? or how do the absence seizures change over time? (temporal analysis)

Three scenarios were considered for modeling the recorded absence seizures to answer the mentioned questions.

In the first scenario, a spatio-temporal model was considered for the epileptic activities generating the spikes of absence seizures. Then, a factor analysis method was employed to find the epileptic activities. One of the interesting results obtained in this scenario was that a common or a background epileptic activity exists during the recorded absence seizures. This result motivated us to propose the second scenario for analyzing the absence seizures. In the second scenario, a static-dynamic model was considered for the sources generating the spikes of absence seizures. Then, a source separation method was employed to find the sources and their structures. The drawback of the aforementioned scenarios was in the absence seizures in which performing the spike detection is not possible. Hence, we proposed the last scenario. In the third or last scenario, we proposed a blind deconvolution method to directly estimate the epileptic activities producing the absence seizures without employing any spike detection step.

It is worth mentioning that we proposed a validation framework corresponding to each scenario. Hence, all of the obtained results were cross validated, and the generality of the considered models in different absence seizures were confirmed. Based on the obtained results, we found that:

1. There is a background event or activity during the absence seizures, and a circuit between layers II/III and VI of somatosensory cortex generate this background event.
2. There are a few events which randomly activate with the background event during the absence seizures, however, there is no specific pattern in the activation of these events. Layers I and V or II/III and VI of somatosensory cortex participate in the generation of these epileptic events.
3. The contribution of the epileptic events in generating the absence seizures of a GAERS are stationary random processes. This means that the epileptic events on average have similar behavior during different absence seizures of a GAERS.
4. The origin of the obtained epileptic events are the same in different GAERS.

As the future work for the continuation of this thesis, it would be interesting to:

1. analyze the data recorded between absence seizures. The data in these time intervals are highly noisy, and it is not possible to employ the proposed methods in this study to analyze them. The data in these time intervals could be useful for predicting the onset time of absence seizures.
2. find that what is going on at the beginning and at the end of absence seizures. We need to understand why an absence seizure starts and why it ends, or in other words, why the duration of an absence seizure is limited.

CONCLUSION AND PERSPECTIVES

3. record data from multiple areas of the cortex using several electrodes with high spatial resolution, and then, find the interaction of these areas during absence seizures.

6 PUBLICATIONS

JOURNAL PAPERS

[1] S. Akhavan, R. Phlypo, H. Soltanian-Zadeh, M. Kamarei and C. Jutten, "A Dictionary Learning Approach for Spatio-Temporal Characterization of Absence Seizures", *Physiological Measurement*, Vol. 112, pp. 1320-1341, 2019

[2] S. Akhavan, R. Phlypo, H. Soltanian-Zadeh, M. Kamarei and C. Jutten, "Separation of Static and Dynamic Sources in Absence Epileptic Seizures Using Depth Cortical Measurements", *Elsevier, Signal Processing*, Vol. 166, pp. 107235, 2019

CONFERENCE PAPERS

[3] S. Akhavan, R. Phlypo, H. Soltanian-Zadeh, F. Studer, A. Depaulis and C. Jutten, "Characterizing absence epileptic seizures from depth cortical measurements," 25th European Signal Processing Conference (EUSIPCO), Kos, pp. 444-448, 2017

[4] S. Akhavan, R. Phlypo, H. Soltanian-Zadeh, M. Kamarei and C. Jutten, "Static and dynamic modeling of absence epileptic seizures using depth recordings ," 14th International conference on Latent Variable Analysis and Signal Separation (LVA ICA), Guildford, pp. 534-544, 2018

[5] S. Akhavan, R. Phlypo, H. Soltanian-Zadeh and C. Jutten, "Unmixing of Absence Epileptic Seizures in GAERS", 2018 IEEE 10th Sensor Array and Multichannel Signal Processing Workshop, Sheffield, pp. 198-202, 2018

A EFFECT OF FIRST-ORDER MARKOVIAN DEPENDENCY ON PARAMETERS ESTIMATION

Using a simple example, we show why the Markovian dependency does not affect on estimation of the parameters when the data is noiseless.

Example: Assume that there are $S = 2$ states with $J = 1$ factor in each one, and at most one factor participates in generating the 2×1 ($E = 2, T = 1$) dimensional signals. Now, we want to estimate the state of the observed signal \mathbf{X}_k , or in other words, select the best factor for \mathbf{X}_k . The scatter plot for \mathbf{X}_{k-1} and \mathbf{X}_k , in the presence of additive noise is schematically shown in Fig. A.1, and assume that \mathbf{X}_{k-1} has been assigned to state 2, i.e., $q_{k-1} = 2$.

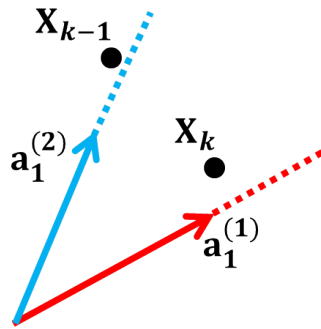


Figure A.1: Scatter plot of two consecutive signals generated under first-order Markovian model. Assigning \mathbf{X}_k to one of the states is not independent from the activated state for \mathbf{X}_{k-1} . Assume that $\mathbf{a}_1^{(s)}$ shows the factor associated with the s^{th} state.

APPENDIX A. EFFECT OF FIRST-ORDER MARKOVIAN
DEPENDENCY ON PARAMETERS ESTIMATION

Since there is a first-order Markovian dependency in activation of the states, if we use the maximum a posteriori (MAP) estimator to find q_k , we get

$$\underbrace{p(q_k = 1 | \mathbf{X}_k, q_{k-1}, \mathbf{A})}_{f_1} \stackrel{2}{\leq} \underbrace{p(q_k = 2 | \mathbf{X}_k, q_{k-1}, \mathbf{A})}_{f_2}. \quad (\text{A.1})$$

where $\mathbf{A} = [\mathbf{a}_1^{(1)} \ \mathbf{a}_1^{(2)}]$. According to Bayes' rule, the left and right sides of (A.1) can be simplified and written as

$$\begin{aligned} f_1 &= \frac{\overbrace{p(q_k = 1 | q_{k-1})}^{p_{21}} p(\mathbf{X}_k | q_k = 1, \mathbf{a}_1^{(1)})}{p(\mathbf{X}_k | \mathbf{A})}, \\ f_2 &= \frac{\overbrace{p(q_k = 2 | q_{k-1})}^{p_{22}} p(\mathbf{X}_k | q_k = 2, \mathbf{a}_1^{(2)})}{p(\mathbf{X}_k | \mathbf{A})}. \end{aligned} \quad (\text{A.2})$$

It can be seen that not only are the conditional probabilities of \mathbf{X}_k important for estimating q_k , but also the probabilities of transition between the states affect the decision making for q_k .

Based on Fig. A.1 and (A.2), whenever the signal to noise ratio (SNR) increases, the produced error decreases. For instance, if the signals were noise free, which is not a practical assumption, the parameters could be learned without any error. Moreover, whenever the probabilities of transition among the states become close to the uniform distribution, i.e., the states become independent, the produced error would decrease. For instance, if p_{21} and p_{22} were equal to 0.5 in (A.2), they would not affect the decision making.

B PERFORMING THE EXPECTATION STEP IN SPATIO-TEMPORAL MODELING OF ABSENCE SEIZURES

We assume that the set of unknown parameters Θ is known and fixed, and we estimate $p(\mathcal{H}_k^{(s)})$ for $k = 1, 2, \dots, K$ and $s = 1, 2, \dots, S$. We use the forward-backward procedure to estimate $p(\mathcal{H}_k^{(s)})$.

B.1 FORWARD PROCEDURE

The forward variable is defined as follows:

$$\alpha_k(s) = p(\mathbf{X}_1, \mathbf{X}_2, \dots, \mathbf{X}_k, \mathcal{H}_k^{(s)} | \Theta) \quad (\text{B.1})$$

which shows the probability of observing the spikes until the k^{th} spike and observing state s for the k^{th} spike given the model parameters. The forward variable when $k = 1$ ($\alpha_1(s)$) is equal to

$$\alpha_1(s) = \underbrace{p(\mathcal{H}_1^{(s)})}_{\frac{1}{S}} f(\mathbf{X}_1 | \mathcal{H}_1^{(s)}, \Theta). \quad (\text{B.2})$$

We assume that the probabilities of activation of the states for the first spike are equal, hence, $p(\mathcal{H}_1^{(s)}) = \frac{1}{S}$. Moreover, $f(\mathbf{X}_1 | \mathcal{H}_1^{(s)}, \Theta)$ is known according to (2.10) because the model parameters are known in *E-step*. Therefore, $\alpha_1(s)$ is easily calculated. It can be shown that we can use the following

*APPENDIX B. PERFORMING THE EXPECTATION STEP IN
SPATIO-TEMPORAL MODELING OF ABSENCE SEIZURES*

recursive expression to calculate $\alpha_k(s)$:

$$\alpha_k(s) = \left[\sum_{q=1}^S \alpha_{k-1}(q) p_{qs} \right] f(\mathbf{X}_k | \mathcal{H}_k^{(s)}, \Theta) \quad (\text{B.3})$$

where p_{qs} shows the $(q, s)^{th}$ entry of the transition probability matrix which is known in this step. Therefore, $\alpha_k(s)$ for $k = 1, 2, \dots, K$ and $s = 1, 2, \dots, S$ can be easily calculated using (2.10), (B.2) and (B.3).

B.2 BACKWARD PROCEDURE

In a similar manner, we define the backward variable as follows:

$$\beta_k(s) = p(\mathbf{X}_{k+1}, \mathbf{X}_{k+2}, \dots, \mathbf{X}_K | \mathcal{H}_k^{(s)}, \Theta) \quad (\text{B.4})$$

which shows the probability of observing spikes from the $(k+1)^{th}$ spike until the last spike, given state s for the k^{th} spike and given the model parameters. Assuming $\beta_K(s) = 1$, again, it can be shown that there is the following recursive expression for calculating $\beta_k(s)$:

$$\beta_k(s) = \sum_{q=1}^S p_{sq} f(\mathbf{X}_{k+1} | \mathcal{H}_{k+1}^{(q)}, \Theta) \beta_{k+1}(q) \quad (\text{B.5})$$

Therefore, $\beta_k(s)$ for $k = 1, 2, \dots, K$ and $s = 1, 2, \dots, S$ can be easily calculated using (2.10) and (B.5).

Now, we estimate $p(\mathcal{H}_k^{(s)})$ using the forward and backward variables. According to the conditional probability rule, $p(\mathcal{H}_k^{(s)})$ can be expressed as

$$p(\mathcal{H}_k^{(s)}) = \frac{p(\mathcal{H}_k^{(s)}, \mathcal{T}_{train} | \Theta)}{p(\mathcal{T}_{train} | \Theta)} = \frac{p(\mathcal{H}_k^{(s)}, \mathbf{X}_1, \mathbf{X}_2, \dots, \mathbf{X}_K | \Theta)}{\sum_{q=1}^S p(s_k = q, \mathbf{X}_1, \mathbf{X}_2, \dots, \mathbf{X}_K | \Theta)} \quad (\text{B.6})$$

By considering the definition of the forward and backward variables in (B.1) and (B.4), it can be seen that

$$p(\mathcal{H}_k^{(s)}, \mathbf{X}_1, \mathbf{X}_2, \dots, \mathbf{X}_K | \Theta) = \alpha_k(s) \beta_k(s). \quad (\text{B.7})$$

Therefore, we can calculate $p(\mathcal{H}_k^{(s)})$ for $k = 1, 2, \dots, K$ and $s = 1, 2, \dots, S$ as

$$p(\mathcal{H}_k^{(s)}) = \frac{\alpha_k(s) \beta_k(s)}{\sum_{q=1}^S \alpha_k(q) \beta_k(q)}. \quad (\text{B.8})$$

APPENDIX B. PERFORMING THE EXPECTATION STEP IN
 SPATIO-TEMPORAL MODELING OF ABSENCE SEIZURES

Here, the explanation of the *E-step* is finished. However, we also calculate another conditional probability which will be used in the Maximization step (*M-step*) to estimate the transition probability matrix. The probability of being in state m for the k^{th} spike and being in state n for the $(k + 1)^{th}$ spike given the observations and the model parameters is calculated as follows in a similar way to (B.6), (B.7) and (B.8):

$$p(\mathcal{H}_k^{(m)}, \mathcal{H}_{k+1}^{(n)}) = \frac{\alpha_k(m)p_{mn}f(\mathbf{X}_{k+1}|\mathcal{H}_{k+1}^{(n)}, \Theta)\beta_{k+1}(n)}{\sum_{q=1}^S \sum_{r=1}^S \alpha_k(q)p_{qr}f(\mathbf{X}_{k+1}|\mathcal{H}_{k+1}^{(r)}, \Theta)\beta_{k+1}(r)} \quad (\text{B.9})$$

C EXTRACTING THE MODEL PARAMETERS IN STATIC AND DYNAMIC MODELING OF ABSENCE SEIZURES

C.1 EXTRACTION OF THE STATIC STRUCTURE IN STATIC AND DYNAMIC MODELING OF SEIZURES

By assuming $\mathbf{Z}^{(k)} = \mathbf{R}_y^{(k)} - \mathbf{R}_B^{(k)}$, we get:

$$\begin{aligned} \mathbf{A}^* &= \underset{\mathbf{A}}{\operatorname{argmin}} \sum_{k=1}^K \|\mathbf{Z}^{(k)} - \mathbf{A}\boldsymbol{\Lambda}_s^{(k)}\mathbf{A}^T\|_F^2 \\ &s.t. \quad \operatorname{diag}(\mathbf{A}^T\mathbf{A}) = \mathbf{I} \end{aligned} \tag{C.1}$$

We solve this optimization problem using gradient projection (GP) method. We iteratively perform the following steps (gradient and projection) until convergence of \mathbf{A} .

Gradient Step: In the gradient step, we use the Newton method to speed up the convergence. The gradient and Hessian of the objective function

APPENDIX C. EXTRACTING THE MODEL PARAMETERS IN
STATIC AND DYNAMIC MODELING OF ABSENCE SEIZURES

with respect to \mathbf{A} is calculated as follows:

$$\begin{aligned}\mathbf{G} &= \sum_{k=1}^K 4\mathbf{A}\boldsymbol{\Lambda}_s^{(k)}\mathbf{A}^T\mathbf{A}\boldsymbol{\Lambda}_s^{(k)} - 2\mathbf{Z}^{(k)}\mathbf{A}\boldsymbol{\Lambda}_s^{(k)} \\ \mathbf{H} &= \sum_{k=1}^K 4(\boldsymbol{\Lambda}_s^{(k)}\mathbf{A}^T\mathbf{A}\boldsymbol{\Lambda}_s^{(k)} \otimes \mathbf{I}) + 4(\boldsymbol{\Lambda}_s^{(k)}\mathbf{A}^T \otimes \mathbf{A}\boldsymbol{\Lambda}_s^{(k)})\boldsymbol{\Pi} \\ &\quad + 4(\boldsymbol{\Lambda}_s^{(k)} \otimes \mathbf{A}\boldsymbol{\Lambda}_s^{(k)}\mathbf{A}^T) - 2(\boldsymbol{\Lambda}_s^{(k)} \otimes \mathbf{Z}^{(k)})\end{aligned}\quad (\text{C.2})$$

where \otimes denotes the Kronecker product, $\mathbf{I} \in \mathbb{R}^{n \times n}$ is the identity matrix, and $\boldsymbol{\Pi} \in \mathbb{R}^{n^2 \times n^2}$ is the permutation matrix which provides the following equality:

$$\text{vec}(\mathbf{A}^T) = \boldsymbol{\Pi} \text{vec}(\mathbf{A}) \quad (\text{C.3})$$

where $\text{vec}(\mathbf{A})$ denotes a long vector obtained by stacking the columns of \mathbf{A} . Hence, by considering $\mathbf{a} = \text{vec}(\mathbf{A})$ and $\mathbf{g} = \text{vec}(\mathbf{G})$, we perform the following iteration in this step:

$$\mathbf{a} \leftarrow \mathbf{a} - \mathbf{H}^{-1}\mathbf{g}$$

Then, we reshape \mathbf{a} to construct its matricization form.

Projection Step: In this step, each column of \mathbf{A} is normalized.

C.2 EXTRACTING AUTO-CORRELATION MATRIX OF STATIC SOURCES IN STATIC AND DY- NAMIC MODELING OF SEIZURES

By assuming $\mathbf{Z}^{(k)} = \mathbf{R}_y^{(k)} - \mathbf{R}_B^{(k)}$, we get:

$$\begin{aligned}\boldsymbol{\Lambda}_s^{(k)*} &= \underset{\boldsymbol{\Lambda}_s^{(k)}}{\text{argmin}} \|\mathbf{Z}^{(k)} - \mathbf{A}\boldsymbol{\Lambda}_s^{(k)}\mathbf{A}^T\|_F^2 \\ \text{s.t. } \boldsymbol{\Lambda}_s^{(k)} &= \text{diag}(\boldsymbol{\Lambda}_s^{(k)}), \boldsymbol{\Lambda}_s^{(k)} \succeq 0\end{aligned}\quad (\text{C.4})$$

We consider the vectorized form of the proposed objective function as:

$$\lambda_s^{(k)*} = \underset{\lambda_s^{(k)}}{\text{argmin}} \|\mathbf{z}^{(k)} - \mathbf{Q}\lambda_s^{(k)}\|_2^2 \quad (\text{C.5})$$

APPENDIX C. EXTRACTING THE MODEL PARAMETERS IN
STATIC AND DYNAMIC MODELING OF ABSENCE SEIZURES

where $\lambda_s^{(k)} = \text{vec}(\mathbf{\Lambda}_s^{(k)}) \in \mathbb{R}^{m^2}$, $\mathbf{z}_s^{(k)} = \text{vec}(\mathbf{Z}^{(k)}) \in \mathbb{R}^{n^2}$, $\mathbf{Q} = \mathbf{A} \otimes \mathbf{A} \in \mathbb{R}^{n^2 \times m^2}$, and \otimes denotes the Kronecker product. Since we know that $\lambda_s^{(k)}$ just has n non-zero entries, we consider the non-zero entries of $\lambda_s^{(k)}$ in $\lambda_{s_1}^{(k)} \in \mathbb{R}^m$, and also, the columns of \mathbf{Q} corresponding to the non-zero entries of $\lambda_s^{(k)}$ in $\mathbf{Q}_1 \in \mathbb{R}^{n^2 \times m}$. Hence, (C.4) can be expressed as:

$$\begin{aligned} \lambda_{s_1}^{(k)*} &= \underset{\lambda_{s_1}^{(k)}}{\text{argmin}} \|\mathbf{z}^{(k)} - \mathbf{Q}_1 \lambda_{s_1}^{(k)}\|_2^2 \\ \text{s.t. } \lambda_{s_1}^{(k)} &\geq 0 \end{aligned} \quad (\text{C.6})$$

where $\lambda_{s_1}^{(k)} \geq 0$ means each entry of $\lambda_{s_1}^{(k)}$ must be non-negative. This optimization problem is a non-negative least square (NNLS) problem. There are many toolboxes that can be employed to solve this problem very fast (e.g., *nnls* function in MATLAB).

C.3 EXTRACTION OF $\mathbf{R}_B^{(k)}$ IN STATIC AND DYNAMIC MODELING OF SEIZURES

By assuming $\mathbf{Z}^{(k)} = \mathbf{R}_y^{(k)} - \mathbf{A} \mathbf{\Lambda}_s^{(k)} \mathbf{A}^T$, we get:

$$\begin{aligned} \mathbf{R}_B^{(k)*} &= \underset{\mathbf{R}_B^{(k)}}{\text{argmin}} \|\mathbf{Z}^{(k)} - \mathbf{R}_B^{(k)}\|_F + \lambda^{(k)} \text{Tr}(\mathbf{R}_B^{(k)}) \\ \text{s.t. } \mathbf{R}_B^{(k)} &\succeq 0 \end{aligned} \quad (\text{C.7})$$

If we consider $\mathbf{r} = \text{vec}(\mathbf{Z}^{(k)} - \mathbf{R}_B^{(k)}) \in \mathbb{R}^{n^2}$, we can write (C.7) as:

$$\begin{aligned} \mathbf{R}_B^{(k)*} &= \underset{t, \mathbf{R}_B^{(k)}}{\text{argmin}} t + \lambda^{(k)} \text{Tr}(\mathbf{R}_B^{(k)}) \\ \text{s.t. } \mathbf{R}_B^{(k)} &\succeq 0, \quad \sqrt{\mathbf{r}^T \mathbf{r}} \leq t \end{aligned} \quad (\text{C.8})$$

Moreover, using a Schur complement argument, the constraint $\sqrt{\mathbf{r}^T \mathbf{r}} \leq t$ is equivalent to:

$$\begin{bmatrix} t\mathbf{I} & \mathbf{r} \\ \mathbf{r}^T & t \end{bmatrix} \succeq 0 \quad (\text{C.9})$$

*APPENDIX C. EXTRACTING THE MODEL PARAMETERS IN
STATIC AND DYNAMIC MODELING OF ABSENCE SEIZURES*

where $\mathbf{I} \in \mathbb{R}^{n^2 \times n^2}$ is the identity matrix. Hence, we can express (C.7) as the following semidefinite programming (SDP) problem:

$$\begin{aligned} \mathbf{R}_B^{(k)*} = \underset{t, \mathbf{R}_B^{(k)}}{\operatorname{argmin}} \quad & t + \lambda^{(k)} \operatorname{Tr}(\mathbf{R}_B^{(k)}) \\ \text{s.t.} \quad & \begin{bmatrix} \mathbf{R}_B^{(k)} & 0 & 0 \\ 0 & t\mathbf{I} & \mathbf{r} \\ 0 & \mathbf{r}^T & t \end{bmatrix} \succeq 0 \end{aligned} \quad (\text{C.10})$$

This kind of problems can be solved using well known solvers like `sdpt3` and `cvx` Toh et al. (1999). Regarding the penalty term, we can consider the proposed value in square-root LASSO problem Belloni et al. (2011) because the two problems are the same. The penalty term is independent of the noise variance and obtained as follows according to Belloni et al. (2011):

$$\lambda^{(k)} = \frac{c}{n} \phi^{-1}\left(1 - \frac{\alpha}{2n^2}\right) \quad (\text{C.11})$$

where $c > 1$ is a constant, ϕ is the cumulative distribution function (CDF) of a zero-mean and unit variance Gaussian variable, and $1 - \alpha$ is the probability of detection.

BIBLIOGRAPHY

- Alotaiby, T. N., Alshebeili, S. A., Alshawi, T., Ahmad, I., and Abd El-Samie, F. E. (2014). EEG seizure detection and prediction algorithms: a survey. *EURASIP Journal on Advances in Signal Processing*, 2014(1):183.
- Amini, L., Jutten, C., Pouyatos, B., Depaulis, A., and Roucard, C. (2014). Dynamical analysis of brain seizure activity from EEG signals. In *2014 22nd European Signal Processing Conference (EUSIPCO)*, pages 36–40.
- Amor, F., Baillet, S., Navarro, V., Adam, C., Martinerie, J., and Le Van Quyen, M. (2009). Cortical Local and Long-range Synchronization Interplay in Human Absence Seizure Initiation. *Neuroimage*, 45(3):950–962.
- Archer, J. S., Abbott, D. F., Waites, A. B., and Jackson, G. D. (2003). fMRI “deactivation” of the posterior cingulate during generalized spike and wave. *NeuroImage*, 20(4):1915 – 1922.
- Arora, S., Ge, R., Moitra, A., and Sachdeva, S. (2015). Provable ica with unknown gaussian noise, and implications for gaussian mixtures and autoencoders. *Algorithmica*, 72(1):215–236.
- Avoli, M. (2012). A brief history on the oscillating roles of thalamus and cortex in absence seizures. *Epilepsia*, 53(5):779–789.
- Baier, G., Goodfellow, M., Taylor, P., Wang, Y., and Garry, D. (2012). The importance of modeling epileptic seizure dynamics as spatio-temporal patterns. *Frontiers in Physiology*, 3:281.

- Becker, H., Comon, P., Albera, L., Haardt, M., and Merlet, I. (2012). Multi-way space–time–wave-vector analysis for EEG source separation. *Signal Processing*, 92(4):1021–1031.
- Belloni, A., Chernozhukov, V., and Wang, L. (2011). Square-root lasso: pivotal recovery of sparse signals via conic programming. *Biometrika*, 98(4):791.
- Bernhardt, B. C., Rozen, D. A., Worsley, K. J., Evans, A. C., Bernasconi, N., and Bernasconi, A. (2009). Thalamo–cortical network pathology in idiopathic generalized epilepsy: Insights from MRI-based morphometric correlation analysis. *NeuroImage*, 46(2):373 – 381.
- Boudet, S., Peyrodie, L., Gallois, P., and Vasseur, C. (2007). Filtering by optimal projection and application to automatic artifact removal from EEG. *Signal processing*, 87(8):1978–1992.
- Boyd, S. and Vandenberghe, L. (2004). *Convex optimization*. Cambridge university press.
- Cabasson, A. and Meste, O. (2008). Time delay estimation: A new insight into the Woody’s method. *IEEE Signal Processing Letters*, 15:573–576.
- Candes, E. J. and Plan, Y. (2010). Matrix completion with noise. *Proceedings of the IEEE*, 98(6):925–936.
- Caraballo, R. H., Fontana, E., Darra, F., Bongiorni, L., Fiorini, E., Cersosimo, R., Fejerman, N., and Bernardina, B. D. (2008). Childhood absence epilepsy and electroencephalographic focal abnormalities with or without clinical manifestations. *Seizure*, 17(7):617 – 624.
- Cardoso, J. F. and Souloumiac, A. (1993). Blind beamforming for non-gaussian signals. *IEEE Proceedings F - Radar and Signal Processing*, 140(6):362–370.

BIBLIOGRAPHY

- Chi, Y. (2016). Guaranteed blind sparse spikes deconvolution via lifting and convex optimization. *IEEE Journal of Selected Topics in Signal Processing*, 10(4):782–794.
- Chipaux, M., Vercueil, L., Kaminska, A., Mahon, S., and Charpier, S. (2013). Persistence of cortical sensory processing during absence seizures in human and an animal model: evidence from EEG and intracellular recordings. *PLoS One*, 8(3):e58180.
- Comon, P. and Jutten, C. (2010). *Handbook of Blind Source Separation: Independent Component Analysis and Applications*. Elsevier.
- Dai, B., Wang, T., Wu, J., and Bao, Z. (2015). Adaptively iterative weighting covariance matrix estimation for airborne radar clutter suppression. *Signal Processing*, 106:282–293.
- Danober, L., Deransart, C., Depaulis, A., Vergnes, M., and Marescaux, C. (1998). Pathophysiological Mechanisms Of Genetic Absence Epilepsy In The Rat. *Progress in Neurobiology*, 55(1):27 – 57.
- Das, A., Folland, R., Stocks, N. G., and Hines, E. L. (2006). Stimulus reconstruction from neural spike trains: Are conventional filters suitable for both periodic and aperiodic stimuli? *Signal processing*, 86(7):1720–1727.
- Depaulis, A., David, O., and Charpier, S. (2016). The genetic absence epilepsy rat from strasbourg as a model to decipher the neuronal and network mechanisms of generalized idiopathic epilepsies. *Journal of neuroscience methods*, 260:159–174.
- Depaulis, A. and Van Luijtelaar, G. (2005). Genetic models of absence epilepsy in the rat. *Models of Seizures and Epilepsy*, pages 233–248.
- Du, B., Sun, Y., Wu, C., Zhang, L., and Zhang, L. (2017). Real-time tracking based on weighted compressive tracking and a cognitive memory model. *Signal Processing*, 139:173–181.

- Einevoll, G. T., Kayser, C., Logothetis, N. K., and Panzeri, S. (2013). Modelling and analysis of local field potentials for studying the function of cortical circuits. *Nature Reviews Neuroscience*, 14:770–785.
- Gonzalez-Navarro, P., Moghadamfalahi, M., Akçakaya, M., and Erdogmus, D. (2017). Spatio-temporal EEG models for brain interfaces. *Signal processing*, 131:333–343.
- Hamandi, K., Laufs, H., Nöth, U., Carmichael, D. W., Duncan, J. S., and Lemieux, L. (2008). Bold and perfusion changes during epileptic generalised spike wave activity. *NeuroImage*, 39(2):608 – 618.
- Hu, M., Liu, Z., Zhang, J., and Zhang, G. (2017). Robust object tracking via multi-cue fusion. *Signal Processing*, 139:86–95.
- Kelley, C. (1999). *Iterative Methods for Optimization*. Frontiers in Applied Mathematics. Society for Industrial and Applied Mathematics.
- Killory, B. D., Bai, X., Negishi, M., Vega, C., Spann, M. N., Vestal, M., Guo, J., Berman, R., Danielson, N., Trejo, J., Shisler, D., Novotny, E. J., Constable, R. T., and Blumenfeld, H. (2011). Impaired attention and network connectivity in childhood absence epilepsy. *NeuroImage*, 56(4):2209 – 2217.
- Koochakzadeh, A., Malek-Mohammadi, M., Babaie-Zadeh, M., and Skoglund, M. (2015). Multi-antenna assisted spectrum sensing in spatially correlated noise environments. *Signal Processing*, 108:69–76.
- Li, Y., Lee, K., and Bresler, Y. (2016). Identifiability in blind deconvolution with subspace or sparsity constraints. *IEEE Transactions on Information Theory*, 62(7):4266–4275.
- Ludwig, K. A., Miriani, R. M., Langhals, N. B., Joseph, M. D., Anderson, D. J., and Kipke, D. R. (2009). Using a common average reference to improve cortical neuron recordings from microelectrode arrays. *Journal of Neurophysiology*, 101(3):1679–1689.

BIBLIOGRAPHY

- Malek-Mohammadi, M., Babaie-Zadeh, M., and Skoglund, M. (2015). Performance guarantees for Schatten-p quasi-norm minimization in recovery of low-rank matrices. *Signal Processing*, 114:225–230.
- Marten, F., Rodrigues, S., Suffczynski, P., Richardson, M. P., and Terry, J. R. (2009). Derivation and analysis of an ordinary differential equation mean-field model for studying clinically recorded epilepsy dynamics. *Phys. Rev. E*, 79:021911.
- Mazzoni, A., Logothetis, N. K., and Panzeri, S. (2013). Information content of local field potentials. *Principles of Neural Coding*, pages 411–429.
- Meeren, H. K. M., Pijn, J. P. M., Coenen, A. M. L., and Lopes Da Silva, O. H. (2002). Cortical Focus Drives Widespread Corticothalamic Networks During Spontaneous Absence Seizures in Rats. *J. Neurosci*, 22:1480–1495.
- Moeller, F., LeVan, P., Muhle, H., Stephani, U., Dubeau, F., Siniatchkin, M., and Gotman, J. (2010). Dynamic analysis of absence seizures in humans: all the same but all different. *Neuropediatrics*, 41(02):V1287.
- Moeller, F., Siniatchkin, M., LeVan, P., Stephani, U., Dubeau, F., and Gotman, J. (2009). Dynamic analysis of absence seizures in humans—an EEG fMRI study. *Neuroimage*, (47):91.
- Mulaik, S. A. (2009). *Foundations of factor analysis*. CRC press.
- Panayiotopoulos, C. P. (2008). Typical absence seizures and related epileptic syndromes: Assessment of current state and directions for future research. *Epilepsia*, 49(12):2131–2139.
- Panayiotopoulos, C. P. (2010). *A Clinical Guide to Epileptic Syndromes and their Treatment*. Springer, London.
- Pardoe, H., Pell, G. S., Abbott, D. F., Berg, A. T., and Jackson, G. D. (2008). Multi-site voxel-based morphometry: Methods and a feasibility demonstration with childhood absence epilepsy. *NeuroImage*, 42(2):611 – 616.

- Paxinos, G. and Watson, C. (2009). *The Rat Brain In Stereotaxic Coordinates: Compact 6th Edition*. Academic press.
- Pettersen, K. H., Devor, A., Ulbert, I., Dale, A. M., and Einevoll, G. T. (2006). Current-source density estimation based on inversion of electrostatic forward solution: Effects of finite extent of neuronal activity and conductivity discontinuities. *Journal of Neuroscience Methods*, 154(1–2):116 – 133.
- Polack, P.-O. (2016). Sensory processing during absence seizures. *The Journal of physiology*, 594(22):6439–6440.
- Polack, P.-O., Guillemain, I., Hu, E., Deransart, C., Depaulis, A., and Charpier, S. (2007). Deep Layer Somatosensory Cortical Neurons Initiate Spike-and-Wave Discharges in a Genetic Model of Absence Seizures. *The Journal of Neuroscience*, 27(24):6590–6599.
- Quiroga, R. Q., Nadasdy, Z., and Ben-Shaul, Y. (2004). Unsupervised Spike Detection And Sorting With Wavelets And Superparamagnetic Clustering. *Neural Comput*, 16(8):1661–1687.
- Rabiner, L. R. (1989). A tutorial on hidden markov models and selected applications in speech recognition. *Proceedings of the IEEE*, 77(2):257–286.
- Recht, B., Fazel, M., and Parrilo, P. A. (2010). Guaranteed minimum-rank solutions of linear matrix equations via nuclear norm minimization. *SIAM Review*, 52(3):471–501.
- Reitz, J. R., Milford, F. J., and Christy, R. W. (2008). *Foundations of electromagnetic theory*. Addison-Wesley Publishing Company.
- Seth, A. K., Barrett, A. B., and Barnett, L. (2015). Granger causality analysis in neuroscience and neuroimaging. *Journal of Neuroscience*, 35(8):3293–3297.

BIBLIOGRAPHY

- Steriade, M. (2003). *Neuronal Substrates of Sleep and Epilepsy*. Cambridge University Press.
- Toh, K. C., Todd, M. J., and Tütüncü, R. H. (1999). SDPT3 — a matlab software package for semidefinite programming, version 1.3. *Optimization Methods and Software*, 11(1-4):545–581.
- Vlachos, I., Krishnan, B., Treiman, D. M., Tsakalis, K., Kugiumtzis, D., and Iasemidis, L. D. (2017). The concept of effective inflow: Application to interictal localization of the epileptogenic focus from iEEG. *IEEE Transactions on Biomedical Engineering*, 64(9):2241–2252.
- Wang, Z., Zhao, Z., Ren, C., and Nie, Z. (2018). Cfar subspace detectors with multiple observations in system-dependent clutter background. *Signal Processing*.
- Williams, M. S., Altwegg-Boussac, T., Chavez, M., Lecas, S., Mahon, S., and Charpier, S. (2016). Integrative properties and transfer function of cortical neurons initiating absence seizures in a rat genetic model. *The Journal of physiology*, 594(22):6733–6751.
- Wu, C., Xiang, J., Sun, J., Huang, S., Tang, L., Miao, A., Zhou, Y., Chen, Q., Hu, Z., and Wang, X. (2017). Quantify neuromagnetic network changes from pre-ictal to ictal activities in absence seizures. *Neuroscience*, 357:134–144.
- Yeredor, A. (2002). Non-orthogonal joint diagonalization in the least-squares sense with application in blind source separation. *IEEE Transactions on Signal Processing*, 50(7):1545–1553.
- Zhu, J., Wang, X., Huang, X., Suvorova, S., and Moran, B. (2018). Detection of moving targets in sea clutter using complementary waveforms. *Signal Processing*, 146:15–21.